UNIVERSITY OF CATANIA

DEPARTMENT OF CHEMICAL SCIENCES

INTERNATIONAL PhD IN CHEMICAL SCIENCES – XXXII CYCLE

Rossella Migliore

SUPRAMOLECULAR AMPHIPHILES:
FROM HOST-GUEST COMPLEXES
TO EFFECTIVE CATANIONIC MIXTURES

PhD Thesis

Tutor:
Prof. Giuseppe Arena

PhD Coordinator:
Prof. Salvatore Sortino

TABLE OF CONTENTS

ABSTRACT

p-sulfonatocalix[n]arenes are 3-D shaped macrocyclic receptors that are found to be very effective hosts for the construction of supramolecular amphiphiles. Despite reasonable interest in calixarene-based supramphiphiles, a quantitative characterization of the binding features and driving forces of the host-guest formation as well as of the aggregation processes occurring in neutral aqueous solution has not been reported yet.

In this work, complex species, binding constants and forces driving the formation of supramphiphiles made of a *p*-sulfonatocalix[4]arene (**C4TS**) and positively charged long-tailed guests in neutral (buffered) aqueous solution have been determined by isothermal titration calorimetry (ITC) in order to find out the best systems and conditions for the assembly of efficient micellar-like aggregates. The aggregation features of the most promising host–guest complexes have been also studied by ITC in neutral aqueous solution, determining critical aggregation concentration and micellization enthalpy values ($\Delta H^{0}_{mic.}$) of the micellar-like aggregates formed by different supramolecular surfactants. The results highlighted the crucial role played by the calixarene scaffold in the formation of efficient self-aggregating systems.

Since in most biological, material and industrial related applications mixtures of surfactants are used, mixtures formed by selected cationic surfactants in combination with the anionic **C4TS** have been studied varying the complexation ratio of surfactant. The species and the binding constant values have permitted a fine control of the composition of the mixtures so to switch from a single anionic surfactant (i.e., the anionic supramolecular amphiphile) to a catanionic mixture in which the supramphiphile and the

excess of free surfactant coexist. A macroscopic evaluation on the effect of the composition on the phase behaviour of these systems has been accurately carried out.

These mixed systems have been investigated by surface tension measurements that enabled both to determine the variation of the CAC values upon changing the amount of **C4TS** in the mixtures and to evaluate the existence of a synergistic behaviour.

The structure of the aggregates has been systematically studied by means of static and dynamic light scattering in a broad range of scattering angles examining different molar fractions in order to determine structural changes when varying the amount of the free surfactant. The structural characterization showed that in the presence of an excess of free uncomplexed surfactant these systems behave like intrinsic catanionic surfactant mixtures, thereby allowing to fine tune the aggregation features by controlling the mixing ratio.

Finally, mixed systems have been studied at the solid/liquid interface at different compositions and concentrations by using a quartz crystal microbalance with dissipation monitoring (QCM-D). The varying mixture conditions employed have caused significant changes in the mass adsorbed onto gold surfaces as well as in the shape of the kinetic profiles which have been associated to different adsorption mechanisms.

LIST OF ABBREVIATIONS

C4TS	*p*-sulfonatocalix[4]arene
CAC	critical aggregation concentration
CetPyr	cetylpyridinium bromide
CMC	critical micelle concentration
CTAB	cetyltrimethylammonium bromide
D3MIC	1-decyl-3-methylimidazolium
DeTAB	decyltrimethylammonium bromide
DLS	dynamic light scattering
DoPyC	1-dodecylpyridinium chloride
DTAB	dodecyltrimethylammonium bromide
ITC	isothermal titration calorimetry
OPyC	octylpyridinium chloride
OTAB	trimethyloctylammonium bromide
QCM-D	quartz crystal microbalance with dissipation monitoring
SCnAs	*p*-sulfonatocalix[n]arenes
SDBS	sodium dodecyl benzene sulphonate
SDS	sodium dodecyl sulfate
SLS	static light scattering
ST	surface tension

CHAPTER 1 – INTRODUCTION

Surfactants, also commonly known as surface active agents, exhibit superficial or interfacial activity and have characteristic structures possessing both hydrophobic (non-polar) and hydrophilic (polar) groups. The polar groups generally contain heteroatoms, such as O, S, P or N, in their functional groups (alcohol, thiol, ester, acid, sulfate, sulfonate, phosphate, amide, amine, etc.). The non-polar part of the structure usually consists of hydrocarbon groups (in the simplest case a long alkyl chain) typically with more than eight carbon atoms. The polar groups of surfactants have a strong affinity for polar solvents, particularly water, and are termed hydrophilic whereas the non-polar part of the surfactant is called hydrophobic; surfactants with dual affinity are called amphiphiles. The word amphiphile was coined by Paul Winsor 50 years ago. It comes from two Greek words: the prefix amphi (άμφί) which means "double" ("from both sides") and the root philos (φιλέω, to love) which expresses friendship or affinity. An amphiphilic substance exhibits a double affinity, resulting from a polar-apolar functionality. (**Figure 1**).
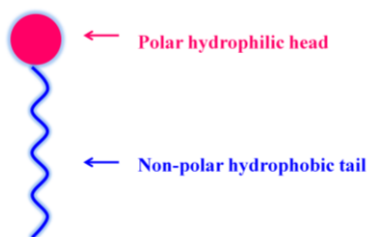
Figure 1. Schematic representation of an amphiphile.

Amphiphilic surfactants have a strong tendency to migrate to interfaces or surfaces to orient themselves. Because of their nature, they do not feel "at ease" in any solvent, be it polar or non-polar, since there is always one of the two groups of an amphiphilic surfactant that does not like the solvent environment.[1] When amphiphiles are on air-water or oil-water interfaces they align so as to expose the hydrophilic part to water and hydrophobic part to air (or oil).

An energetically favourable form/aggregate of surfactant molecules in aqueous solution are micelles in which the hydrophobic tails are protected by the hydrophilic head groups (**Figure 2**). At low surfactant concentration the surfactant molecules arrange on the surface. When more surfactant is added, the surface tension of the solution starts to rapidly decrease due to the crowding of surfactant molecules on the surface. When the surface becomes saturated, the addition of surfactant molecules will lead to the formation of micelles. The concentration value at which the association process begins is termed critical micelle concentration (CMC).
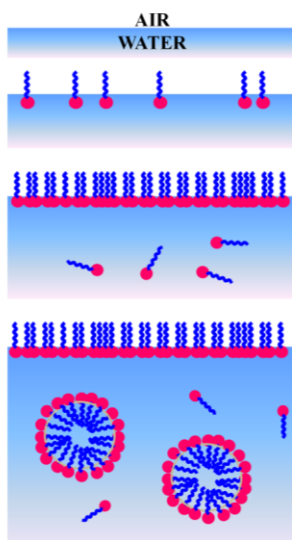
Figure 2. Schematic representation of micelles formation.

Surfactants classification

From the commercial point of view, surfactants are often classified according to their use. However, this is not a convenient definition and may generate confusion owing to the multiple uses for which surfactants may be employed. The most accepted and scientifically valid classification of surfactants is based on their dissociation in water. According to this classification, surfactants can be divided into four categories[2] (**Figure 3**):

- Anionic surfactants
- Cationic surfactants
- Non-ionic surfactants
- Amphoteric/Zwitterionic surfactants
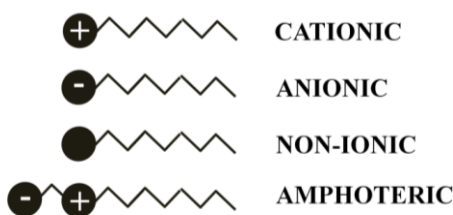
Figure 3. Surfactant classification based on the nature of their polar head.

Anionic surfactants

When dissolved in water, anionic surfactants dissociate to form an amphiphilic anion and a cation. Typical anionic surfactants include soaps, alkylbenzene sulfonates, alkyl sulfonates, alkyl sulfates, salts of fluorinated fatty acids, silicones, etc. Within the anionic surfactant class there is only a limited number of hydrophilic groups whilst there are several types of hydrophobic groups. The raw materials of important functional hydrophilic groups include carboxylic acid, sulfonic acid and phosphoric acid esters; the

raw materials from which hydrophobic groups are derived include animal and vegetable fats and their hydrolysis products. Anionic surfactants have excellent penetration, wetting, emulsification, dispersion, solubilisation, foaming, decontamination, anti-static and smoothing properties. They have the largest yield among different categories of surfactants and can be used in combination with non-ionic and amphoteric surfactants. They cannot be mixed with cationic surfactants owing to the formation of a precipitate.

This class of surfactants is commonly used as detergent, wetting, emulsifying and dispersing agents. Anionic surfactants find applications in many fields, some examples are reported below.

- In cosmetics as foaming agent of shampoos, bath creams, toothpastes;
- In food industry as emulsifier, dispersant, preservative, solubilizer, protein stabilizing agents;
- In medicine as an emulsifier, dispersant, preservative, solubilizer, protein stabilizing agents;
- In textile industry as oiling agent, dyeing auxiliarie, bleaching agent, soft processing agents;
- in the field of pesticides as spraying and emulsifying agent.

Anionic surfactants find also applications in other fields such as polymer industry, paint, ink, transportation, ship-breaking.

Cationic surfactants

Cationic surfactants dissociate in water to form an amphiphilic cation and an anion. These are mainly quaternary ammonium compounds and account for only 5-6% of the total surfactant production. They are neither good

detergents nor foaming agents. However, they are extremely useful for some specific uses, thanks to their peculiar properties. Their positive charge allows for their adsorption on solid surfaces that are negatively charged at neutral pH. This characteristic confers an antistatic feature and a softening action for fabric and hair rinsing. Moreover, thanks to their positive charge they may be used as floatation collectors, hydrophobating agents, corrosion inhibitors as well as solid particle dispersants. They are used as emulsifiers in asphaltic emulsions and coatings in general, in inks, wood pulp dispersions, magnetic slurry, etc. In addition, many cationic surfactants are bactericides. They are used to clean and sterilize surgery hardware, to formulate heavy duty disinfectants for domestic and hospital use, and to sterilize food bottle or containers, particularly in the dairy and beverage industries. Examples include alkyltrimethylammonium alides, cetrimide, benzalkonium chloride, etc.

Non-ionic surfactants

Non-ionic surfactants do not produce ions in aqueous solution. As a consequence, they are compatible with the other types of surfactants and are excellent candidates to enter complex mixtures, as found in many commercial products. These are the most commonly used surfactants. They are much less sensitive to electrolytes, particularly divalent cations, than ionic surfactants and can be used with high salinity or hard water. The hydrophilic region contains polyoxyethylene or polyols derivatives while the hydrophobic region contains saturated or unsaturated fatty acids or fatty alcohols.

Non-ionic surfactants are good detergents, wetting agents and emulsifiers. Some of them have also good foaming properties. Some categories exhibit a

very low toxicity level and are used in pharmaceuticals, cosmetics and food products. Non-ionic surfactants are found today in a large variety of domestic and industrial products, such as powdered or liquid formulations. Poloxameres and polysorbates are the most commonly used non-ionic surfactants.

Amphoteric/zwitterionic surfactants

Amphoteric/zwitterionic surfactants exhibit both cationic and anionic dissociation features. These surfactants are scarcely aggressive and may be anionic, cationic or non-ionic depending on the pH of the solution. They are ubiquitous in biological systems (e.g. components of membrane bilayers) and are used for numerous technological and industrial applications spanning from common cleaning detergents to oil recovery, pharmaceutical and cosmetic formulations, drug delivery systems, catalysis and synthesis of nanostructured advanced materials, just to name a few. All of these applications arise from the ability of these molecules to adsorb at surfaces and interfaces and to self-assemble into more or less defined aggregates of nanometric dimensions. Alkylbetaine is an example of amphoteric surfactant.

Nature of the hydrophobic group

Differences in the nature of the hydrophobic groups (usually long-chain hydrocarbon residues) are less pronounced than those of the hydrophilic groups. However, the characteristics of the hydrophobic group affect some proprieties of surfactants, as briefly illustrated below.

- Length of the hydrophobic group. An increase of the length of the hydrophobic group *i.* decreases the solubility of the surfactant in water and increases its solubility in organic solvents, *ii.* causes closer packing of the surfactant molecules at the interface (if the area occupied by the hydrophilic group at the interface allows for it), *iii.* increases the tendency of the surfactant to adsorb at an interface or to form aggregates (micelles), *iv.* increases the melting point of the surfactant and of the adsorbed film as well as the tendency to form liquid crystal phases in the solution, and *v.* for ionic surfactants makes it easier for a counter ion to precipitate the surfactant from water.

- Branching, unsaturation. The introduction of branching or unsaturation into the hydrophobic group *i.* increases the solubility of the surfactant in water or in organic solvents (compared to straight-chain, saturated isomers), *ii.* decreases the melting point of the surfactant as well as of the adsorbed film, *iii.* causes a looser packing of the surfactant molecules at the interface (the *cis* isomer is particularly loosely packed while the *trans* isomer is packed almost as closely as a saturated isomer) and inhibits liquid crystal phase formation in solution, *iv.* may cause oxidation and the appearance of a color in unsaturated compounds, *v.* may decrease biodegradability in branched-chain compounds, and *vi.* may increase thermal instability.

- Aromatic nucleus. The presence of an aromatic nucleus in the hydrophobic group may *i.* increase the adsorption of the surfactant onto polar surfaces, *ii.* decrease its biodegradability, and *iii.* cause looser packing of the surfactant molecules at the interface.[3-8]

Mixed surfactant systems

Mixtures of surfactants, rather than individual surfactants, are used in most practical applications. In some cases, this is not done purposely, since commercial surfactants are mixtures of surface-active materials due to the non-homogeneous raw materials used in their manufacture and/or the presence of unreacted raw materials and process by-products. In other cases, different types of surfactants are intentionally mixed to improve the properties of the final product.

Aqueous solutions of surfactants, whether mixtures or single surfactants, exhibit a variety of interesting and useful phenomena. Even at low concentrations of surfactant in water, peculiar effects can be observed at interfaces with the solution.

The most pronounced effect is a lowering of interfacial tension due to the preferential adsorption of surfactant molecules at solution interfaces. With increasing surfactant concentration, monolayers or bilayers are formed at solution interfaces and, when the critical micellar concentration is reached, surfactant molecules self-aggregate to yield micelles. In this process, there may be both ideal and non-ideal mixing contributions. Since the overall micellization process is driven by the hydrophobic effect, that does not depend on the surfactant head group, the formation of randomly mixed surfactant aggregates will tend to be favoured.[9] Thus, the hydrophobic effect may be considered the ideal contribution to the formation of aggregates. In the case of mixtures with different surfactant types, electrostatic interactions between head groups are the "non-ideal" contribution to the formation of aggregates.[10]

A mixed micellar solution is schematically illustrated in **Figure 4** where the two different colours indicate different surfactants. A mixed micelle, a mixed

monolayer at the air/solution interface as well as a mixed bilayer aggregate at the solid/solution interface are also schematically shown.
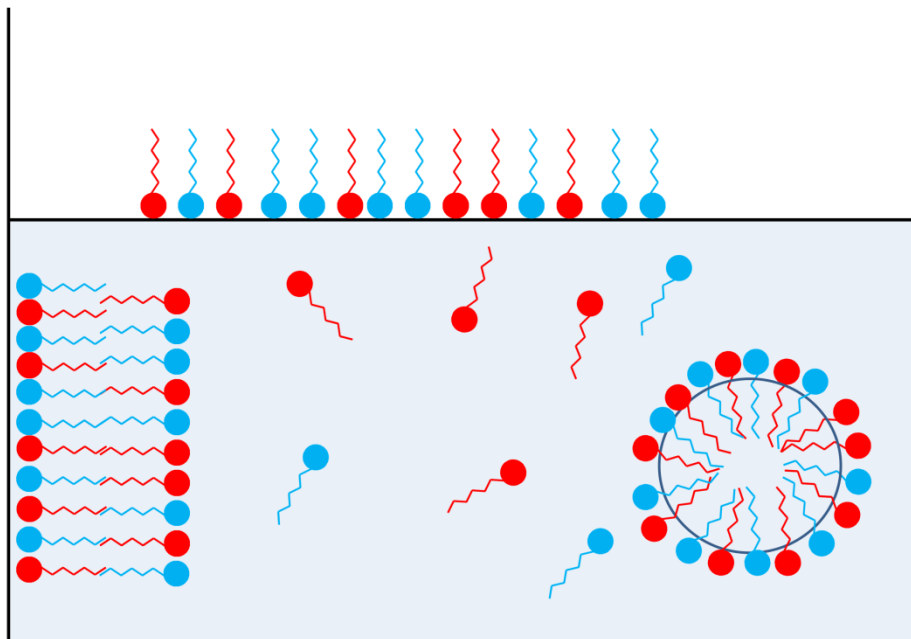
Figure 4. Schematic representation of phenomena in a mixed micellar solution of two different surfactants.

There are several examples of surfactant mixtures. As it is a well-established idea that cationic and anionic surfactants cannot be present in the same formulation, surfactant mixtures are usually obtained by combining anionic/anionic, cationic/cationic, non-ionic/non-ionic, amphoteric/ amphoteric, anionic/non-ionic, cationic/non-ionic or amphoteric/non-ionic surfactants.

In most cases, when different types of surfactants are purposely mixed, synergism is the main goal, i.e. the condition in which the properties of the mixture are better than those attainable with the individual components themselves.[11-16] Although the existence of synergistic relations between

certain types of surfactants has been known and utilized for many years, the investigation of synergism in quantitative terms is a recent development based upon a simple, convenient method for measuring molecular interactions between surfactants. The molecular interactions between two different surfactants adsorbed at various interfaces are measured by a parameter, β, that indicates the nature and strength of such interactions.

The value of the β parameter relates to the free energy change upon mixing of the two surfactants. A negative β value indicates that, upon mixing, the two surfactants experience either greater attraction or less repulsion than before mixing; by contrast, a positive β value, indicates that the two surfactants experience less attraction or greater repulsion upon mixing than before mixing. A value close to zero indicates little or no change upon mixing. Since, in mixtures containing ionic surfactants, there is always a repulsive interaction between the ionic surfactant molecules before mixing, the β parameter is almost always negative, if only because of the dilution effect upon mixing with a second surfactant, except for anionic–anionic mixtures. Steric effects contribute to the value of the β parameter when the size of the hydrophilic head group or the branching of the hydrophobic groups of the two surfactants vary.[17] The relevant properties of the individual surfactants and the values of the molecular interaction parameters help predicting whether there will be synergism in a mixture of surfactants and also give indications on the component ratio maximizing the optimum value of the relevant surface property in that specific point.

In any case, synergism increases as charge difference increases indicating that synergism between anionic/anionic or non-ionic/non-ionic surfactants is lower than that occurring between anionic/non-ionic or cationic/non-ionic, which, in turn, is lower than that between cationic/anionic. Thus, a higher synergism is obtained by mixing anionic and cationic surfactants, and

therefore, a better understanding of that system may broaden the horizon for new formulations.[18]

In practical applications the surfactant mixtures that behave synergistically, provide more desirable properties than individual surfactants.

In skin care applications, mixtures of surfactants, that may act as chemical penetration enhancers (CPEs) have already been shown to yield formulations that do not enhance skin irritation. The ability of surfactants to self-assemble into micelles allows for more complex interactions with skin; synergism in a surfactant mixture decreases the total surfactant concentration, reducing skin irritation.[19]

In the area of detergency, mixtures of anionic and non-ionic surfactants have gained increased attention thanks to their widespread applications. The addition of a non-ionic surfactant has been reported to significantly improve the detergency of anionic surfactants and to maximize water hardness tolerance.[20]

As to mixtures containing zwitterionic surfactants, betaines are widely used as foam booster in commercial shampoos or hair conditioners.[21]

Finally surfactants mixtures, especially cationic/anionic mixtures, can yield the formation of microstructures, such as vesicles, that can be used as templates for drug-delivery applications as well as in nano-drug carrier synthesis.[22,23]

Supramolecular amphiphiles

Supramolecular amphiphiles or supra-amphiphiles are a new class of amphiphilic compounds that has attracted the attention of researchers in recent years. The main difference between conventional and supramolecular amphiphiles is that in the first case the hydrophilic and hydrophobic segments are linked by covalent bonds, while in the second case these segments are held together by non-covalent interactions.

Non-covalent synthesis is regarded as a kind of self-assembly method that is very useful in the construction of chemical structures with a high degree of structural complexity. Furthermore a non-covalent synthesis allows to overcome the problems associated with the more complex and longer procedures typical of covalent syntheses. Supramphiphiles of different topologies and functions can be easily fabricated; in addition different type of non-covalent interactions can be employed for their preparation, such as host-guest and metal-ligand as well as electrostatic interactions and hydrogen bonding formation.

However, it should be pointed out that in most cases the formation of supramphiphiles is not driven by a single kind of interaction, but rather by the combination of different forces, though one driving force may play the leading role.[24]

Hydrogen bonding

Kunitake and Kimizuka reported on the use of hydrogen bonding for the formation of supra-amphiphiles based on building blocks such as melamines and isocyanuric acid derivatives. These complementary groups can form extended hydrogen bonded arrays having amphiphilic properties (**Figure 5**).[25]
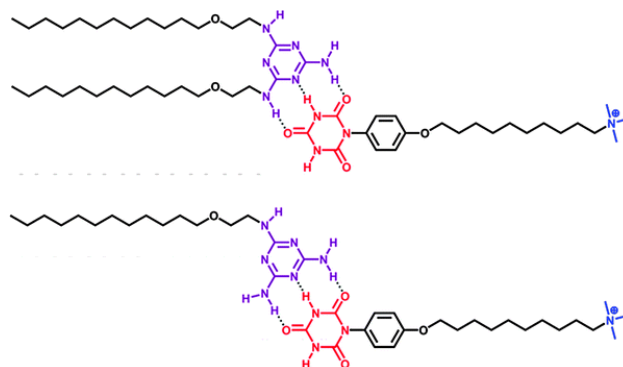
Figure 5. Supra-amphiphiles based on hydrogen bonding.[25]

Metal–ligand coordination

Metal ligand coordination is stronger than most intermolecular interactions; however, its reversibility makes it function as a sort of supramolecular bond. Schubert *et al.* have suggested the use of metal-ligand coordination to link hydrophilic and hydrophobic blocks, that yields a supramolecular amphiphilic polymer (**Figure 6**).[26]
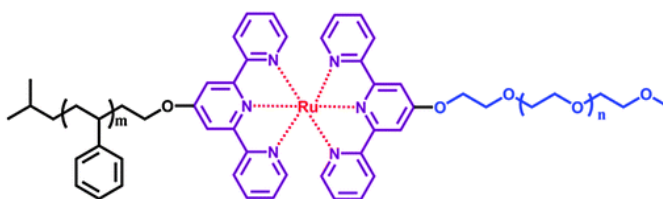
Figure 6. Metal supramolecular diblock copolymer reported by Schubert *et al.*[26]

Electrostatic interaction

Eisenberg *et al.* showed that the complexes formed in aqueous solutions by block copolymers containing ionic and non-ionic water-soluble segments (block ionomers) and oppositely charged single-tail surfactants

spontaneously arrange in small vesicles. This was observed for a variety of cationic surfactants, differing for the length of the aliphatic radical and the size of the head group.[27] MacKintosh et al. reported that a cationic gemini surfactant with a chiral counterion behaves as a supramolecular gemini system. When the counterion is L-tartrate, this supramolecular gemini structure forms gels in both water and some organic solvents by creating extended networks of multilamellar twisted ribbons (**Figure 7**).[28]
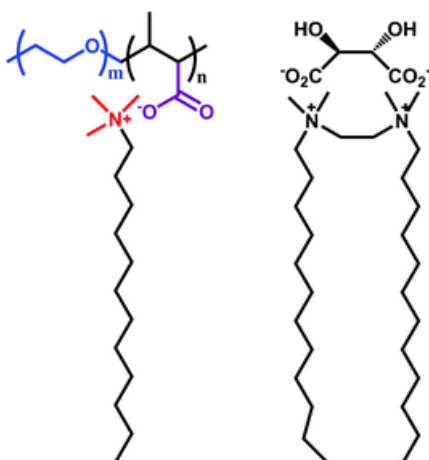
Figure 7. Supra-amphiphiles based on electrostatic interactions.[28]

Charge transfer interaction

Zhang et al. demonstrated that well-defined nanostructures may be obtained by using charge transfer interaction between electron donors and acceptors. By designing and synthesizing different building blocks, X-shape or H-shape super-amphiphiles were successfully assembled, which can be used to create tunable supramolecular nanostructures (**Figure 8**).[29]
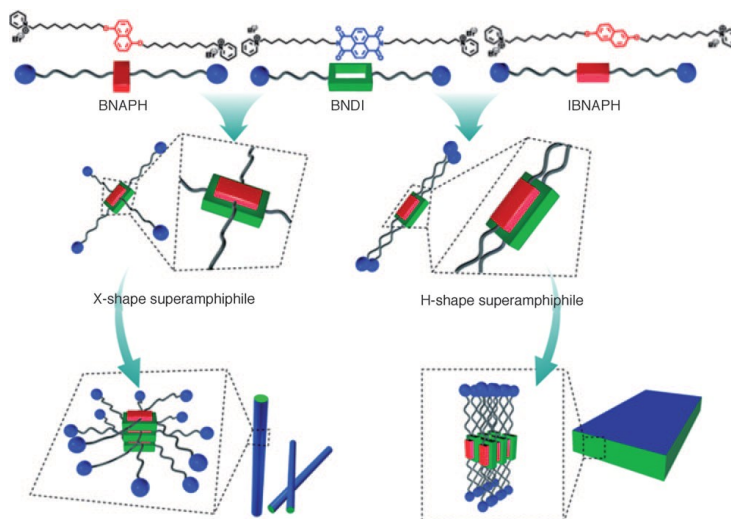
Figure 8. Schematic representation of the X- and H-shape supramphiphiles and their assembly into one-dimensional and two-dimensional nanostructures, respectively.[29]

Host–guest recognition

Finally, host–guest recognition can be used for the assembly of supramolecular amphiphiles. The host (e.g. a cyclodextrin, a calixarene or a cucurbituril) can form stable inclusion complexes with appropriate guests to obtain a supramolecular structure having amphiphilic properties (**Figure 9**). The inclusion complex obtained with a β-cyclodextrin and a fatty alcohol or acid, functioning as a non-ionic supramolecular amphiphiles. provides a good example.[30]

Cucurbiturils, well-known macrocyclic cavitands, can be also used for the construction of supramolecular amphiphiles. Kim et al. have employed a stable ternary complex driven by charge transfer interaction between the electron-deficient cucurbituril host and an electron-rich guest molecule to form supramphiphiles able to trigger the spontaneous formation of giant vesicles.[31]
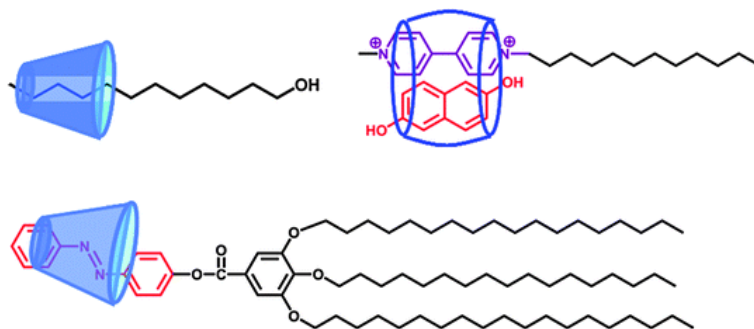
Figure 9. Some examples of supramphiphiles based on host-guest complex formation.[24]

Last but not least, calixarenes may act as building block for the development of supramphiphiles with improved features compared to conventional amphiphiles.

Calixarene-based supramphiphiles

Calixarenes

Calixarenes are a class of organic macrocyclic hosts formed by the *ortho* condensation of *para*-substituted phenols with formaldehyde. During the eighties, Gutsche *et al.* provided evidence for both the macrocyclic nature of the calixarenes and the presence of cycles containing four, six and eight phenolic units, by NMR studies.[32] Gutsche was the first to suggest the term "calixarenes" for these molecules due to the structural analogy with the shape of the ancient Greek calix crater vases.

The simplified nomenclature of the calixarenes uses [n] to denote the number of phenolic units in the macrocycle (e.g., the calix[4]arene contains four aromatic units). Sketches for a calix[4]arene, a calix[6]arene and a calix[8]arene are showed in **Figure 10**.

Calix[4]arene   Calix[6]arene   Calix[8]arene
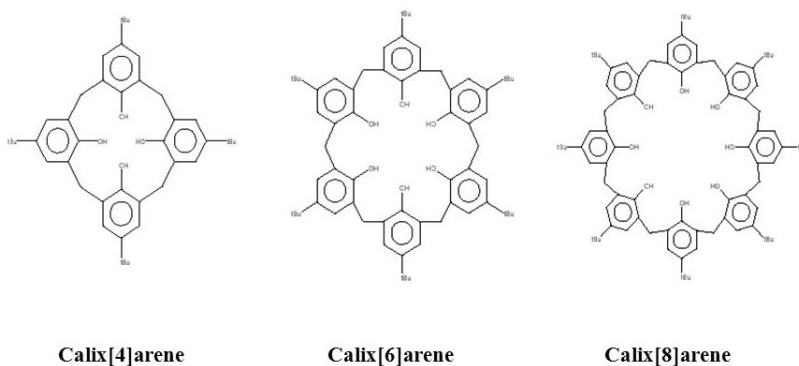
Figure 10. Calix[n]arenes.

The presence of methylene bridges linking the phenolic units in the calix[n]arene scaffolds drives the conformational mobility of these macrocycles (**Figure 11**).[33] For calix[n]arenes having no substituents at the

lower rim, the formation of annular intra-molecular hydrogen bonds may stabilize the cone conformation.
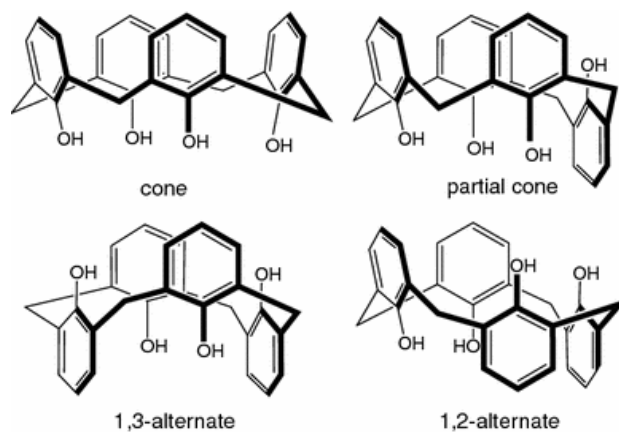
Figure 11. Conformations of calix[4]arene.[34]

However, the inclusion capabilities of the cavities of unmodified calixarenes are not as good as those of other common macrocycles such as crown ethers, cyclodextrins and cucurbiturils; extensive chemical modification of calixarenes is necessary to achieve efficient endo-complexation and, when needed, to render them water-soluble. Fortunately, they have been described as "macrocycles with (almost) unlimited possibilities" for their relative facile modification at both the upper and the lower rim.[35]

p-sulfonatocalix[n]arenes (SCnAs, n = 4−8; **Figure 12**), first reported by Shinkai *et al.* in 1984,[36] are a prominent family of water-soluble calixarene derivatives with a strong ability to bind guests in their cavities in aqueous media.[37] SCnAs have been used for molecular recognition and sensing, crystal engineering, catalysis, enzyme assays, and biological/medicinal chemistry.
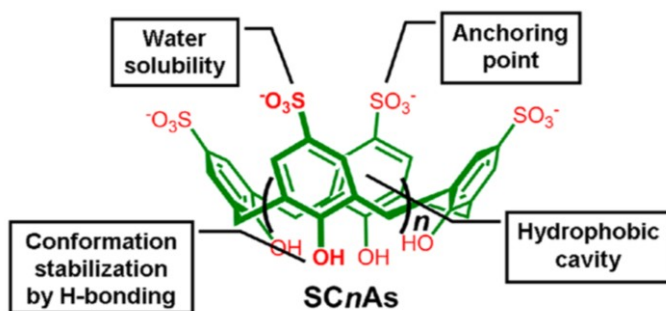
Figure 12. Structure and features of *p*-sulfonatocalix[n]arene.[38]

p-sulfonatocalix[n]arenes have several advantages:

1) Facile synthesis: they can be prepared easily with satisfactory yields by direct sulfonation of the upper rim of simple calixarenes;

2) Solubility: they are highly water-soluble and this is a remarkable advantage as the driving forces for guest inclusion in the cavity, such as hydrophobic and π-stacking interactions, are more effective in aqueous than in organic media;

3) Binding ability and selectivity: the sulfonate groups at the upper rim provide anchoring points that supplement the binding interactions intrinsic of the π-electron-rich cavities; as a result, SCnAs display robust capacity of binding and high selectivity toward various organic cations;[39-41]

4) Biocompatibility: this property makes SCnAs suitable for diverse biological and pharmaceutical applications.[42,43] For example, it has been reported that a single injection of SC4A to mice at doses equivalent to 2−5 g in humans has no acute toxicity; in addition, the compound is rapidly cleared via urine without accumulating in the liver.[44]

In addition to these properties, properly modified *p*-sulfonatocalix[*n*]arenes also show amphiphilic properties, self-aggregating into well-defined

nanostructures, such as micelles, when placed in aqueous solution. *p*-sulfonatocalixarene-based amphiphiles can be simply obtained by attaching hydrophobic alkyl chains to the phenolic oxygen atoms. In principle, these compounds can be included in the same category of oligomeric surfactants (such as gemini, trimeric and tetrameric surfactants).[45-48]

Compared to conventional surfactants, besides a lower critical micelle concentration (CMC) calixarene-based surfactants are characterized by a host-guest recognition site, able to bind guest molecules and ions. The first example of calixarenes with surface active properties was reported by Shinkai *et al.,* who described the synthesis of *p*-sulfonatocalix[6]arenes bearing alkyl chains at the lower rim and discussed possible structure-aggregation relationships.[49-51]

Following Shinkai's pioneering work, among the researchers that have studied the aggregation behaviour of amphiphilic *p*-sulfonatocalixarenes emerged the work of Basilio *et al.*. They reported different studies on the self-assembly of *p*-sulfonatocalix[n]arenes amphiphiles (**Figure 13**).
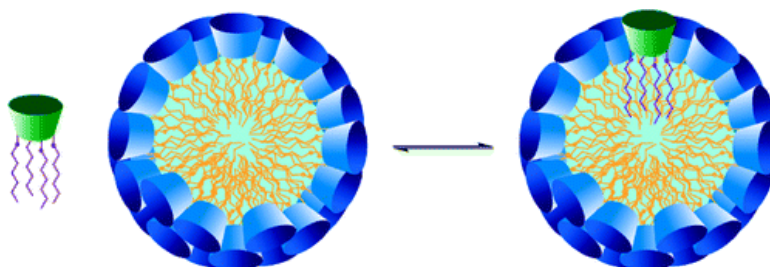
Figure 13. Schematic representation of amphiphilic *p*-sulfonatocalixarene micellization.[52]

Firstly the micellization of three calix[4]arene derivatives with alkyl chains of different lengths at the lower rim together with a calix[6]arene and a calix[8]arene, both bearing alkyl chains of the same length (hexyl) at the

lower rim, were investigated (**Figure 14**). Then the correlations between the micellization properties with both the alkyl chain length and the number of phenolic units present in the macrocyclic ring (*i.e.*, the ring size) were examined. [52-54]
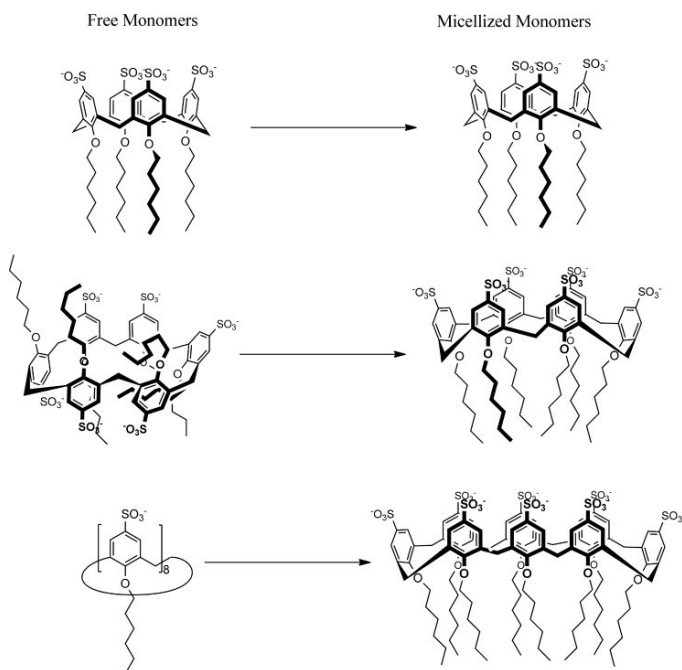
Figure 14. Structures of the conformations adopted by a calix[4]arene calix[6]arene and a calix[8]arenes derivative as free and micellized monomers.[54]

The work done demonstrated the high potential of these compounds in the fields of surfactant or colloidal chemistry. When compared with traditional single chain surfactants, amphiphilic *p*-sulfonatocalix[n]arene present a higher tendency to self-aggregate and special structural features, such as variable flexibility and conformational reorganization ability, which makes these compounds of special interest to study the effects of these properties on the aggregation of amphiphilic molecules.

p-sulfonatocalixarene-based supramolecular amphiphiles

p-sulfonatocalixarenes exhibit different cavity structures, framework rigidity and complexation driving forces and therefore may afford significant recognition and assembly features when used in host−guest systems. In the presence of properly chosen amphiphilic guests molecules, the recognition abilities of *p*-sulfonatocalixarenes make them promising building blocks for the construction of supramolecular amphiphiles.

Garcia-Rio and co-workers reported on the formation of micelles resulting from the complexation of a single chain surfactant with calixarene derivatives in aqueous solution. In that work, besides the formation of the host-guest complex between the alkyltrimethylammonium cation and the hexamethylated *p*-sulfonatocalix[6]arene, the formation of micellar aggregates was observed at a concentration lower than the CMC of the pure surfactant, suggesting that the calixarene promotes the formation of micelles. The system was characterized by a wide variety of techniques, including NMR, surface tension and dynamic light scattering. The results indicate that for concentrations below the critical aggregation concentration (CAC), the calixarene forms a discrete 1:1 host-guest complex with the alkyltrimethylammonium guests that further aggregates into micelles (**Figure 15**).[55-57]
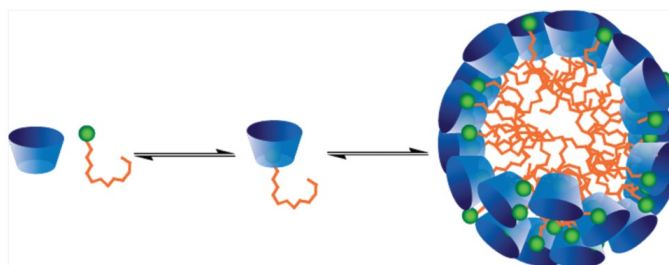
Figure 15. Aggregation of alkyltrimethylammonium surfactants in the presence of calix[6]arene.[55]

Interestingly, a smaller and preorganized calixarene, such as *p*-sulfonatocalix[4]arene, with a single chain surfactant leads to the formation of vesicles in aqueous solution. After sonication, the unilamellar vesicles resulting from the complex formed by tetratrimethylammonium bromide and *p*-sulfonatocalix[4]arene have a diameter of about 120 nm with the potential of being stored by lyophilization and then rehydrated without significant change in size or shape.[58]

Significant contributions to the field of *p*-sulfonatocalixarene based supramphiphiles were made by Liu and co-workers. In one of their works, *p*-sulfonatocalix[4]arene and *p*-sulfonatocalix[5]arene were used as hosts and different molecules with amphiphilic properties were employed as guests in order to construct self-aggregating supramolecular systems. For example, when calix[5]arene as hosts and 1- pyrenemethylaminium (PMA) were used as host and guest, respectively, they obtained self-assembled binary supramolecular vesicles with a structure that can respond to multiple external stimuli, such as temperature or host-guest competitive binding. With this approach, the authors were able to release the entrapped drugs inside the vesicles (**Figure 16**).[59-63]
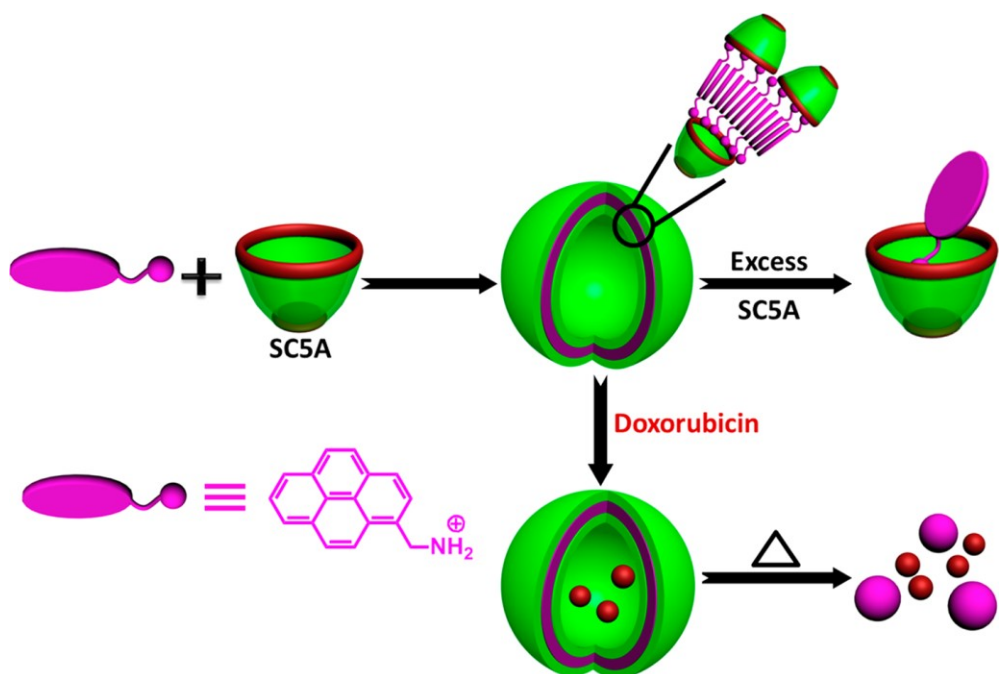
Figure 16. Construction of supramolecular binary vesicles and temperature-responsive drug release from the vesicles.[59]

p-sulfonatocalix[*n*]arene-based supramolecular amphiphiles have already provided promising results and potential applications in the fields of smart materials and controlled delivery systems. The basic idea consists in the use of the recognition abilities of *p*-sulfonatocalix[n]arenes to form supramolecular complexes with (improved) amphiphilic properties. Due to the inherent reversibility of the non-covalent interactions, the assembly/disassembly process can be conveniently controlled with appropriate stimuli.

However, the structure and composition of the complex or complexes of calixarene-based supramphiphiles are not currently known and further microstructure characterization studies are needed to fully elucidate the aggregation process.

CHAPTER 2 - SOLUTION THERMODYNAMICS OF CALIXARENE-BASED SUPRAMPHIPHILES IN BUFFERED AQUEOUS SOLUTION

Two different aspects are to be considered when surfactant solutions are investigated: the air/liquid interfacial properties and the bulk properties. The latter features show an unusual behaviour indicating the presence of colloidal particles in solution. In almost every curve in which the value of a measurable physical property (that depends on size or number of particles) is plotted against an increasing concentration of surfactant solution, a break is observed. This break correspond to the formation of micelles; the related concentration value is called critical micelle concentration (CMC).

The CMC value is commonly determined by using the breaks in the electrical conductivity, surface tension, light scattering, or fluorescence spectroscopy–concentration curves.

Due to the large amount of data concerning this phenomenon, a picture of the process of micellization and the structure of the micelles formed has slowly emerged.

When a surfactant is dissolved in water, the hydrophobic group distorts the structure of water and therefore increases the free energy of the system. In order to minimize the free energy of the all system, surfactants concentrate at the surface by orienting their hydrophobic groups away from the solvent. However, there is another way to minimize the free energy in these systems. The distortion of the solvent structure can also be decreased (and consequently the free energy of the solution reduced) by the aggregation of the surface-active molecules into clusters (micelles) in which the

hydrophobic groups are oriented towards the interior of the cluster and the hydrophilic groups are oriented towards the solvent.

Micellization is therefore a mechanism alternative to adsorption at the interfaces thanks to which hydrophobic groups move away from polar environments, thereby reducing the free energy of the system. When the hydrophobic group causes minor distortion of the structure of the solvent (e.g., when the hydrophobic group of the surfactant is short), the chance of having micellization is little.

Though removing the hydrophobic group from water may result in a decrease in the free energy of the system, the surfactant molecule may also experience some loss of freedom as a result of confinement within the micelle and, in the case of ionic surfactants, the onset of electrostatic repulsion between similarly charged surfactant molecules in the micelle. These forces increase the free energy of the system and thus hamper micelles formation. Therefore, the micellization process is the result of the balance between the factors promoting micellization and those opposing it.

According to the above, a better understanding of the process of micellization is necessary for a rational explanation of the effects of structural and environmental factors on the value of the CMC. To this end the determination of thermodynamic parameters of micellization ΔG_{mic}, ΔH_{mic}, and ΔS_{mic} has played an important role.

For non-ionic surfactants, the standard free energy of micellization is given by

$$\Delta G_{mic} = RT ln X_{CMC} \quad (1)$$

Where X_{CMC} is the critical micelle concentration expressed as mole fraction, T is the absolute temperature and R is the gas constant.

When the CMC value is 10^{-2} M or less, equation (1) can be approximated without significant error by

$$\Delta G_{mic} = 2.3RTlog\left(\frac{CMC}{\omega}\right) \quad (2)$$

where the CMC is expressed in molar units and ω is the number of moles of water per liter of water at the temperature T.

For ionic surfactants, a standard free energy change of micellization, ΔG_{mic}, can be calculated by taking into account also the degree of binding of the counterion to the micelle.

The data available (mainly for aqueous systems) indicate that the negative values of ΔG_{mic} result from the large positive values of ΔS_{mic}. ΔH_{mic} is often positive and, even when negative, is much smaller than the value of $T\Delta S_{mic}$.

Therefore, the micellization process is governed primarily by the entropy gain associated with it, thus the driving force for the process is the tendency of the hydrophobic group of the surfactant to move from the solvent environment to the interior of the micelle.

The large entropy increase during the micellization process in aqueous medium has been explained in two ways: *i.* a change in the structure of water molecules surrounding the hydrocarbon chains in aqueous medium, when the hydrocarbon chains are removed from the aqueous medium to the interior of the micelle; *ii.* increased freedom of the hydrophobic chain in the non-polar interior of the micelle compared to the aqueous environment. Any structural or environmental factors that may affect water-hydrophobic group interactions or interactions among hydrophobic groups in the interior of the micelle will therefore affect ΔG_{mic} and consequently the value of CMC. [64-69]

ITC: a valuable tool for the study of micellization processes

Calorimetry has evolved significantly since its early beginning and thanks to the most recent technological evolution has become a unique technique to monitor chemical or biological events, due to both its high sensitivity and to the fact that almost all processes are associated with adsorption (or release) of heat.

One of the most common calorimetric techniques is called titration calorimetry, in which the system composition is varied by addition of one or more components followed by measurement of heat exchange. These experiments are typically run under isothermal conditions hence it is most commonly referred to as Isothermal Titration Calorimetry (ITC).

Titration calorimetry is becoming one of the most used techniques to investigate surfactant association in solution.

The main advantage of ITC is providing direct access to all the information necessary to determine with a single experiment the most important thermodynamic functions associated with micellization, namely the variations in Gibbs energy (ΔG_{mic}), enthalpy (ΔH_{mic}) and, hence, the changes in entropy (ΔS_{mic}). Furthermore, combination of ITC experiments at varying temperatures allows the determination of changes in heat capacity, which may be an useful parameter for the evaluation of hydrophobic contributions. Modern ITC has a sensitivity low enough to allow for the monitoring of most processes in the micromolar concentration range. In addition, it has been widely demonstrated, that the van't Hoff approach is not capable of accounting for parallel changes in the surfactant aggregates with temperature and, therefore, does not provide accurate values for enthalpy and entropy changes upon micellization. Moreover, the direct determination of enthalpy yields more accurate values. In general, the enthalpy of micellization

determined via ITC have an uncertainty of less than 1%. Consequently also the derived thermodynamic parameters derived from these values are characterized by small uncertainties. In conclusion, the use of ITC may provide a full thermodynamic characterisation and a better accuracy of micellization data. [70-72]

Aim of the work

The tendency of supramolecular amphiphiles to form aggregates with different size and shape has been widely demonstrated. [52-63] However, an in-depth investigation of the host-guest complex formation represents a crucial step for the understanding of the aggregation process, providing essential information about the supramphiphile itself, that is the monomeric unit of the aggregates. Furthermore, the thermodynamic characterization of the self-aggregation process allows to develop new and more efficient supramphiphiles and may highlight the crucial role played by the calixarene scaffold in the formation of more effective self-aggregating systems. Indeed, literature data have shown that supramolecular amphiphiles self-aggregate at a much lower concentration than conventional surfactants, and this has made them more efficient than the free uncomplexed surfactants.

The aggregation of supramolecular amphiphiles based on water soluble *p*-sulfonatocalix[n]arenes and cationic organic guests has attracted the attention of some research groups during the last few years. Despite the widespread interest in these systems, a quantitative characterization of the interactions, the binding features of the host-guest systems and the micellization processes occurring in neutral (buffered) aqueous solution have not been reported yet.

Aim of the initial step of the present work is the determination of the binding constants, the thermodynamic parameters and the forces driving the formation of supramphiphiles in buffered aqueous solution (pH 7.2); this would help finding out the best host-guest systems and the conditions which may be employed for the formation of efficient micellar aggregates (**Scheme 1**) .
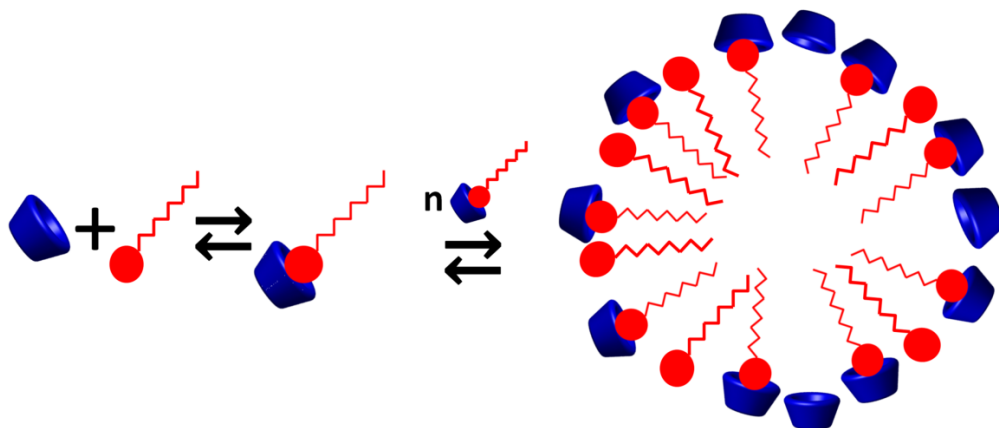
Scheme 1. Sketch of the equilibrium studied

In this context, 1:1 host–guest complexes made of a *p*-sulfonatocalix[4]arene and positively charged surfactants having either aliphatic or aromatic head and alkyl tails of increasing length have been studied by ITC experiments in neutral aqueous solution (**Scheme 2**). ITC experiments also allowed for the determination of CMC and ΔH^0_{mic} of the micelles formed by the different supramolecular surfactants and these have highlighted the crucial role played by the calixarene scaffold in the formation of efficient self-aggregating systems. The significant influence of both the pH and the ionic medium on the parameters determined will be also critically discussed.
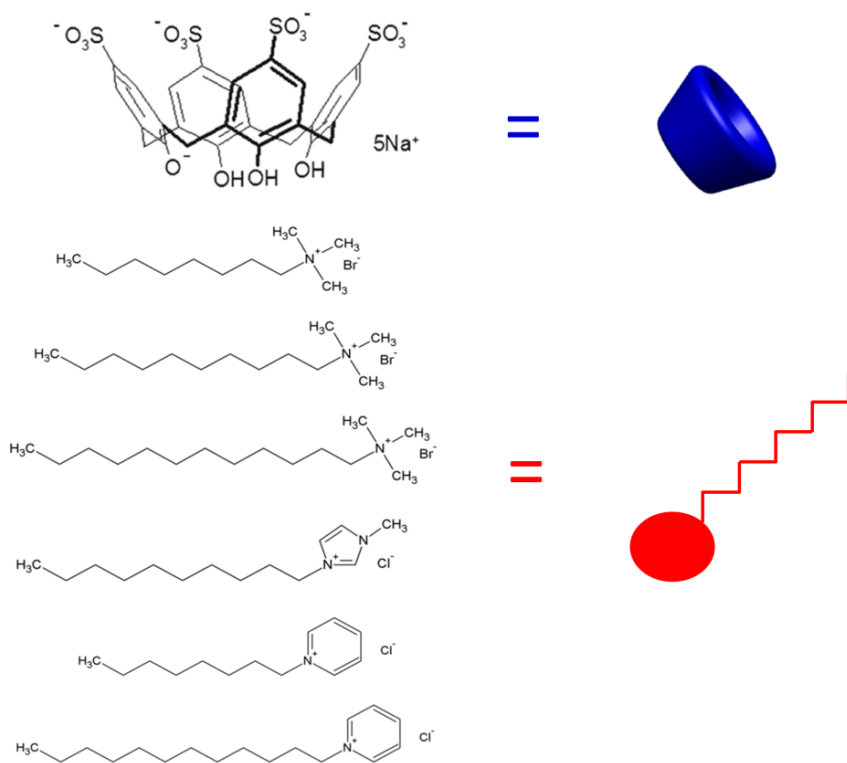
Scheme 2. Host and guests investigated.

Preliminary study and role of the buffer on micelle formation

A preliminary ITC study was carried out using common cationic and anionic surfactants to find the optimal experimental conditions for the accurate determination of the thermodynamic parameters associated to micelle formation in aqueous solution (**Figure A1-A5**). The CMC and ΔH_{mic} values determined at 25 °C in plain water for surfactants studied are reported in **Table A1**. The difference between the values determined in the present investigation and literature (when available)[73-76] values is always smaller than 5%, which shows that both experimental conditions for the study of micelle formation in solution and data analysis for parameters determination have been appropriately set up.

However, biologically relevant molecules are usually studied in buffered aqueous solution, rather than in plain water. It has been widely demonstrated that the presence of an electrolyte such as a buffer causes a variation of the CMC values. This effect is more pronounced for ionic surfactants, due to the reduction of charge repulsions between the surfactants polar heads caused by the oppositely charged ions from the buffering salt.

When micellization processes are investigated by ITC, ionic strength causes dramatic changes of the shape and the magnitude of the calorimetric curves and thus very often CMC and ΔH^0 values can be hardly determined for common cationic surfactants in presence of a buffering salt. [77] In some cases the ITC curve does not even display a "suitable" pattern (or break) for the CMC and ΔH_{mic} values to be accurately determined (**Figure A6**).

By contrast, a significant change of the shape of the calorimetric curve is obtained in the presence of a buffer for the anionic surfactants, which allows for the determination of the relevant thermodynamic parameters. In this case

a dramatic decrease of the CMC value has been observed for anionic surfactants.[78] (**Figure A7**).

Thus, a systematic study of the behaviour of the anionic surfactant sodium dodecylbenzensulphonate, (**SDBS**) in the presence of the most common buffers (phosphate or MOPS) or electrolytes (NaCl), that is in the presence of a ionic background was carried out in order to evaluate the effect of the ionic strength on the calorimetric curves and, ultimately, on the micellization process (**Figure A8-A10**).

The values obtained (**Table A2**) show that in all cases the presence of the electrolyte causes a considerable decrease of CMC compared to plain water, where the CMC value is 0.0152 M. The values of both the CMC and the micellization enthalpy do not differ significantly from those determined in pure water.

Remarkably, both values are not affected by the specific ionic medium employed as much as by the ionic strength of the solution.

Host-guest complex formation

The preliminary studies reported above show that the ionic medium may affect significantly the shape of the calorimetric curve for cationic surfactants to such an extent as to render impossible to determine the thermodynamic parameters in some cases. On the other hand, for anionic surfactants the effect of ionic strength may be determined by using ITC.

Owing to the potential applications of supramphiphile-based aggregates in the biological field, it is essential to carry out the investigation in buffered solution in order to reproduce the physiological conditions, since the influence of buffer cannot be ignored. Furthermore, the pH control gives an idea of the species existing in a given specific condition and hence of the overall charge of calixarene scaffold.

The ability of *p*-sulfonato-calix[4]arene (**C4TS**) to complex ammonium and pyridinium guests has been widely reported.[79-81] In order to design efficient supramphiphiles formed by **C4TS** (host) and proper long-tailed molecules (guest) complexes, a calorimetric study of the binding features of different cationic surfactants (having different alkyl chain length or nature of the polar head, (**Scheme 1**) with **C4TS** was carried out in presence of phosphate buffer at pH 7.2 (**Figure A11-A15**). A typical ITC titration for the **DoPyC-C4TS** system in neutral aqueous solution (pH 7.2, phosphate buffer) at 25 °C is shown in **Figure 17**.
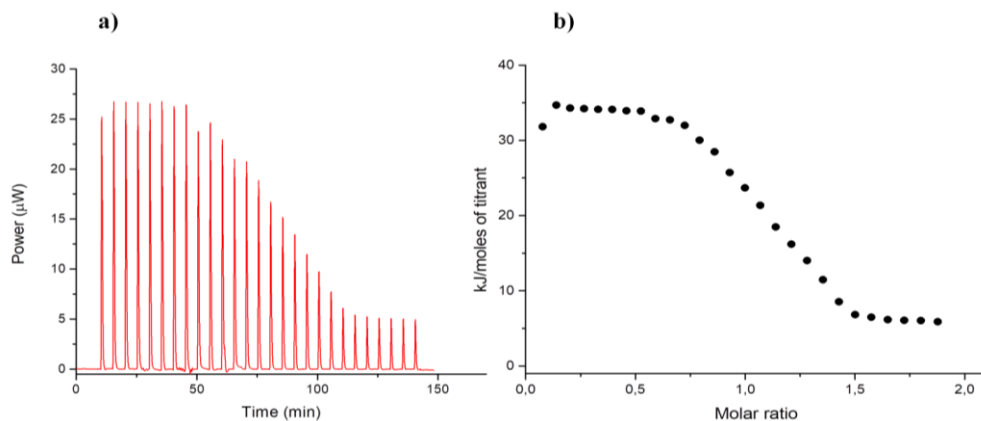
Figure 17. a) Titration of dodecylpyridinium chloride 3 mM (**DoPyC**) into **C4TS** 0.3 mM at 25 °C in buffered aqueous solution (phosphate buffer, pH 7.2); **b)** Integrated heat data.

The calorimetric data were analysed by HypCal to determine the species formed in solution, their stability constants, and the value of ΔH^0 and ΔS^0 concerning the formation of each species.[82] A typical HypCal output for the simultaneous refinement of four titration for the **DoPyC-C4TS** system is shown in **Figure 18**.
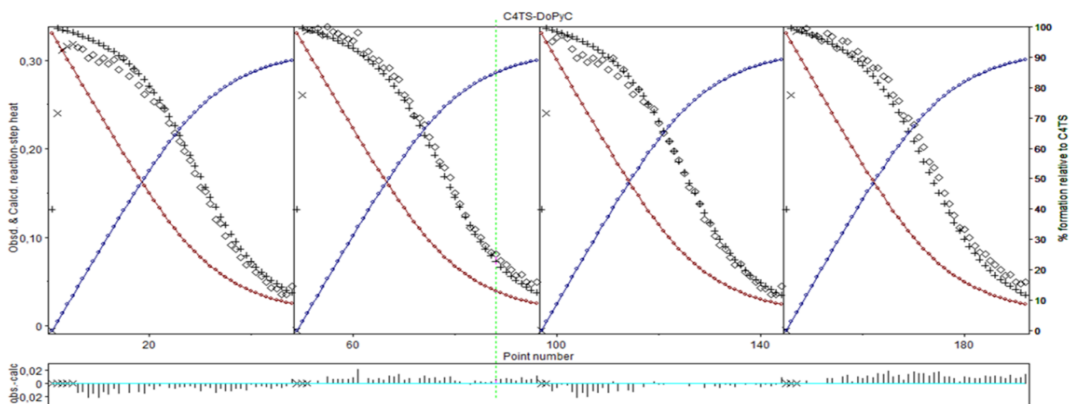
Figure 18. HypCal output for the complexation of **DoPyC** (G) with **C4TS** (H): experimental heats (diamonds); calculated heats (crosses). The species distribution diagram [free H (brown), HG (blue)] is also shown in the same windows. Residuals (observed - calculated values) are shown at the bottom of the curves. × indicates that the specific titration point has been excluded from the refinement.

The binding constants and the thermodynamic parameters for the host-guest complex formation are reported in **Table 1**.

Table 1. LogK values and thermodynamic parameters for the **C4TS**-guest complex formation at 25 °C in neutral aqueous solution (pH 7.2, phosphate buffer).

Guest	Equilibrium	logK	$\Delta H°$ (kJ mol^{-1})	$\Delta S°$ (J deg^{-1} K^{-1})
OTAB	H + G ⇆ HG	4.75 (6)*	-31.29 (1)	-14 (2)
DeTAB	H + G ⇆ HG	4.71 (8)	-30.55 (1)	-12 (2)
DTAB	H + G ⇆ HG	4.60 (2)	-33.64 (1)	-24.7 (5)
OPyC	H + G ⇆ HG	4.60 (5)	-28.78 (1)	-8 (1)
DoPyC	H + G ⇆ HG	4.70 (5)	-36.39 (1)	-32 (2)
D3MIC	H + G ⇆ HG	4.57 (8)	-28.47 (1)	-7 (2)

*σ in parenthesis

The results suggest that stable host–guest complexes are formed with all guests. The stability of the host-guest complexes is not affected by either the length of the alkyl chain or the nature of the polar head of the surfactant. Although several conditions and concentrations were tested, the titration of **CTAB** or **CetPyr** into **C4TS** never provided calorimetric curves that could be satisfactorily fit; the very long and flexible alkyl chain (16 C) of both these surfactants somehow hampers the formation of the host-guest complex due to possible tail entanglement. The reason of this is not clear at the moment and deserves further investigations.
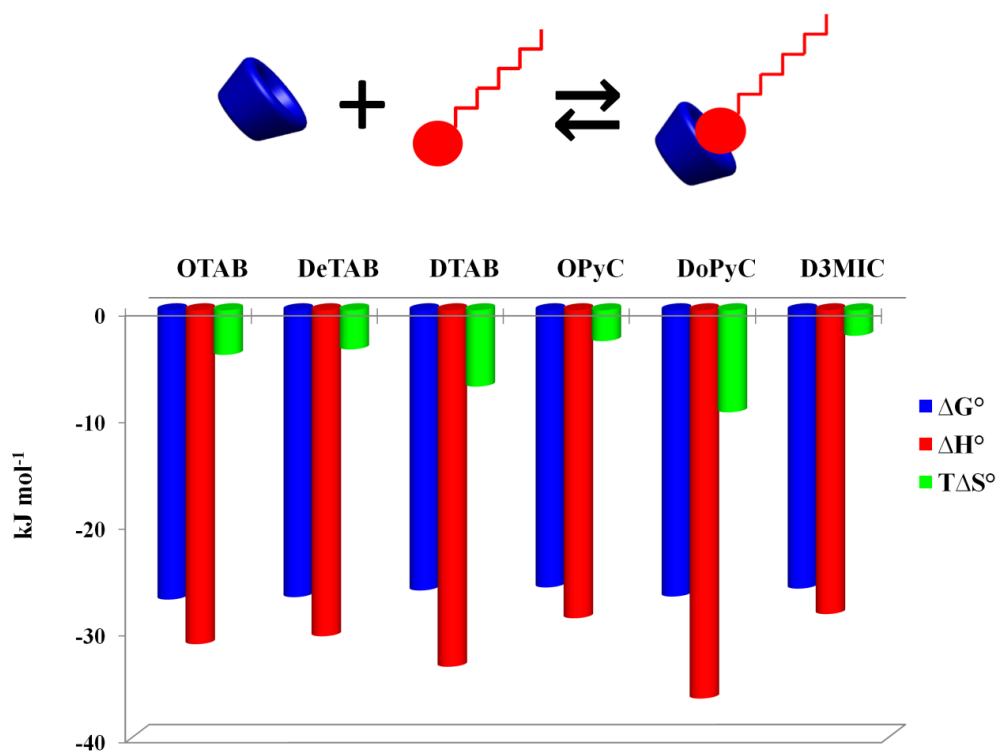
Figure 19. Thermodynamic parameters for the formation of HG complexes at 25 °C in neutral aqueous solution

In general terms, the driving forces for the complexation process consist of both specific interactions between guest and host functional groups, non-specific weak interactions as well as desolvation of host and guest that must occur upon guest inclusion. These factors have different and often opposing enthalpic and entropic contributions and thus splitting the standard Gibbs energy term into the $\Delta H°$ and $T\Delta S°$ components may help understanding relevant details of the binding process that are not expressed in the $\Delta G°$ term. Coulombic forces, hydrogen bonds, CH-π, π-stacking, and van der Waals interactions mainly contribute to the enthalpy changes, whereas

conformational and/or structural rearrangements and desolvation mainly contribute to the entropy changes.

Concerning the systems investigated, we found that the supramphiphile formation is always driven by enthalpy (**Figure 19**). Electrostatic interactions between the positive charge of the guests and the sulfonato groups at the upper rim of the host, along with CH–π and/or π–π interactions with the **C4TS** cavity, drive the host–guest complex formation. These enthalpically favourable contributions override the energy cost needed for the desolvation of the interacting reagents. The unfavourable entropic contribution is the result of the balance between host and guest desolvation ($\Delta S^0 > 0$) and the loss of degrees of freedom due to HG complex formation ($\Delta S^0 < 0$), the latter being the prevaling contribution.

The large stability of these host–guest complexes makes them promising candidates as supramolecular amphiphiles. Indeed, this class of surfactants can be easily prepared by just mixing the host and the proper long-tailed guest at a 1:1 ratio in order to have the expected supramphiphile complex as (basically) the only reaction product. More precisely, a small excess of **C4TS** (5% in excess of surfactant concentration) was used in order to avoid the presence of free surfactant. This allows for a simple and accurate study of the micellization processes without dealing with free cationic surfactants, that might themselves aggregate. The distribution diagram under these conditions (**Figure 20)** shows that the amount of free guest is negligible over a wide interval of guest concentration.
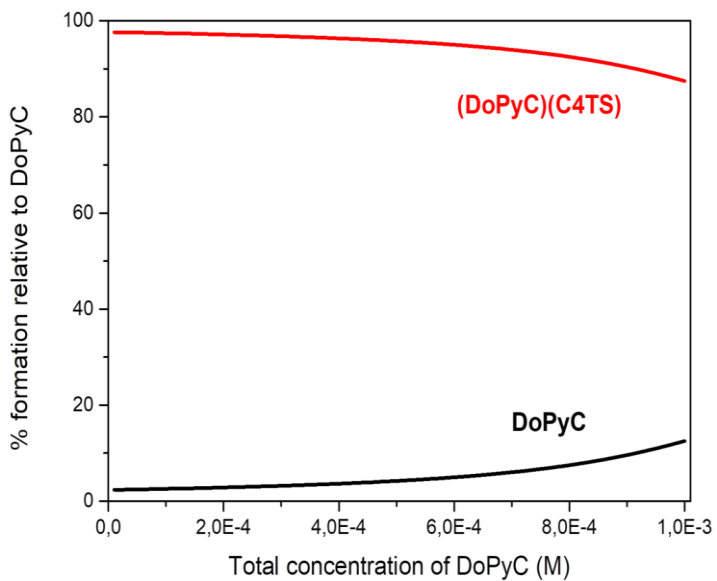
Figure 20. Species distribution for supramphiphile (**DoPyC**)(**C4TS**) computed by using the data shown in **Table 1.**

Supramphiphiles self-aggregation

The calorimetric study of the micelle formation process using supramphiphiles formed by **C4TS** and cationic surfactants was carried out at 25 °C at pH 7.2 (phosphate buffer) (**Figure A16-A20**). A typical thermogram for the micellization process of the (**DoPyC)(C4TS**) supramphiphile is shown in **Figure 21c**. Remarkably, the thermograms of the sole guest (**Figure 21a**) or host (**Figure 21b**) indicate that no micelles are formed.
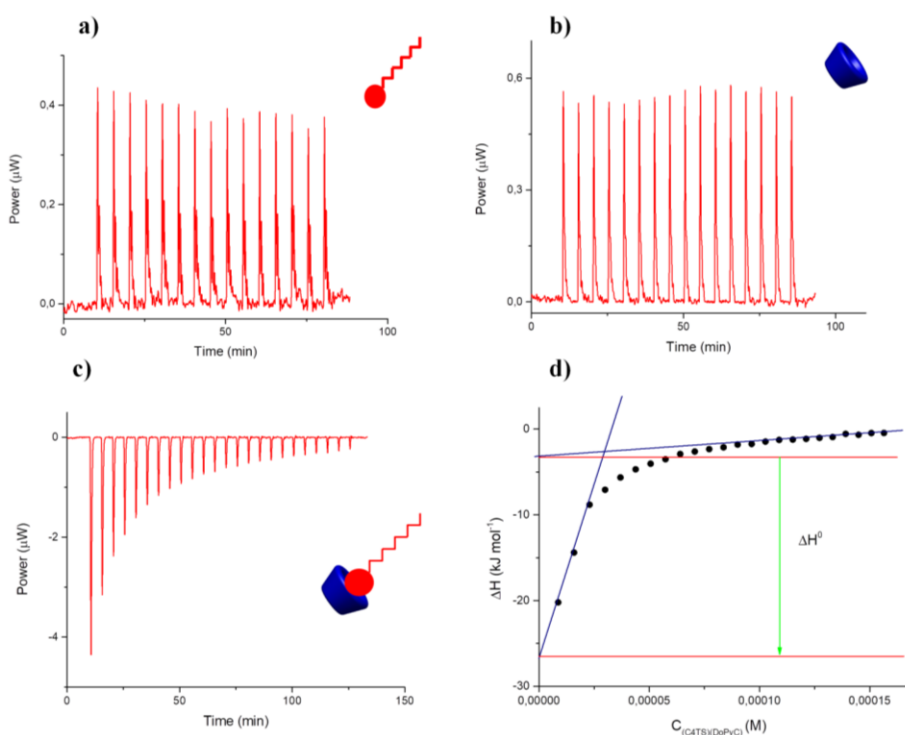
Figure 21.a) Titration of **DoPyC** (1 mM) into phosphate buffer (pH 7.2); **b)** Titration of **C4TS** (1 mM) into phosphate buffer (pH 7.2) **c)** Typical curve obtained from ITC experiments carried out with a (**C4TS**)(**DoPyC**) supramphiphile 1 mM solution at 25 °C and pH 7.2 (phosphate buffer); **d)** integrated heat data.

Table 2 shows the CMC and ΔH^0_{mic} values determined as reported above at 25 °C for six different supramphiphiles. The table also shows the values of ΔG^0_{mic} and ΔS^0_{mic} calculated through the pseudophase separation model as well as the CMC values of the free (uncomplexed) cationic surfactants in plain water for comparison.

Table 2. CMC values and thermodynamic parameters for the micelle formation at 25 °C in neutral aqueous solution (pH 7.2, phosphate buffer).

Supramphiphile	CMC* (mM) *free surfactant in plain water	CMC (mM)	$\Delta G^0_{mic.}$ (kJ mol^{-1})	$\Delta H^0_{mic.}$ (kJ mol^{-1})	$\Delta S^0_{mic.}$ (J mol^{-1} K^{-1})
(OTAB)(C4TS)	300[83]	0.076 (2)*	-66.9 (1)	-14.4 (1)	176 (4)
(DeTAB)(C4TS)	94.7[84]	0.058 (2)	-68.2 (1)	-19.8 (1)	162 (3)
(DTAB)(C4TS)	15.22 (3)	0.048 (1)	-69.2 (1)	-26.5 (1)	143 (5)
(OPyC)(C4TS)	220[85]	0.091 (2)	-66.0 (1)	-14.9 (1)	171 (4)
(DoPyC)(C4TS)	14.62 (5)	0.069 (1)	-67.4 (1)	-23.0 (1)	148 (5)
(D3MIC)(C4TS)	41[86]	0.051 (1)	-68.8 (1)	-17.9 (1)	170 (3)

pH 7.2, phosphate buffer

*σ in parenthesis

In all cases, the host–guest complexes (supramphiphiles) formed by **C4TS** and cationic surfactants self-aggregate at a much lower concentration than

the free uncomplexed surfactant. CMC values decrease by up to more than three orders of magnitude (4000 fold (**OTAB**)) in the presence of the calixarene receptor, thus indicating that these supramphiphiles are able to form very effective self-aggregating systems in buffered solutions. Supramolecular micellar-like aggregates are characterized by CMC values much smaller than those observed in plain water; this indicates that the cavity effectively shields the polar head of the surfactant. The CMC of both alkylammonium or pyridinium derivatives systems decreases as the tail length of the supramphiphile increases. However, the trend observed for the supramphiphiles of comparable length parallels that observed for the free surfactant in plain water. Finally, it is important to underline that the calixarene reduces the CMC values for each surfactant, levelling them at the same order of magnitude despite the corresponding free surfactants have CMC values that differ by orders of magnitude. This further emphasizes the crucial role of the calixarene in the micellization process.

Negative values of ΔH^0_{mic} and ΔG^0_{mic} and positive values of ΔS^0_{mic} are found for all supramphiphiles. The major driving force for surfactant micelle formation can figured out by comparing ΔS^0_{mic} and ΔH^0_{mic} micellization values. In most cases, hydrophobic interactions are the most prominent driving forces for micelle formation. The entropy contribution usually dominates the micellization process in aqueous solutions whilst enthalpy plays a minor role (i.e. $|T\Delta S| > |\Delta H|$).

In some cases, besides hydrophobic interactions, other forces such as electrostatic attraction/repulsion may contribute to the micellization process.[87] For example, the formation of a micelle from monomeric ionic surfactants results from the balance between *i.* attractive molecular driving forces between the hydrophobic surfactant tails arising from the hydrophobic interactions, *ii.* attractive and repulsive electrostatic interactions between

their hydrophilic charged head groups, and *iii.* attractive and repulsive electrostatic interactions with and between the counterions.

The observed enthalpy and entropy values indicate that the formation of the micelles is driven primarily by the entropy gain and to a lesser extent by the enthalpic contribution (**Figure 22**). Increasingly favorable $\Delta H^0{}_{mic}$ values result from a stronger hydrophobic interactions occurring between the alkyl chains of supramphiphiles occurring among longer alkyl chains. The large positive entropy results from the exclusion of ordered water molecules from the micellar interior (desolvation) upon the formation of aggregates. Indeed, the structures of the water molecules surrounding the hydrocarbon chains of the surfactants are destroyed when the hydrocarbon chains are removed from the bulk aqueous medium to form the interior domain of the micelles.
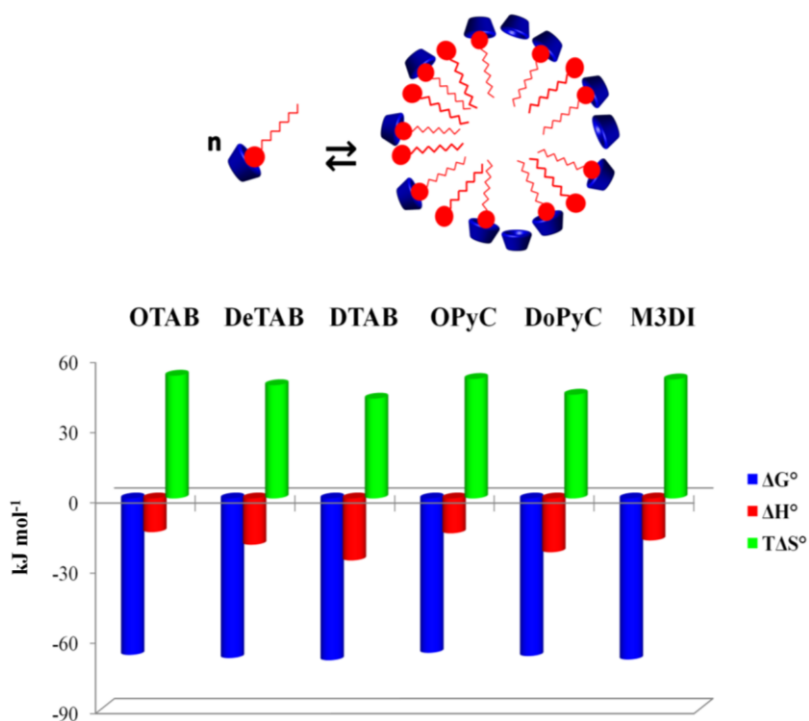
Figure 22. Thermodynamic parameters for the micellization process of different supramphiphiles at 25 °C in neutral aqueous solution.

Experimental

Materials

The host, *p*-sulfonato-calix[4]arene (**C4TS**), and the guests octyltrimethylammonium bromide (**OTAB**), decyltrimethylammonium bromide (**DeTAB**), dodecyltrimethylammonium bromide (**DTAB**), 1-decyl-3-methylimidazolium chloride (**D3MIC**), dodecylpyridinium chloride (**DoPyC**), cetylpyridinium bromide (**CetPyr**), cetyltrimethylammonium bromide (**CTAB**), sodium dodecylsulphate (**SDS**) and sodium dodecylbenzensulphonate (**SDBS**) were purchased from Sigma-Aldrich; octylpyridinium chloride (**OPyC**) was purchased from AKos GmbH.

High purity water (Millipore, Milli-Q Element A 10 ultrapure water) and A grade glassware were employed throughout.

ITC titrations

ITC titrations were carried out at 25 °C with a nano-isothermal titration calorimeter (TA Instruments) having an active cell volume of 0.988 mL and equipped with a 250 μL injection syringe. The reaction mixture in the sample cell was stirred at 250 rpm during the titration. Measurements were run in the overfilled mode which does not require any correction for liquid evaporation and the presence of the vapor phase.[88,89] The power curve was integrated by using a software (NanoAnalyze, TA Instruments) to obtain the gross heat involved in the reaction. The calorimeter was calibrated chemically by a test HCl/TRIS reaction according to the procedure previously described.[90] The instrument was also checked through an electrical calibration.

Host-guest complex formation

ITC measurements for the study of the HG (H= host, G =guest) complex formation were carried out by titrating a solution of the proper guest (3–4 mM) into a **C4TS** solution (0.2–0.4 mM). Both **C4TS** and guests were dissolved in 25 mM phosphate buffer (pH 7.2). The buffer was used to keep the host in its penta-anionic form and to minimize any contribution resulting from the interaction of either the host or the guests with the proton. Typically, 3–4 independent titrations were run for each **C4TS**-guest system in order to collect a proper number of points to obtain a satisfactory fit of the curve. The heats of dilution were determined in separate blank experiments by titrating solutions of each guest (prepared in phosphate buffer) into a solution containing phosphate buffer only (**Figure 23**).
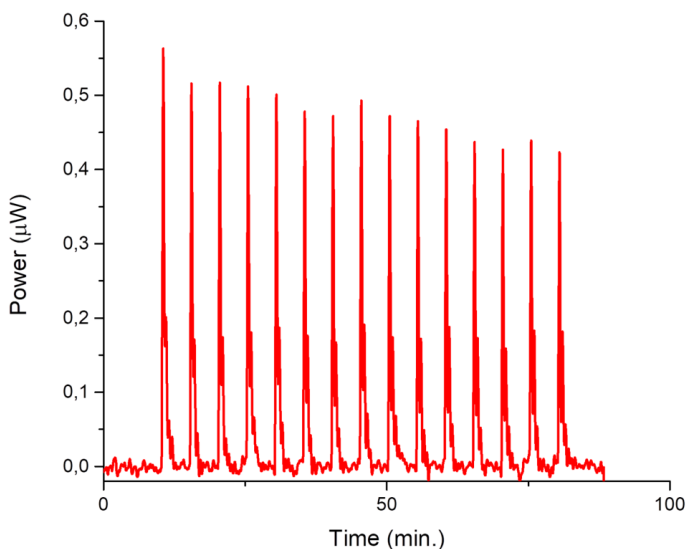
Figure 23. Typical "blank" experiment. Titration of **DoPyC** (3 mM) into phosphate buffer (pH 7.2)

Since blank titrations usually involve relatively small heats and, consequently, introduce an additional noise into the net reaction heat some blank titrations were run and then optimized to obtain the "best blank" in order to minimize the background noise (**Figure 24**). The "best blank" incremental heat corresponding to a given addition can be easily obtained from a plot of the type shown in the figure by subtracting the nth from the nth-1 point.
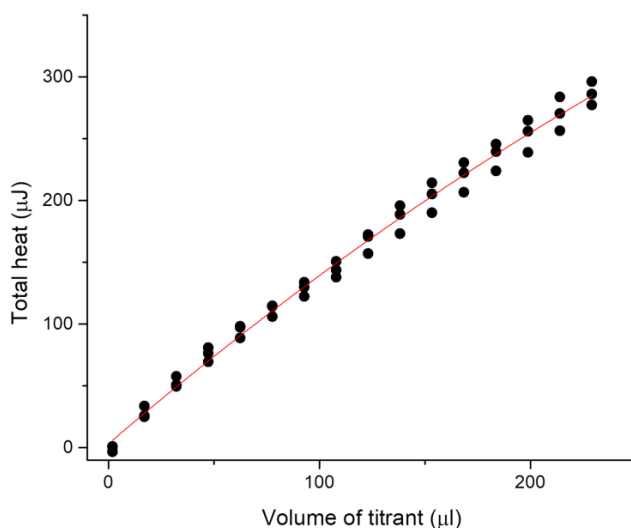
Figure 24. Optimized "blank." The *red line* represents the "best" blank heat. The blank incremental heats are obtained by subtracting the nth from the $(n-1)$th value.

The net heats of reaction, obtained by subtracting the heat evolved/absorbed in the blank experiments, were analyzed by HypCal. This software is specifically designed for the determination of equilibrium constants and formation enthalpies of complexes in solution by a non-linear least-squares minimization of the function

$$U = \Sigma(Q_{obs.} - Q_{calc.})^2 \quad (3)$$

where $Q_{obs.}$ is the observed heat for a given reaction step, corrected for the dilution (blank) effects, while $Q_{calc.}$ is calculated as

$$Q_{calc.} - \Sigma \, \delta n \Delta H^0 \quad (4)$$

where δn is the change in the number of moles of a reaction product and ΔH^0 is the molar formation enthalpy of the reaction product. The summation is carried out over all the reaction steps of the specific chemical system. The squared residuals $(Q_{obs.} - Q_{calc.})^2$ are summed over all the titration points. For each host–guest system, log$K$ values and thermodynamic parameters were obtained by analyzing the calorimetric data obtained from different titrations simultaneously.

Micelle formation

ITC is the only technique that allows to obtain two different thermodynamic parameters i.e. the critical micellar concentration (CMC) and the enthalpy of micellization (ΔH_{mic}^{0}) for the aggregation of surfactants directly from a single experiment,.[91] Typically, 3–4 independent titrations were run for each commercial surfactant or supramphiphile in order to obtain accurate values for both thermodynamic parameters. A typical micellization experiment consists of a stepwise titration of a concentrated surfactant solution into the reaction cell, containing water or the buffer solution, at a constant temperature. To ensure that the titrant (surfactant) reaches the CMC in the course of a titration, its concentration in the syringe must be appropriately chosen. However, the choice of the concentration of the micellar solution used as the titrant may be difficult when no information is available about the CMC of the surfactant. In such a case, several ITC experiments have to

be carried out by varying the concentration of the surfactant in the syringe. When experimental conditions are adequately chosen, CMC is progressively reached during the experiment and the heats recorded may allow for the direct determination of the parameters. A schematic representation of the processes occurring in the calorimetric vessel during the titration of a concentrated solution of surfactant is schematically depicted in **Figure 25**.
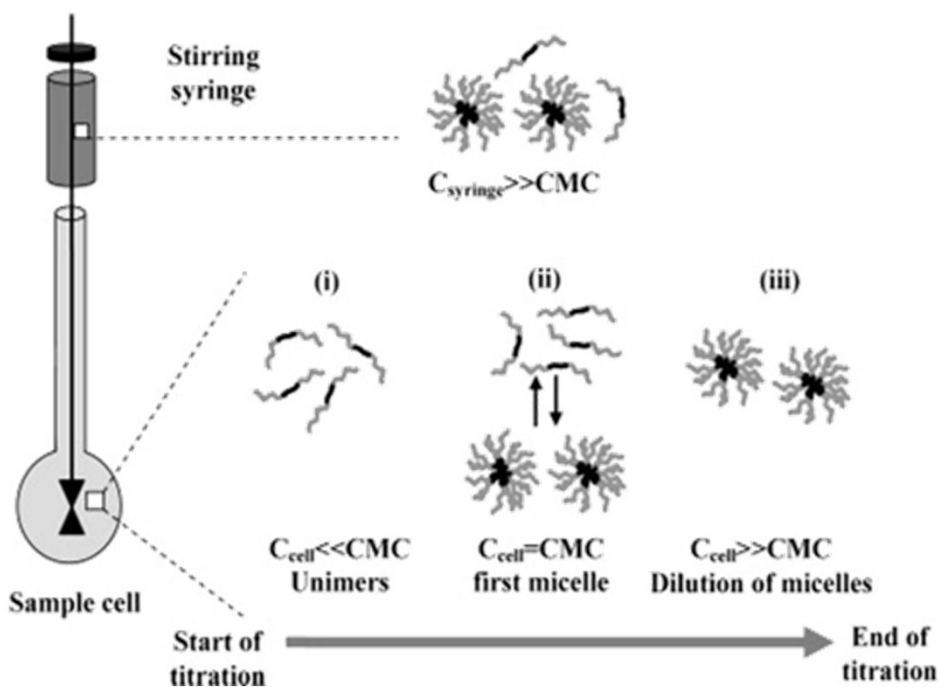
Figure 25. Schematic representation of the events occurring during the ITC experiment. $\Delta H_{(i)}$: enthalpy of unimer dilution, $\Delta H_{(ii)}$ (or ΔH_{mic}): enthalpy of micellization, $\Delta H_{(iii)}$: e enthalpy of micelle dilution (adapted from Bouchemal et al.)[92]

Thermograms can exhibit a variety of shapes. For sigmoidal curves (**Figure 26**) linear fits of the data sets in the lower and upper concentration

domains are performed as shown in **Figure 27 a)**. The difference between the two intercepts of the two tangent lines yields the value of the enthalpy of micellization. The CMC is determined by taking the inflection point of a plot of the enthalpy of dilution versus the total surfactant concentration curve. In more precise mathematical terms, the CMC is defined as the concentration at which the first derivative of the curve displays a minimum (or a maximum), as shown in **Figure 27 b)**.
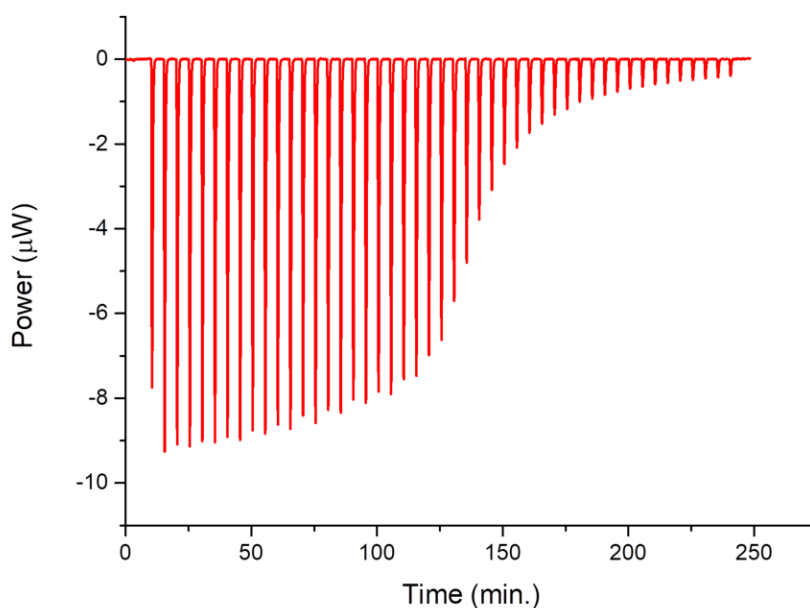
Figure 26. Titration of cetylpyridinium bromide (**CetPyr**, 5 mM) at 25 °C in pure water
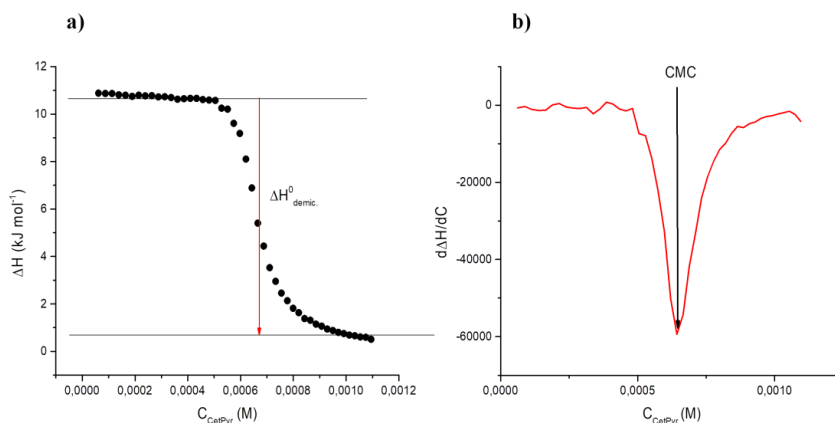
Figure 27. a) Enthalpy curve for the titration of cetylpyridinium bromide (**CetPyr**) into plain water at 25 °C as a function of the total surfactant concentration; **b)** first derivative of the enthalpy curve.

CMC values may also be determined by plotting the cumulative (or total) enthalpy of dilution values vs. the total surfactant concentration; the plot shows a slope change at a concentration which corresponds to the CMC at that specific temperature. This value is correctly determined by selecting suitable data below and above the inflection of the curve, fitting these data to straight lines by a linear regression and taking their intersection point (**Figure 28**).[93]
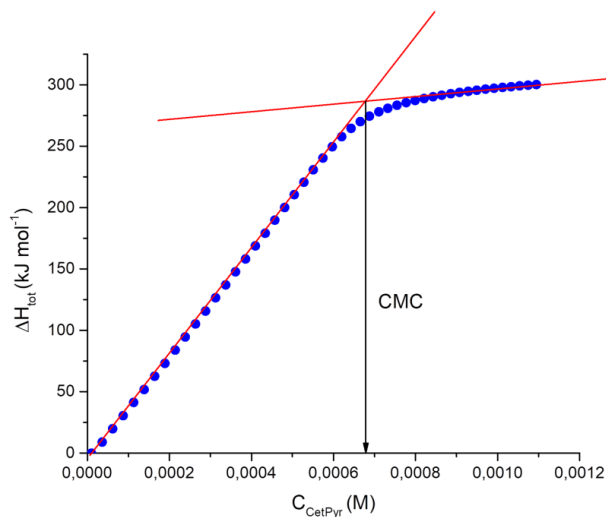
Figure 28. Cumulative enthalpy of dilution of Cetylpyridinium bromide in pure water at 25 °C against surfactant concentration. The intersection of the two tangents may be identified as the CMC.

When the curve does not show a clear sigmoidal trend (**Figure 29a**), the analysis may be performed as suggested by different authors.[94,95] In such cases a linear fit of the data sets in the lower and upper concentration domain is performed as shown in **Figure 29b**. The intercepts of the two straight lines are then determined and the value of the enthalpy of micellization is obtained by taking the difference between the two intercepts.
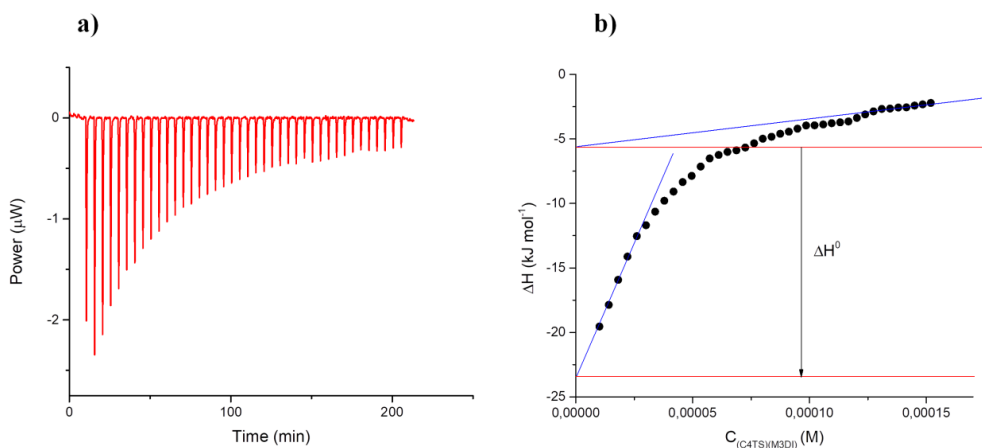
Figure 29. a) Typical non sigmoidal curve obtained from ITC experiments carried out with a supramphiphile solution at 25 °C and pH 7.2 (phosphate buffer); **b)** integrated heat data.

The change of the Gibbs free energy ΔG_{mic}^{0} of a micellization process can be obtained by using different models. In the pseudophase separation model, the micelle part is treated as a separate phase and the value of Gibbs free energy is calculated from the CMC values according to the following equation:[96]

$$\Delta G_{mic}^{0} = 2RTln\chi_{CMC} \quad (5)$$

where χ_{CMC} is the critical micellar concentration expressed as mole fraction, T is the absolute temperature and R is the gas constant.

ΔS_{mic}^{0} can be easily obtained by the equation:

$$\Delta S_{mic} = (\Delta H_{mic} - \Delta G_{mic})/T \quad (6)$$

CHAPTER 3 - INTRINSIC CATANIONIC MIXTURES

Mixtures of anionic and cationic surfactants present some peculiar properties: they have much lower critical aggregation concentrations (cac) than single pure surfactants;[97] they are usually more surface active than both pure surfactants; and they can yield microstructures (such as vesicles and rod-like micelles) not formed by the corresponding pure components. [98,99] They can also decrease the concentration at which liquid crystalline phases form.[100] The above properties can be exploited in many ways. Mixtures with lower cac values may be useful in detergency applications; also, vesicles could eventually be used for controlled drug release, microreactors and model membranes.[101]

For anionic/cationic surfactant mixtures, one can assume that there is a formation of a pseudo double-tailed zwitterionic surfactant, resulting in a decrease in the effective size of the head group and an increase in the volume of the hydrophobic portion as schematically shown in **Figure 30**.
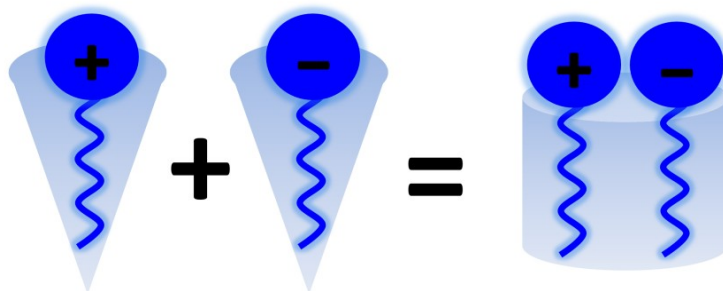
Figure 30. Schematic representation of ion pair formation in catanionic mixtures.

The formation of ion pairs has pronounced influence on the adsorption properties and on the self-assembly of catanionic mixtures. Unlike the solution of individual monomeric surfactants, in catanionic mixtures, aggregates with lower curvature, such as open and closed bilayers (vesicles), are spontaneously formed even at the low surfactant concentrations.[102]

It was found that the extent of the vesicular phase depends on the surfactant structure: when both surfactants are linear and have symmetric in chain length, the precipitate phase dominates the phase behaviour; in such cases, micelles and vesicles are observed only at higher concentrations or for a certain charge asymmetry. Vesicular phases are stable when the surfactants are branched and/or contain a bulky substituent in the tail group. As vesicular phases all present mixed surfactant bilayers, a question that arises is why mixed surfactants form bilayers, when pure surfactants form only micelles, multilayers or exist as monomers in solution.

Spontaneous formation of stable vesicles in these systems can be explained by using the packing parameter (P), which depends on three nominal geometric parameters of surfactant molecules:

$$P = \frac{v_{hc}}{a_0 l_{hc}} \quad (7)$$

Where a_0 is the surface area per head group and v_{hc} and l_{hc} are the volume and fully extended length of the hydrophobic chain of the surfactant, respectively.

The molecular shape and respective P will determine the type of aggregate that is formed:

- $P = 0.33$ → spherical micelles;
- $P \approx 0.33–0.5$ → cylindrical micelles;
- $P \approx 0.5–1$ → bilayer disks and vesicles;
- $P > 1$ → reverse structures.

Considering the geometric constraints, for a given hydrophobic tail size, the preferred structure of the aggregates strongly depends on the effective head group area. In general, the a_0 value depends on two opposite forces: *i.* attractive hydrophobic interactions between hydrocarbon chains at the hydrocarbon-water interface and *ii.* repulsive electrostatic and/or steric interactions. In the case of catanionic ion pairs, the effective head group area decreases, compared to the value of each surfactant, while the volume of the hydrophobic chain increases. As a result, the value of packing parameter is close to 1, that promotes structures with low curvature like vesicles and flexible bilayers.[103]

As the molar mixing ratio of the two surfactants or the total surfactant concentration is varied, different phase transitions involving vesicles are found: micelle-to-vesicle, vesicle-to-lamellar and vesicle-to-solid phase transitions. At the highest excess of the mixture components, mixed micelles of various sizes and shapes can be found, including globular, elongated (worm-like) and branched ones. The size and shape of mixed micelles depend on bulk composition and total surfactant concentration as well as geometry of the surfactants, temperature, salt content, etc.

Supramolecular surfactant mixtures

Since supramolecular amphiphiles are formed by non-covalent interactions between two components, the relative amount of both can be modulated in order to generate a mixed system between supramolecular complex and free components. Two interesting examples are reported in the literature about the formation of mixtures with this approach.

Basilio *et al.* have reported about the formation of mixed micelles composed of dodecyltrimethylammonium bromide (DTAB) and a hexamethylated p-sulfonatocalix[6]arene (SC6HM).

Several qualitative conclusions were drawn on the basis of this study (**Figure 31**).

It was found that above the CAC of this system, the addition of surfactant to the solution leads to the formation of mixed micellar aggregates, and as long as any fraction of calixarene remains free (or as a 1:1 host–guest complex), the further addition of DTAB mainly results in an increase in the concentration of micellized surfactant.

Once all the monomeric calixarene has been consumed, the increase in DTAB concentration causes two main effects: *i.* a small fraction of added DTAB binds to the anionic micelles and this changes the micellar compositions; *ii.* in this concentration range, the vast majority of the added DTAB remains free in solution.

As more surfactant is added, the concentration of free surfactant increases until it equals the CMC of pure DTAB. Above this concentration, pure micelles start to form independently and react rapidly with the mixed micelles with high calixarene content already formed to give mixed micelles with low calixarene content. Finally, when the concentration of DTAB is in great excess amount (and above the CMC), the mixed micelles have such a

low content of SC6HM that their properties resemble those of micelles made from pure DTAB.
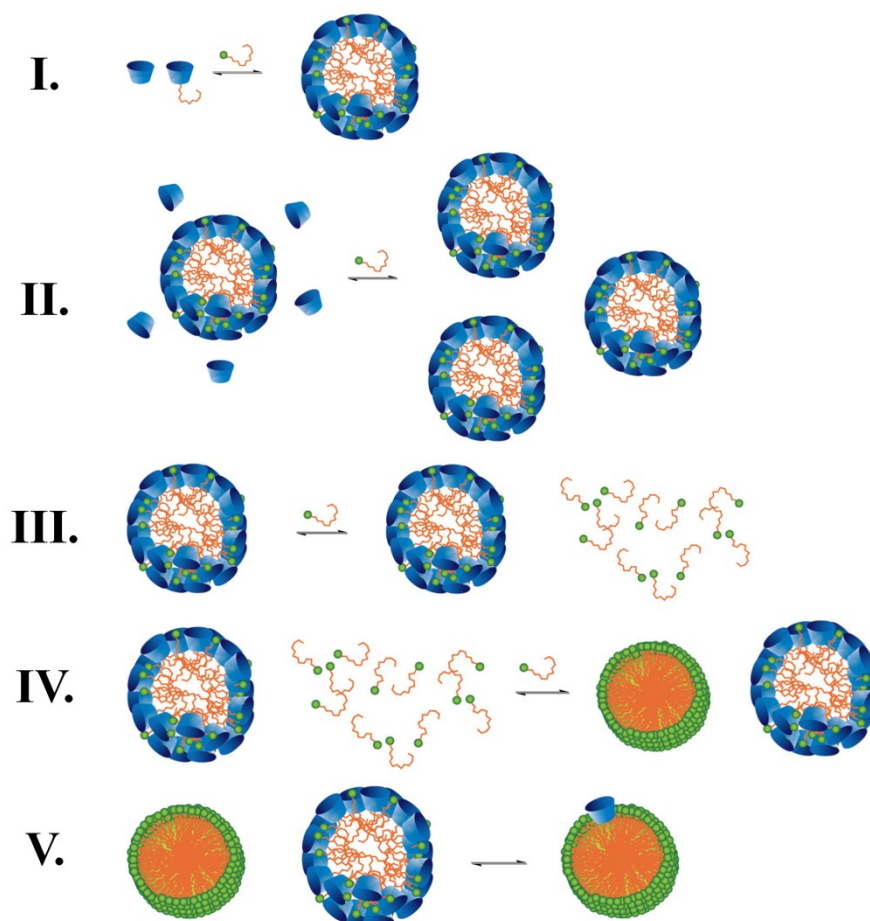
Figure 31. Schematic representation of the evolution of aggregates with the surfactant concentration in SC6HM–DTAB mixed systems: **I.** SC6HM induces the formation of mixed micellar aggregates; **II.** The addition of DTAB to the solution leads to an increase in the concentration of micelles; **III.** the addition of further DTAB results in an increase in the concentration of free surfactant monomers; **IV.** When the concentration of free monomers reaches the CMC of pure surfactant, they independently aggregate to form pure micelles; **V.** The pure and mixed micelles react rapidly to redistribute the SC6HM molecules.[104]

The authors have observed that this aggregation behaviour has many features that are similar to those of more complex systems that involve surfactants in the presence of oppositely charged polyelectrolytes. In this way, calixarenes can serve as simple models to mimic polyelectrolytes and to gain insight into the complex behaviour displayed by these macromolecules.

Costa *et al.* have explored the interactions and morphologies present in mixtures of *p*-sulfonatocalix[4]arene and a cationic serine-based surfactant, resorting to different techniques (**Figure 32**). Complexation of the amino acid-based surfactant by the calixarene leads initially to mixed micelle formation and a significant lowering of the critical micelle concentration with respect to the neat surfactant even for very low content of C4TS. Interestingly, as the C4TS fraction in the system is gradually increased, highly flexible tubular structures and vesicles are assembled. The observed self-assembly was rationalized in terms of electrostatic complexation between the two co-solutes and the preferred packing of the supramolecular complexes formed.
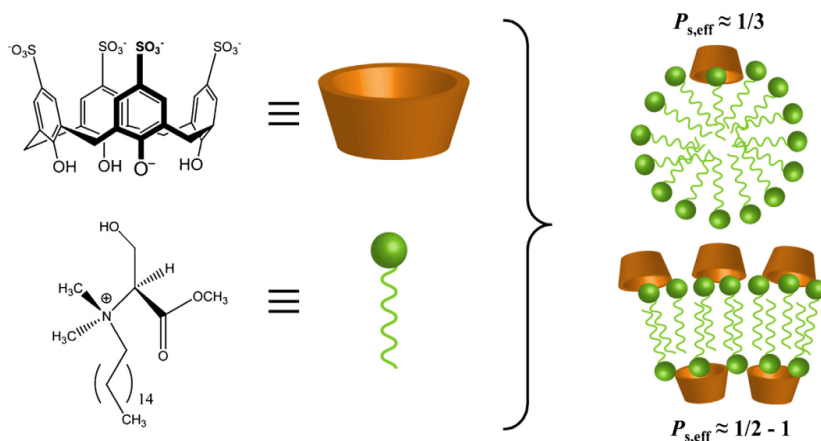
Figure 32. Schematic representation of the aggregation of system formed by *p*-sulfonatocalixarene and serine-based cationic surfactant at low and high calixarene content.[105]

The data obtained have allowed the authors to suggest a gradual structural sequence (micelles→tubules→vesicles), with increasing calixarene content. However this view needs further microstructure characterization.

Aim of the work

Complex species, binding constants and forces driving the formation of supramphiphiles made of a *p*-sulfonatocalix[4]arene (**C4TS**) and positively charged long-tailed guests in neutral (buffered) aqueous solution were investigated in order to find out the best systems and conditions for the assembly of efficient micellar-like aggregates. The aggregation features of the most promising host–guest complexes have been also studied by ITC in neutral aqueous solution. CMC and ΔH_{mic} values of the micellar-like aggregates formed by different supramolecular surfactants highlighted the crucial role played by the calixarene scaffold in the formation of efficient self-aggregating systems. It was suggested that the complexation of the cationic surfactant with **C4TS** yields a species that induces aggregation at lower concentrations than that of free surfactant.

Motivated by these observations, I studied the mixed systems formed by the calixarene **C4TS** with the cationic surfactants dodecyltrimethylammonium bromide (**DTAB**) and dodecylpyridinium chloride (**DoPyC**) (**Scheme 3**). The compounds have been selected in order to understand the effect of the nature of the head group of the cationic surfactant, since no substantial differences have been observed for different alkyl chain lengths in the aggregation features in line with literature values reported for comparable systems.[55,56]

Namely, the cationic surfactants, **DTAB** or **DoPyC**, in combination with the anionic calixarene, **C4TS,** were studied varying the complexation ratio of surfactant for both systems. Indeed, in this way the percentage of the two component can be modulated just by controlling the amount of calixarene (**C4TS**).

This is an interesting variation as by doing so we deal with free cationic surfactants combined with the anionic supramolecular surfactants, i. e. an intrinsic catanionic surfactant mixture.

After the phase behaviour investigation, these systems have been studied by surface tension measurements in order to determine the variation of the CAC value as a function of the amount of the **C4TS** and also to evaluate the synergistic behaviour.
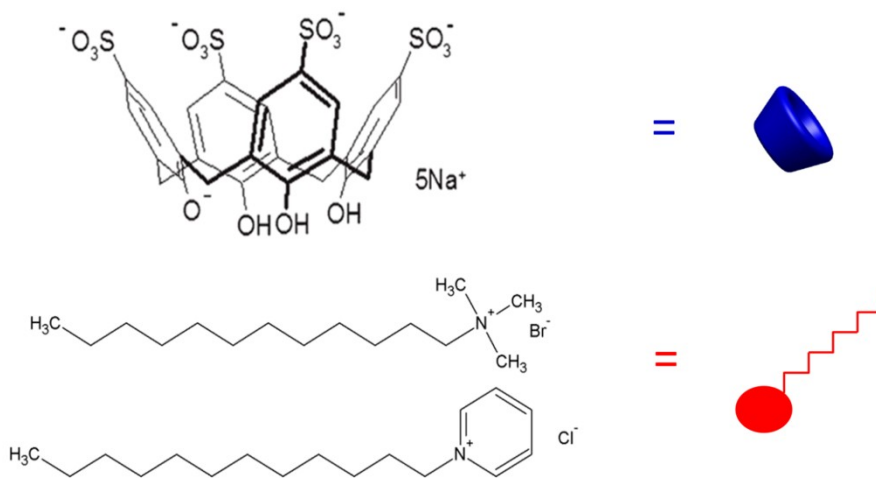
Scheme 3. Host and guests investigated

Composition of the mixtures

Since the systems investigated are formed by an anionic complexing agent (**C4TS)** that behaves as a host and a cationic surfactant (**DTAB** or **DoPyC)** that acts as a guest, when we mix these two reagents we may consider the amount of each species at every composition. The knowledge of the binding constant values allows to well establish the appropriate conditions. Indeed, by using the binding constant values, it is possible to calculate the species concentrations by solving the mass balance equations. The percentage of each component is reported in **Figure 33** and **Figure 34** at all molar fractions investigated considering a total concentration of 0.1 wt%.

The figures show that at X_{surf}<0.5 we are dealing with an increasing amount of complex and an excess of free calixarene and the amount of free surfactant is negligible because it is less than the 5% of the total amount. This indicates that we are just in the presence of an anionic surfactant, i.e. the supramolecular amphiphile. Under these conditions we can also ignore the excess of free calixarene as it is not a surface active agent.

At X_{surf}=0.5 the prominent component of the mixture is the complex. However starting from this point the amount of free surfactant is no longer negligible.

On the other hand, at X_{surf}>0.5 we are dealing with a decreasing amount of complex, an excess of free cationic surfactant and a negligible amount of free calixarene. This indicates that under these conditions we are in the presence of a catanionic mixture formed by the anionic supramphiphile and the free cationic surfactant . [free surfactant]/[complex] ratio as a function of the molar fraction values are reported for **DTAB/C4TS** and **DoPyC/C4TS** systems in **Figure 35**. The plot shows more clearly that only at $X_{surf.} \geq 0.5$ we are dealing with a real mixture, since at lower molar fraction values this
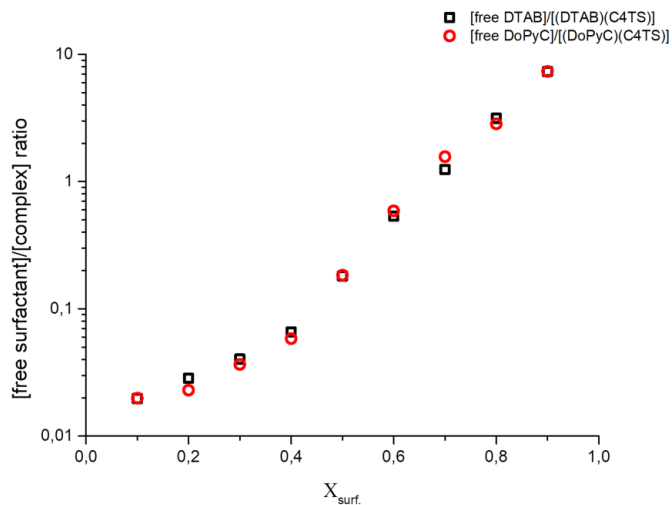
ratio is around 10^{-2} which corresponds to a really small amount of free cationic surfactant.
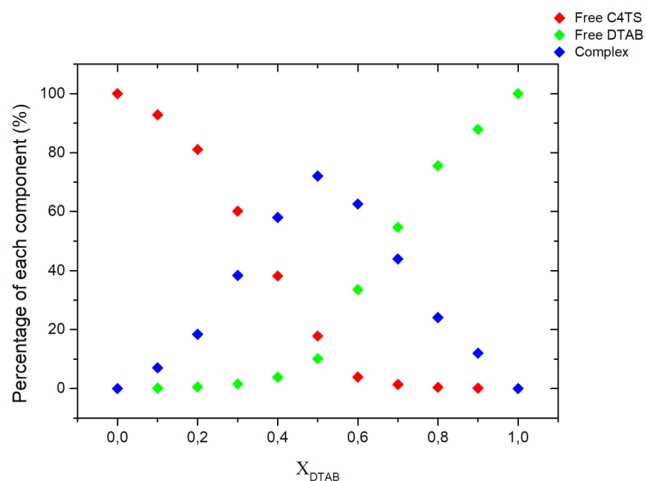
Figure 33. Molar percentage of each component at different molar fractions for **DTAB/C4TS** system.
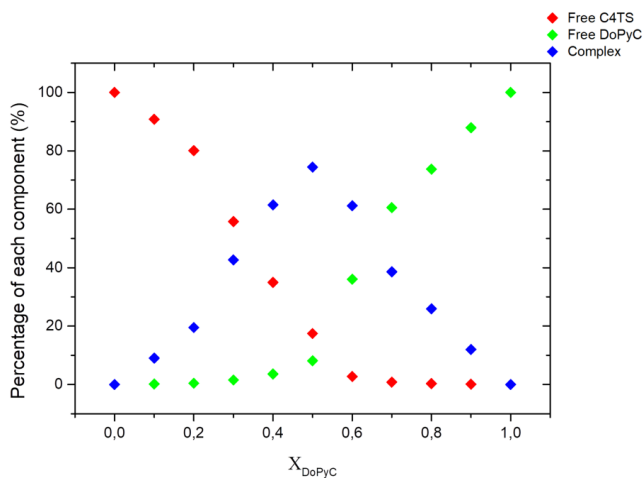
Figure 34. Molar percentage of each component at different molar fractions for **DoPyC/C4TS** system.

Figure 35. [free surfactant]/[complex] ratio as a function of the molar fraction values for **DTAB/C4TS** and **DoPyC/C4TS** systems

In other words, by modulating the amount of cationic surfactant we are switching from a solution containing one anionic surfactant, the supramphiphile to a catanionic mixture when we are in the presence of excess free cationic surfactant.
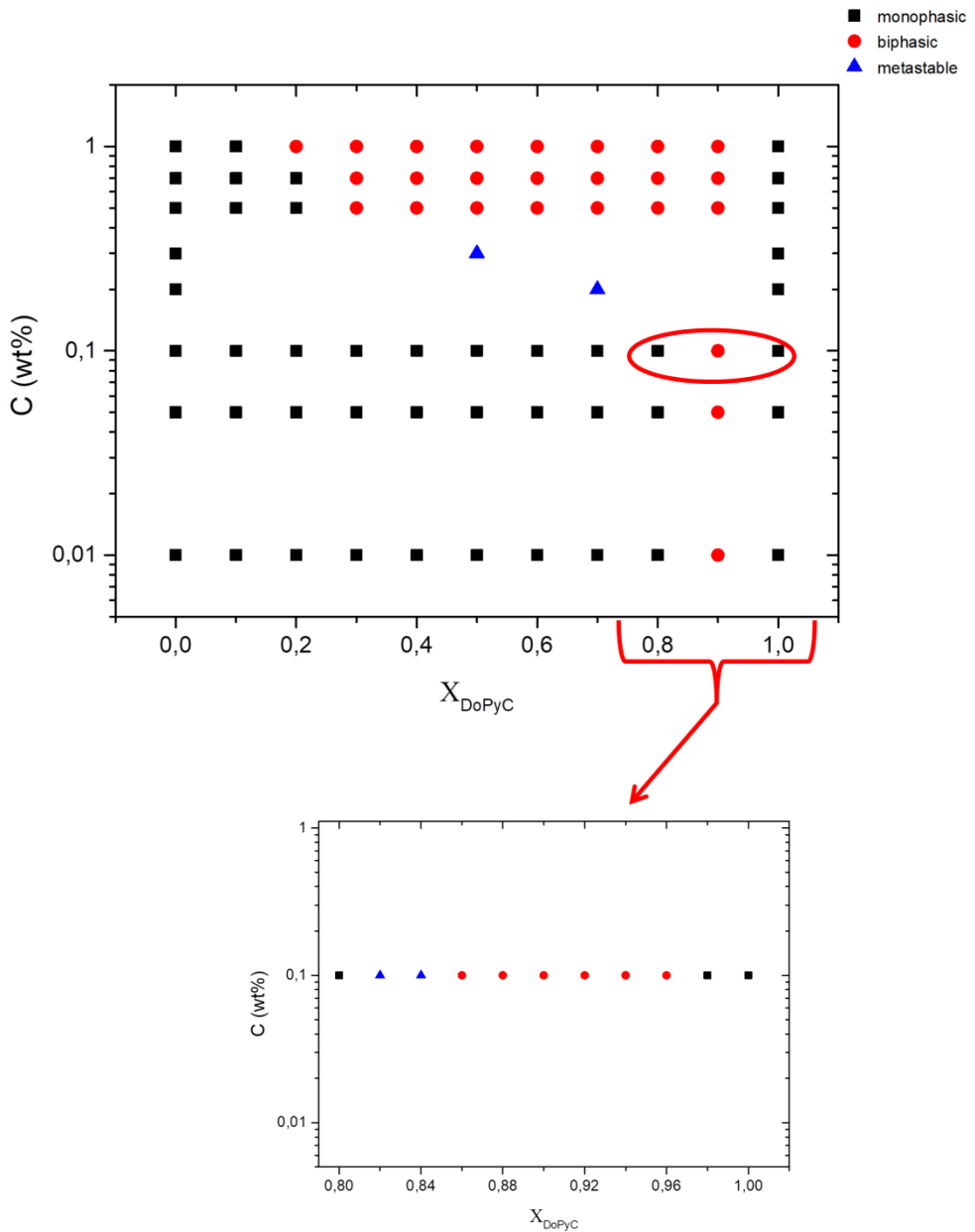
Phase behaviour

If we treat these systems by considering the total number of positive and negative charge, since the free surfactant is cationic and the free calixarene is in a pentanionic form at neutral pH, we may also consider that they have the tendency to form precipitate as commonly oppositely charged mixtures do.

Hence, the determination of the macroscopic phase behaviour is crucial. **DTAB/C4TS** and **DoPyC/C4TS** mixtures at different concentration and molar fractions were investigated, in order to obtain information about the solution stability.

The concentration values investigated are in the range between 0.01 wt% and 1 wt%. Lower concentration values are too much diluted for our purpose as precipitation/phase separation cannot be easily observed and they are also much lower than the CAC values determined by surface tension measurements. On the other hand, higher concentration values are too large to consider worthwhile to use mixed systems rather than the free conventional surfactant. Indeed the concentration value of 1 wt% is already higher than the CMC values of both cationic surfactants.
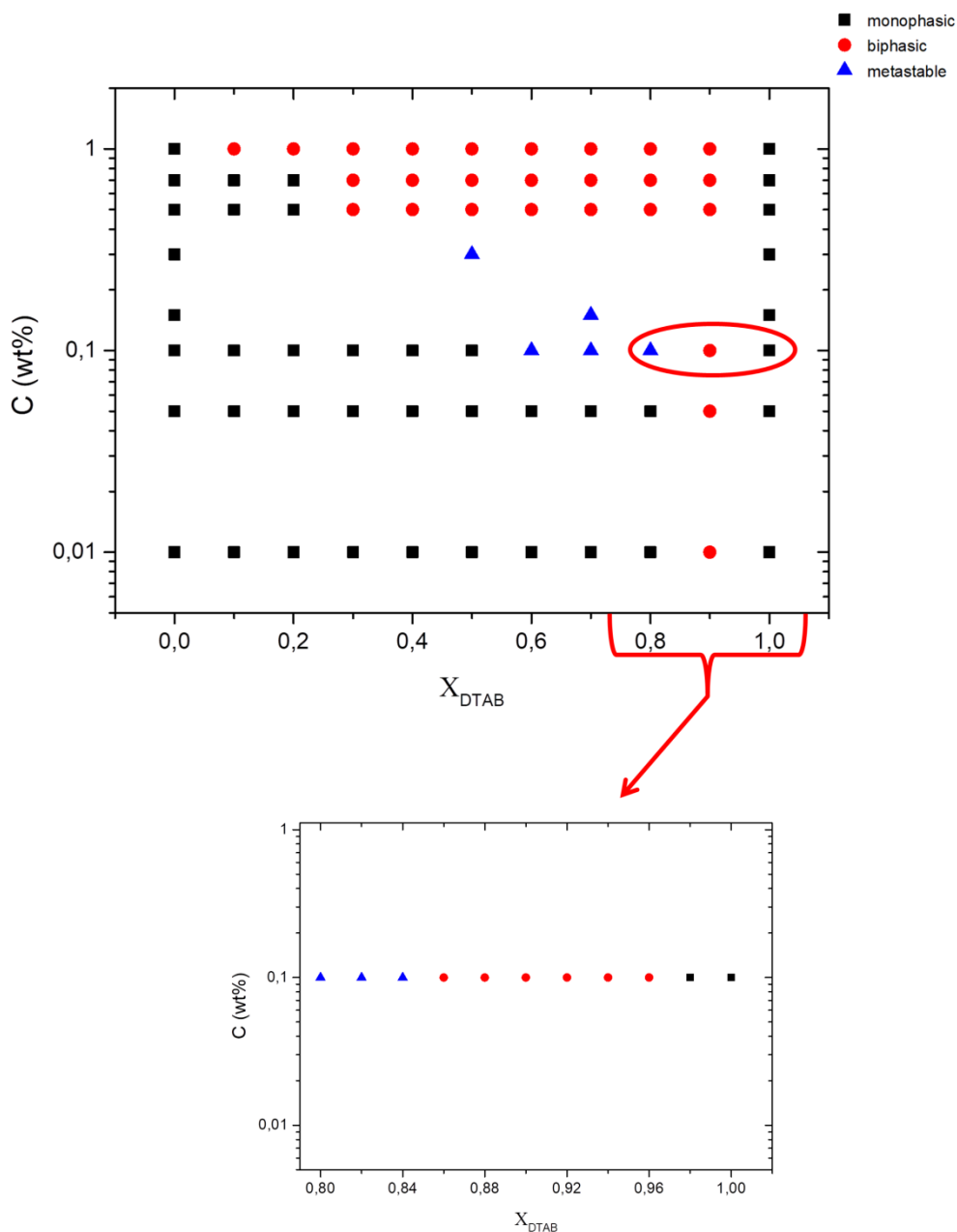
Figure 36. Phase diagram showing the monophasic, metastable and precipitate regions for **DTAB/C4TS** system at different concentration and at different molar fractions.

Figure 37. Phase diagram showing the monophasic, metastable and precipitate regions for **DoPyC/C4TS** system at different concentration and at different molar fractions.

The findings for the phase behaviour for **DTAB/C4TS** system and **DoPyC/C4TS** are schematically reported in **Figure 36** and **Figure 37** while the pictures for both systems are reported in **Figure A21** and **Figure A22**, respectively. The monophasic range at 0.1 wt% concentration is much larger for the **DoPyC/C4TS** system than for the **DTAB/C4TS** system. Probably, for **DoPyC/C4TS** system, the pyridinium ring of the excess free surfactant is interacting with the external cavity of calixarene more than the trimethylammonium group of **DTAB**.

All free components are stable at all concentration values investigated. At 0.1 and 0.2 molar fraction values, the samples are stable up to a concentration value of 0.7 wt% for the **DTAB/C4TS** system while for **DoPyC/C4TS** it is possible to reach the concentration value of 1 wt% at X_{DoPyC}=0.1. The maximum concentration value that can be reached is 0.3 wt% for both system at X_{surf}=0.5. beyond this molar fraction, metastable samples are observed at the concentration value of 0.1 wt% for the **DTAB/C4TS** system while the samples are stable for the **DoPyC/C4TS** system. For both systems the samples are monophasic when they are freshly prepared with milky colour however precipitation occurs after few days in the case of the **DTAB/C4TS** mixture. For the **DoPyC/C4TS** system no precipitation occurs for more than one week but for longer times precipitation was observed too.

Precipitation occurs at $X_{surf.}$=0.9 regardless of the samples concentration because we are too close to total neutrality (which one has at $X_{surf.}$=0.8333) since at working pH (7.2) calixarene **C4TS** is pentanionic.

Finally, in order to evaluate the effect of calixarene on the solubility of the free surfactant and exactly establish the phase boundaries over the molar fraction interval between 0.8 and 1, different composition within this interval were investigated in details. It was found that precipitation occurs in the

interval $0.84 \leq X_{surf} \leq 0.96$. Since the values in this range are quite close to the full neutrality of the system, it is reliable that precipitation phenomena occur.

Samples that do not show precipitate formation after one week were considered as thermodynamically stable single phase systems.

# Surface Tension study of supramolecular catanionic mixtures

Mixtures of two or more different types of surfactants often show a "synergistic" interaction, i.e., the interfacial properties of the mixture are more pronounced than those of the individual components. As a result, instead of individual materials, mixtures of different types of surfactants are used , in many industrial products and processes,.

Knowing the specific interaction between the two surfactants is crucial for the comprehension of mixed micellar systems as it can be easily expressed in terms of the interaction parameter β of the regular solution theory.[106-] Classically, the interaction parameter β is determined by measuring the CMC of the corresponding surfactant mixtures. This was accomplished by measuring the surface tension of **DTAB/C4TS** and **DoPyC/C4TS** systems at different molar fractions as summarized in **Figure 38** and **Figure 39**, respectively.
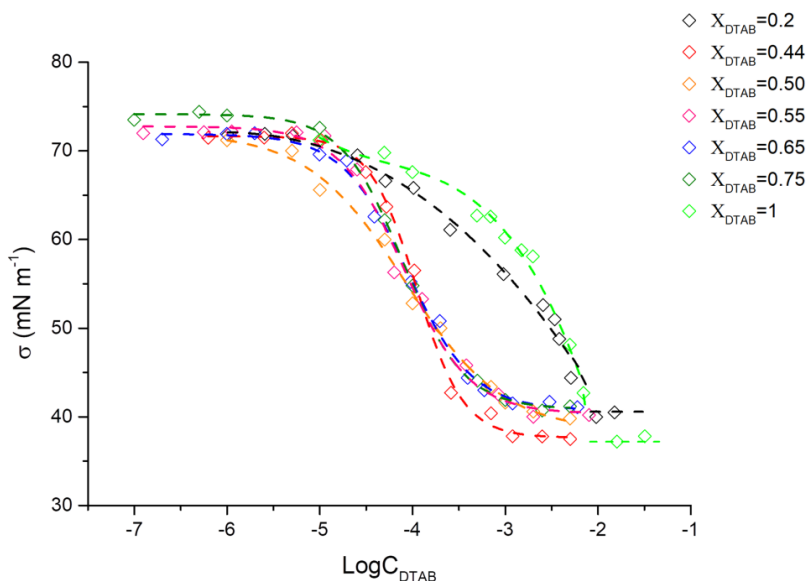
Figure 38. Surface tension curves obtained at different **DTAB/C4TS** molar fractions (lines are guides to the eye).
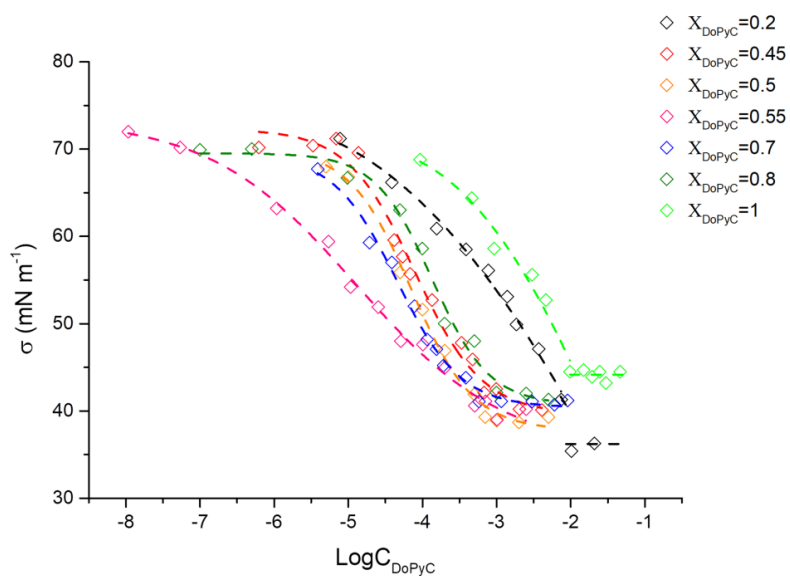
Figure 39. Surface tension curves obtained at different **DoPyC/C4TS** molar fractions (lines are guides to the eye).

The CMC values obtained by the measurements reported above are reported in **Table 3** and **Table 4**, respectively, and are also schematically represented in **Figure 40**.

Table 3. CMC values of **DTAB** determined at different **DTAB/C4TS** fractions at 25 °C.
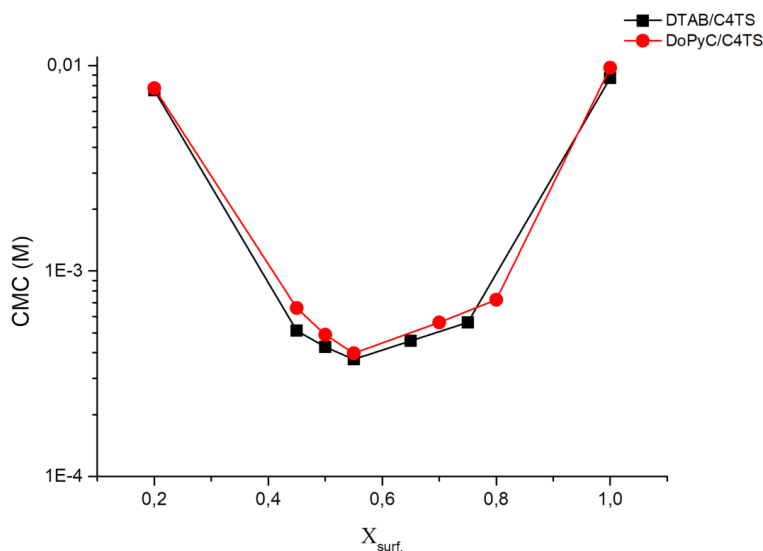
X_{DTAB}	CMC (mM)
0.2	7.59 (2)
0.44	0.51 (3)
0.5	0.43 (1)
0.55	0.37 (2)
0.65	0.46 (2)
0.75	0.56 (3)
1	8.71 (2)

X_{DTAB} is obtained from $\frac{c_{DTAB}}{c_{DTAB}+c_{C4TS}}$

Table 4. CMC values of **DoPyC** determined at different **DoPyC/C4TS** fractions at 25 °C.

X_{DoPyC}	CMC (mM)
0.2	7.76 (2)
0.45	0.59 (3)
0.5	0.49 (2)
0.55	0.40 (1)
0.7	0.56 (1)
0.8	0.72 (2)
1	9.77 (1)

X_{DoPyC} is obtained from $\frac{c_{DoPyC}}{c_{DoPyC}+c_{C4TS}}$

Figure 40. CMC$_{surf}$ values reported as a function of the molar fraction of **surfactant for DTAB/C4TS (black squares) and for DoPyC/C4TS (red circles) sytems.**

Figure 40 clearly shows that for both **DTAB** and **DoPyC** the CMC values of the mixtures are significantly lower than that of the pure surfactant. The marked reduction of the CMC indicates that the interactions between the components of the surfactant mixtures are strongly synergistic, i.e. the properties of the mixture are better than those attainable with the individual components by themselves.

The molecular interactions between two different surfactants can be expressed by a parameter, β, that gives the strength of these interactions. The regular solution equation for β, is

$$\beta = \frac{\left[W_{AB} - \frac{(W_{AA} + W_{BB})}{2}\right]}{RT} \qquad (8)$$

where

W_{AB} is the molecular interaction energy between the mixed surfactants,

W_{AA} is the molecular interaction energy among the first surfactant particles prior to its mixing with the second component,

W_{BB} is the molecular interaction energy among the second surfactant molecules prior to its mixing with the first component,

R is the gas constant,

T is the absolute temperature.

The parameters of this equation help to understand the meaning of β and need no further comments.

The sign of W is negative for attractive interactions, while is positive for repulsive interactions. A negative β value indicates that, upon mixing, the two surfactants experience either greater attraction or less repulsion than before mixing; by contrast, a positive β value indicates a lesser attraction or a greater repulsion upon mixing than that occurring before mixing. A value close to zero indicates little or no change upon mixing.

According to the non-ideal solution theory, for mixed surfactant systems the molecular interaction parameter, β, may be determined by using the following equations:[108,109]

$$x_{surf.}^2 * ln\frac{\alpha_{surf}CMC_{(surf)(C4TS)}}{x_{surf}CMC_{surf}} = (1 - x_{surf})^2 * ln\frac{\alpha_{C4TS}CMC_{(surf)(C4TS)}}{(1-x_{surf})CMC_{C4TS}} \quad (9)$$

$$\beta = \frac{ln[\alpha_{surf} * \frac{CMC_{(surf)(C4TS)}}{(x_{surf}CMC_{surf})}]}{(1-x_{surf})^2} \quad (10)$$

where:

α_{surf} is the total amount of surfactant (**DTAB** or **DoPyC**)

α_{C4TS} is the total amount of **C4TS**

x_{surf} is the amount of free surfactant (**DTAB** or **DoPyC**) in the micelles

$CMC_{(surf)(C4TS)}$ is the critical micellar concentration of the mixed system

CMC_{surf} is the critical micellar concentration of free surfactant (**DTAB** or **DoPyC**)

CMC_{C4TS} is the critical micellar concentration of **C4TS**. This quantity does not really exist, due to the non-amphiphilic nature of calixarene and the values used in this plot are hypothetical values.

However, in the case of catanionic system of this type, in which the anionic component is a non-amphiphilic molecule, more variables have to be considered. Indeed one may consider this system as a mixed surfactant system only when the supramolecular complex is formed (that will be the anionic counterpart of the free cationic surfactant); however its formation depends on both the analytical concentration of **C4TS** and cationic surfactant (**DTAB** or **DoPyC**) and the binding constant value. Furthermore, the critical micellar concentration value for **C4TS** does not exist as it does not form micelles since it is not a surfactant. Nevertheless, the interaction parameter, β, may be calculated from the above equation by assuming different CMC values for **C4TS** and exploring various molar fractions. The results obtained for the **C4TS/DTAB** and **C4TS/DoPyC** systems are reported in **Figure 41** and **Figure 42**, respectively.
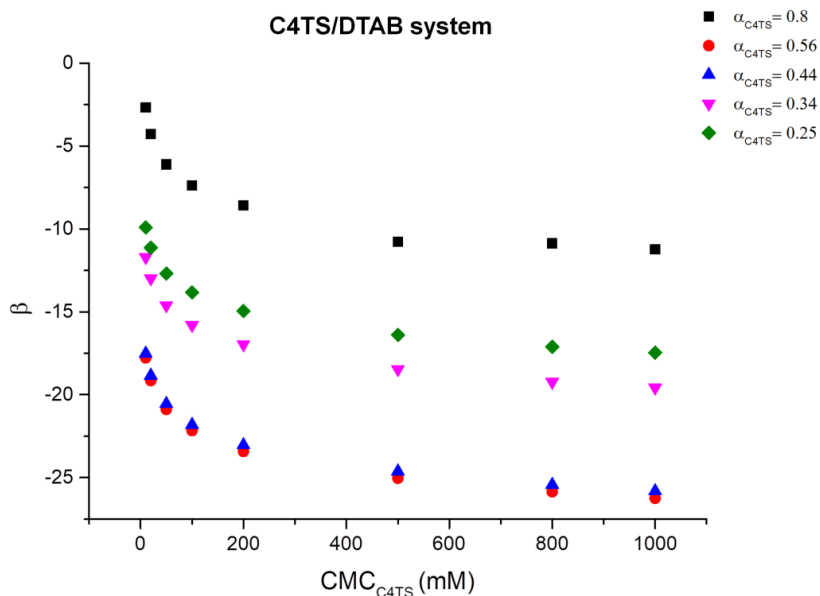
Figure 41. Trends of β values for the **C4TS/DTAB** system considering different molar fractions and introducing increasing CMC values for **C4TS**
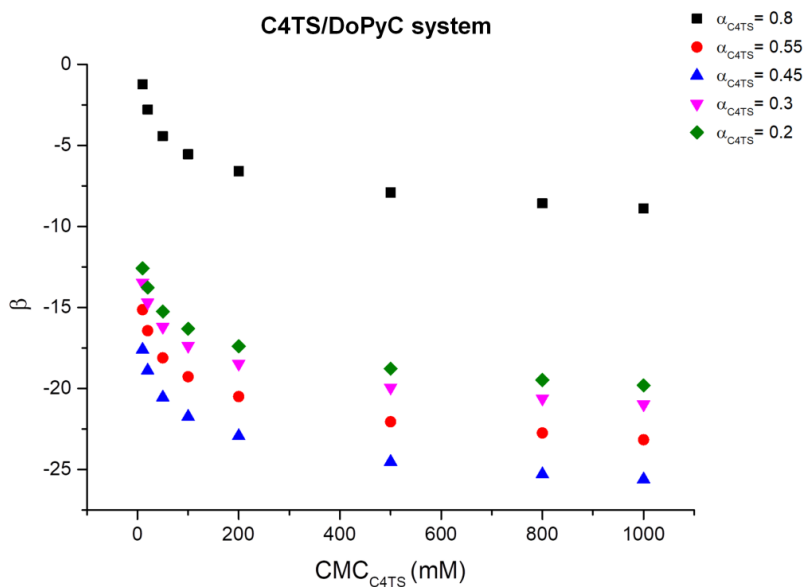
Figure 42. Trends of β values for the **C4TS/DoPyC** system considering different molar fractions and introducing increasing CMC values for **C4TS**

The figures undoubtedly show that β values are always negative for any **C4TS** CMC value and all molar fractions investigated. Due to the non-amphiphilic nature of calixarene, the values reported in the plot are not exact values but they may be employed for comparison purposes. Indeed, when one compares them with the values obtained for conventional catanionic mixtures, β values for supramolecular catanionic mixtures turn out to be fully consistent.

These results emphasise the crucial role played by the calixarene scaffold in the generation of synergetic mixtures.

The surface tension measurements also allowed for the determination of two more closely correlated parameters i.e. the surface excess concentration, Γ, and the area per molecule at the interface, a_s.

The surface excess concentration (Γ) is the area-related concentration of a surfactant at the surface or interface. For surface-active solutes, the surface excess concentration Γ is with a good approximation equal to the actual surface concentration. For a mixture, Γ results from the contribution of all the components of the solution:

$$\Gamma = \sum_i \Gamma_i \quad (11)$$

where Γ_i is the surface excess concentration of each component.

For a mixture of a calixarene (**C4TS)** and a cationic surfactant, the components to be considered are the free calixarene, the free surfactant and the complex. The model may be further simplified by considering the Γ_{app} parameter that can be calculated using the following equation:

$$\Gamma_{app} = - \frac{1}{RT} \left(\frac{d\gamma}{d\ln C} \right) \quad (12)$$

The surface excess concentration may be obtained from the slope of a plot of surface tension values versus log C at constant temperature, namely, directly from the surface tension measurements curves.

From the surface excess concentration, the area per molecule at the interface (a_s), in square angstroms, is calculated from the relation:

$$a_s = \frac{10^{23}}{N\Gamma} \quad (13)$$

where N is Avogadro's number.

The area per molecule at the interface provides information on the degree of packing and the orientation of the adsorbed surfactant molecules.

The values thus obtained are reported in **Table 5.**

Table 5. Surface excess concentration, Γ, and area per molecule at the interface, a_s for all the systems investigated

SYSTEM	$X_{surf.}$	Γ (mol 10^{-3} m^{-2})	a_s (Å^2)
DTAB/C4TS	0.2	0.00250 (1)	66.5 (3)
	0.44	0.00435 (2)	38.2 (2)
	0.5	0.00273 (1)	60.7 (1)
	0.55	0.00378 (2)	43.9 (2)
	0.65	0.00371 (2)	44.8 (2)
	0.75	0.00422 (2)	39.3 (3)
	1	0.00401 (1)	41.4 (2)
DoPyC/C4TS	0.2	0.00278 (1)	59.8 (2)
	0.45	0.00275 (1)	60.4 (3)
	0.5	0.00320 (1)	51.9 (1)
	0.55	0.00214 (2)	77.6 (1)
	0.7	0.00289 (2)	57.4 (1)
	0.8	0.00314 (1)	52.9 (3)
	1	0.00379 (2)	43.8 (2)

The surface excess concentration is a useful measure of the adsorption effectiveness of the surfactant at the L /G or L /L interface.

Since the effect of a surfactant on an interfacial phenomenon is a function of the concentration of surfactant at the interface, we can define the adsorption effectiveness of a surfactant at an interface as the maximum concentration that the surfactant can attain at that interface, i.e., the surface concentration of a surfactant for a saturated surface. As a consequence, this parameter depends on the structural groups in the surfactant molecule and its orientation at the interface.

Since tightly packed, coherent interfacial films have very different interfacial properties compared to loosely packed films, the effectiveness of adsorption is an important factor for the properties (foaming, wetting, and emulsification) of a surfactant.

A plot of the area per molecule at different molar fractions for the systems investigated is reported in **Figure 43.**
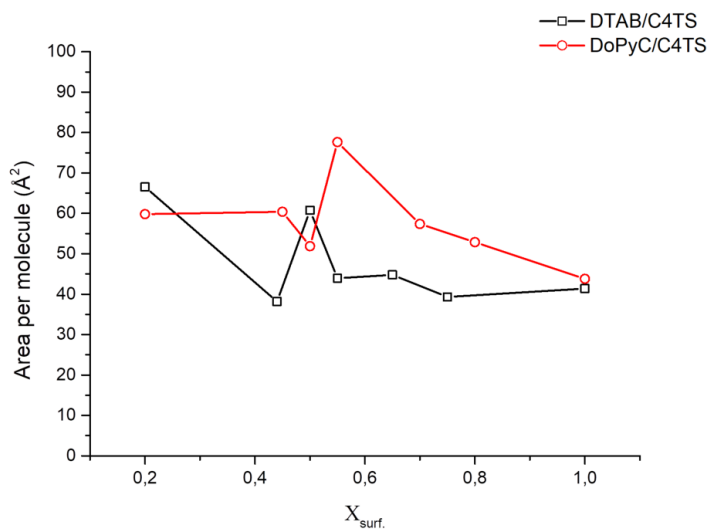
Figure 43. Area per molecule calculated at different molar fractions for the **DTAB/C4TS** and **DoPyC/C4TS** systems, respectively.

If the component is adsorbed onto the substrate surface perpendicularly in a close-packed arrangement, an increase in the length of a straight-chain hydrophobic group would cause no significant change in the number of moles of surfactant adsorbed per unit area of surface for a saturated surface; this is presumably due to the cross-sectional area occupied by the chain oriented perpendicularly onto the interface that does not change with the increase in the number of units in the chain.

Moreover, for a perpendicular orientation the adsorption effectiveness may be determined by the size of the hydrophilic group when the cross-sectional area of the group is greater than that of the hydrophobic chain; larger hydrophilic groups will result in smaller amount of surfactant molecules adsorbed onto a saturated surface.[110,111]

Salt formation between an ionic surfactant and an oppositely charged surfactant of approximately equal hydrophobic chain length produces a large increase in the effectiveness of adsorption, with the area per molecule at the interface approaching that of a close-packed film with the hydrophobic chains oriented perpendicular to the interface. This is probably the result of the combined effects of mutual attraction of ionic groups and mutual attraction of hydrophobic chains.

Accordingly, the area per molecule values decrease in the molar fraction range $0.5 < X_{surf.} < 0.8$, i.e. the molar fraction interval in which we are approaching the neutrality of the mixture.

Experimental

Materials

The host, *p*-sulfonato-calix[4]arene (**C4TS**) and the guests dodecyltrimethylammonium bromide (**DTAB)** and dodecylpyridinium chloride (**DoPyC**), were purchased from Sigma-Aldrich.

High purity water (Millipore, Milli-Q Element A 10 ultrapure water) and A grade glassware were employed throughout.

Both **C4TS** and the guests were dissolved in 25 mM phosphate buffer (pH 7.2). The buffer was chosen to keep the host in the penta-anionic form.

Samples preparation

All samples were prepared by mixing a proper amount of **DTAB** or **DoPyC** stock solutions with a proper amount of **C4TS** stock solution in order to have the desired molar fraction and the desired concentration. Two equations were used to calculate the amount of both components in the mixtures:

$$g_{tot} = g_{surf.} + g_{C4TS} \quad (14)$$

$$X_{surf.} = \frac{\frac{g_{surf.}}{PM_{surf}}}{\frac{g_{surf.}}{PM_{surf}} + \frac{g_{C4TS}}{PM_{C4TS}}} \quad (15)$$

in which g_{tot} are the total grams that allow to obtain the desired weight percent concentration.

Surface Tension Measurements using the Pendant Drop Method

Reduction of surface or interfacial tension is one of the most commonly measured properties of surfactants in solution: it depends directly on the replacement of molecules of solvent at the surface (or interface) by molecules of surfactant.

The surface tension of a surfactant solution decreases continuously as the bulk concentration of the surfactant increases until the concentration reaches a value known as the critical micelle concentration (CMC), above which the tension remains virtually unchanged (**Figure 44**).[112]
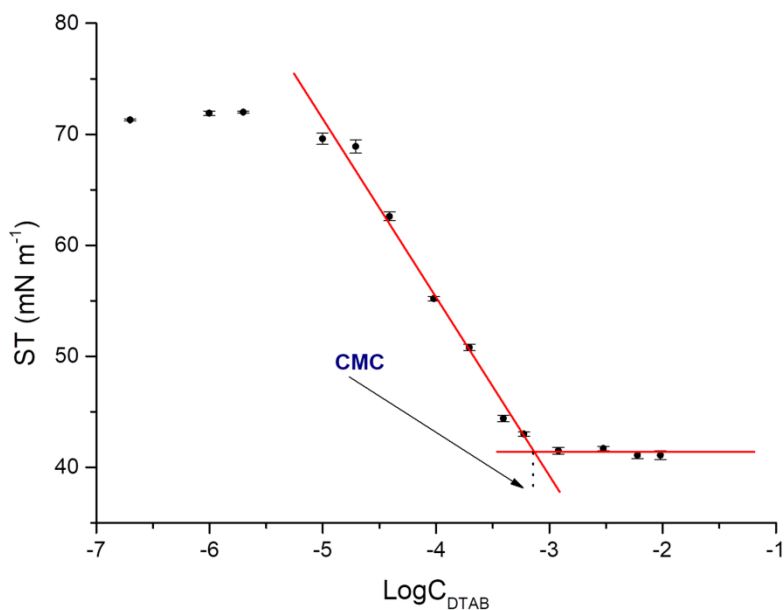
Figure 44. Surface tension-log C plot for pure DTAB illustrating the surface tension reduction at the CMC value.

Among the numerous measuring methods used to measure the surface tension, the optical pendant drop method is particularly convenient. Indeed, it requires only a very small sample volume, a relatively simple apparatus and is a very accurate method when used correctly;[113,114] however it has few limiting conditions.

The principal assumptions are:

- The drop is symmetric about a central vertical axis: this means that the direction from which the drop is viewed is not relevant.

- The drop is not in motion in that viscosity or inertia are playing a role in determining its shape: this means that surface (or interfacial) tension and gravity are the only forces shaping the drop.

The equation describing the pressure difference (Laplace pressure) between the areas inside and outside of a curved liquid surface/interface, with the principal radii of curvature R_i, is:

$$\Delta P = (P_{int} - P_{ext}) = \sigma(\frac{1}{R_1} + \frac{1}{R_2}) \quad (16)$$

The forces that determine the shape of the pendant drop are the surface tension and gravitation. The surface tension seeks to minimize the surface area and confer the a spherical shape. Gravitation, on the other hand, stretches the drop from its spherical shape resulting in the typical pear-like shape.

Gravitation causes a pressure difference across the z-axis according to Pascal's law (hydrostatic pressure). Therefore, the Laplace pressure $\Delta P(z)$ at a distance z from an arbitrary reference plane with Laplace pressure ΔP_0 is:

$$\Delta P(z) = \Delta P_0 \pm \Delta\rho g z \quad (17)$$

For a pendant drop, the principal radii of curvature at the vertex (lowest point of the drop) are: $R_1 = R_2 = R$. Thus, the reference plane is conveniently placed in this point. For every point above it holds that $R_2 = x/\sin\Phi$ (see **Figure 45**).
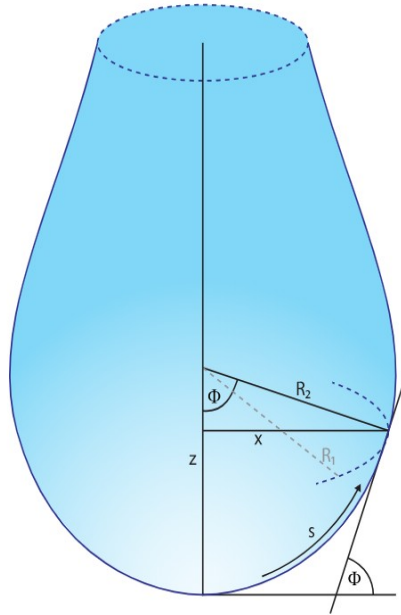
Figure 45. Schematic Young-Laplace fit on a pendant drop.

The above-mentioned equations lead to:

$$\frac{1}{R} + \frac{\sin\Phi}{x} = \frac{2}{R} \pm \frac{\Delta\rho g z}{\sigma} \quad (18)$$

The introduction of a parametrisation using the arc length (s) of the drop shape results in the following set of three first-order differential equations with three boundary values, that may be solved by numerical procedures:

$$\frac{d\Phi}{ds} = -\frac{\sin\Phi}{x} + \frac{2}{R} \pm \frac{\Delta\rho g z}{\sigma} \quad (19)$$

$$\frac{dx}{ds} = \cos\Phi \quad (20)$$

$$\frac{dz}{ds} = \sin\Phi \quad (21)$$

$$0 = x(s = 0) = z(s = 0) = \Phi(s = 0) \quad (22)$$

The numerical fit of the theoretical drop shape to the shape recorded by the camera eventually yields the surface tension. These considerations also apply when the surrounding phase is not air but a liquid. In this case, the interfacial tension is the measured parameter.

Surface Tension measurements were carried out using an optical contact angle measuring and contour analysis system of the OCA series. The setup illustrated in **Figure 46** is used to capture an image of a liquid drop that hangs on a dosing needle and to subsequently analyse it with the DataPhysics Instruments SCA 22 software module.[115] The corresponding evaluation process is called pendant drop method.[116,117]
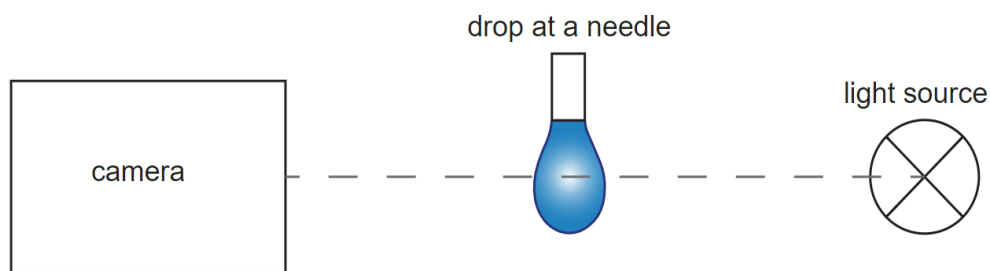
Figure 46. Sketch of the apparatus used for Surface Tension measurements

The solution was introduced into a glass syringe, and then the syringe was mounted onto the experimental equipment. A stainless-steel needle with an outside diameter of 0.52 mm and an inner diameter of 0.25 mm was used to produce the drops. When a liquid drop hangs from the syringe needle, it has a characteristic shape and size that determine the surface tension. The drops were measured in 12/15 independent sets of quintuplicates for each concentration. The uncertainty in the surface tension is less than 0.2 mN/m.

CHAPTER 4 - AGGREGATION BEHAVIOUR OF CALIXARENE-BASED CATANIONIC MIXTURES

Amphiphilic molecules may self-assemble in different morphological structures in aqueous solution.

The shape of the aggregates formed in aqueous media is important to determine various properties of the surfactant solution, such as the viscosity or the solubilisation capacity of water-insoluble molecules of these aggregates.

A variety of different aggregate shapes in surfactants solution have been observed as *i.* relatively small spherical structures (micelles); *ii.* elongated cylindrical rodlike micelles; *iii.* large, flat lamellar micelles; and *iv.* vesicles, more or less spherical structures consisting of bilayer lamellar micelles arranged in one or more concentric spheres.

In aqueous media, the surfactant molecules are oriented, in all these structures, with their polar heads predominantly toward the aqueous phase and their hydrophobic groups away from it. In vesicles, there are also water molecules in the interior of the structure. In ionic micelles, the aqueous solution–micelle interfacial region contains the ionic head groups, the Stern layer of the electrical double layer with the bound counterions as well as water.

The interior region of the micelle, containing the hydrophobic groups, has a radius approximately equal to the length of the fully extended hydrophobic chain. The aqueous phase is believed to penetrate into the micelle beyond the hydrophilic head groups; furthermore there is good evidence that penetration of water molecules into the micellar interior is rather little or basically null

and the first few methylene groups of the hydrophobic tails adjacent to the hydrophilic head are often considered in the hydration sphere.[118] Thus the interior region may be divided into an outer core that may be penetrated by water and an inner core that does not contain water. In non-polar media, the structure of the micelle is similar but reversed, with the hydrophilic heads comprising the interior region surrounded by an outer region containing the hydrophobic groups and nonpolar solvent.

Changes in temperature, concentration of surfactant, additives in the liquid phase, and structural groups in the surfactant may all cause change in the size, shape, and aggregation number of the aggregates, yieldin structures that range from spherical and rod-like micelles to amphiphilic bilayers. [119,120]

A very common method of self-assembly for surfactants is the formation of amphiphilic bilayers, in which the hydrophilic polar heads of the amphiphiles are facing the solvent (water) and the hydrophobic tails of the amphiphiles constitute the interior of the bilayers, respectively. In the simplest arrangement, these bilayers form planar structures only. However, bilayers may also close, forming objects which are called vesicles, that have, in the simplest case, a spherical shape (**Figure 47**).

Vesicles find application in several fields such as cleaning, catalysis, and microencapsulation for drug delivery; the latter one depends on a simple and controlled method for the generation of vesicles with a well-defined average size. In addition, vesicles are often employed as models for biological membranes.
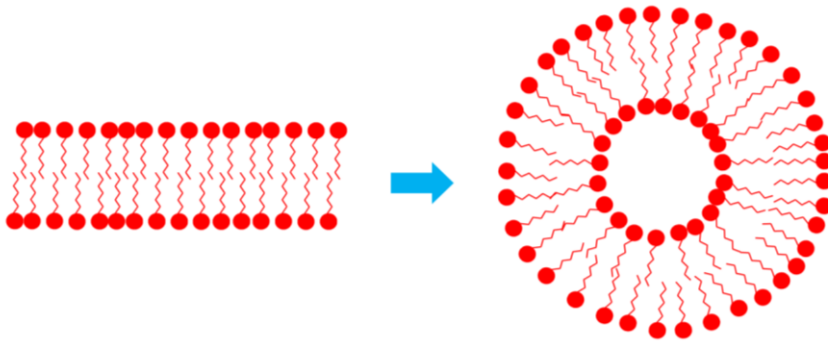
Figure 47. Schematic representation of an amphiphilic bilayer and a vesicle.

Vesicles can be classified into different categories, depending on their structure.[121]

- Unilamellar vesicles (UV). They are formed by a single bilayer. In this case both small unilamellar (SUV; R = 4–50 nm) and large unilamellar vesicles (LUV; R = 50 nm–10 μm) may be obtained. Unilamellar vesicles form isotropic solutions (except for high concentrations, where gels may also be formed).
- Multilamellar vesicles (MLV). In this case different concentric shells of vesicles are present in solution.[122] The most common example is represented by the so-called liposomes.[123,124]

In general, unilamellar vesicles are detected in dilute systems, while MLV are frequently found in more concentrated surfactant systems. Typically, for bilayer-forming amphiphilic systems, as concentration increases, the structure evolves progressively according to the following scheme:

unilamellar vesicles→multilamellar vesicles→planar bilayers.

Although vesicles often form spontaneously *in vivo*, they rarely form as the equilibrium structure of simple surfactant-water systems. For this reason, vesicle preparation is a crucial point for the formation of vesicles, since in several circumstances this process requires an external energy input.[125,126]

Various methods have been proposed for the formation of vesicles from relatively rigid bilayers. For example, phospholipids, the main amphiphiles forming the membranes of living cells, are an example of formation such rigid bilayers.

A typical method of forming phospholipid-based vesicles is by sonication of aqueous dispersions of the lipid.[127-129] In some cases, vigorous shaking or vortexing can be sufficient for the mechanical dispersion of the lipid.[130,131] Noteworthy, such a treatment is a standard procedure for achieving homogenization of surfactant samples. Indeed, in many situations where vesicles are observed experimentally, their formation occurs due to the homogenization of the samples.

Thin film hydration is another classical method. In this case a thin film of amphiphilic material is obtained by evaporating a solution of amphiphile in chloroform or other volatile solvents. The thin film comes then into contact with water and dissolves by forming vesicles.

Another technique for vesicle preparation is by the use of membrane filters of a given pore size. This method allows for the formation of relatively monodisperse vesicles.[132,133]

In many circumstances, vesicles are only formed following an external energy input. Spontaneous formation of vesicles is a very important process as no external driving force is required. A spontaneous vesicle formation was obtained with dialkyl dimethyl ammonium surfactants in which halide counterions were replaced by hydroxide or acetate counterions.[134] The reason for the different behaviour of the hydroxide vs. corresponding halide surfactants is that the hydroxide ion has a much higher affinity to water and it is found, on the average, further away from the charged micellar surface. Thus, the repulsive interactions between the head groups, and hence the whole head group region, of the surfactant molecules at the amphiphilic

interface becomes larger. Accordingly, they do not form planar bilayers but have a tendency to form curved bilayers, i.e. vesicles. In these systems, the size of the vesicles can be even controlled by titration with an acid, which may lead to growth of the expected vesicles.[135] A similar strong dependence of the formation of vesicles on the counterion has been observed for anionic surfactants.[136]

A spontaneous formation of vesicles is also observed for catanionic systems: vesicles are obtained by mixing a cationic and an anionic surfactant. For such catanionic systems, vesicle formation has been observed for a large variety of different situations. Most frequently, mixtures of anionic and cationic single-chain surfactants have been studied. Examples of such systems include SDS/DTAB or DTAB/SDBS mixtures.[137-141] Schmölzer *et al.* have investigated the salt free system TexaponN70-H and TTAOH, showing that after mixing equimolar amounts of surfactant solutions firstly mixed micelles are formed and then spontaneously they form monodisperse unilamellar vesicles.[142]

Typically, for equimolar mixtures of this type precipitation occurs, whilst stable unilamellar vesicles are formed when using an excess of either the cationic or the anionic surfactant. The precipitate often evolves into a vesicle phase upon heating. However, there may also exist the possibility that no precipitate is formed for equimolar catanionic mixtures at room temperature. Of course, the tendency to precipitate increases with the length of the alkyl chains and is more pronounced for chains of similar length.

In addition, the nature of the head group has a strong influence on the formation of precipitate. The tendency to form precipitates depends strongly on the ability of cationic and anionic surfactant molecules to form stable crystalline arrangements and this tendency may be suppressed by reducing the effective electrostatic interaction between the oppositely charged head

groups, as is, for instance, in the case for the bulky triethylammonium head group.

Aim of the work

Initially, mixed systems formed by the calixarene **C4TS** with dodecyltrimethylammonium bromide (**DTAB**) or dodecylpyridinium chloride (**DoPyC**) have been investigated by surface tension measurements in order to determine the variation of the CAC value as a function of the amount of the **C4TS** as well as to evaluate the synergistic behaviour, as reported in the previous chapter.

The structure of these systems was then systematically studied by means of static and dynamic light scattering over a broad range of scattering angles investigating different molar fractions in order to determine structural changes varying the amount of free surfactant.

Mixtures of anionic and cationic surfactants (catanionic mixtures) offer an attractive approach for the construction of complex self-assembled nanostructures. The formation of spontaneous vesicles in mixtures of oppositely charged surfactants was widely demonstrated and intense research has been devoted to the study of self-assembled structures formed in catanionic surfactant systems.[143] The formation of host–guest complexes between macrocyclic hosts and surfactant monomers is a different approach to modulate the physicochemical properties of these systems.[144,145]

Indeed, in this way, we can have a catanionic mixture, and the percentage of the two component can be modulated just by controlling the amount of calixarene (**C4TS**).

The two cationic surfactants, **DTAB** or **DoPyC**, in combination with the anionic calixarene, **C4TS,** have been studied varying the complexation ratio of surfactant for both systems. This is a stimulating variation as we have dealt with free cationic surfactants combined with the anionic supramolecular surfactants, i. e. an intrinsic catanionic surfactant mixture.

Interesting structural changes were observed as such mixtures of surfactants are known to form vesicular or wormlike aggregates (**Scheme 4**).

Detailed knowledge of the structure of these systems is essential in order to further improve this class of systems.
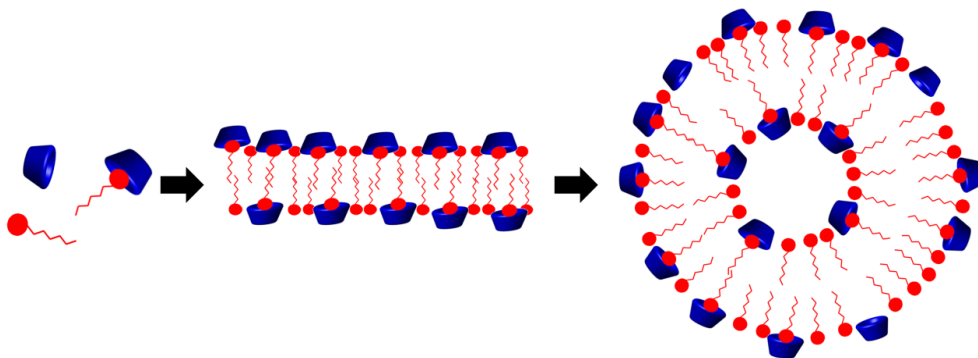
Scheme 4. Supposed aggregation features of the charged systems investigated at proper composition.

Study of the aggregation properties using light scattering

Structural information about supramolecular aggregates was obtained by light scattering measurements. Scattering angles between 30° and 130° with an increment of 10° were investigated. The experiments were carried out by mixing the cationic surfactant (**DTAB** or **DoPyC**) and the calixarene **C4TS** at five different molar fractions in the range of 0.4 to 0.8 (**Figure A23-A32**). Molar fractions were calculated as

$$X_{surf.} = \frac{C_{surf.}}{C_{surf.} + C_{C4TS}}. \quad (23)$$

Significant changes are observed for both the **DTAB/C4TS** and **DoPyC/C4TS** systems in this range. On the other hand, for molar fraction values lower than 0.4 (e.g. $X_{surf.}$=0.1; 0.2; 0.3) the results obtained are not consistent, since the overall scattering intensity is of the same order of magnitude of that of the buffer, thus one can assume that no aggregates of detectable dimensions are formed under these conditions.

The autocorrelation functions obtained for the systems investigated by varying the molar fraction at a scattering angle θ=90° are reported for both systems investigated in **Figure 48** and **Figure 49**, respectively. The autocorrelation functions obtained at the same molar fraction at all scattering angles investigated are showed for both systems in **Figure 50** and **Figure 51**, respectively.
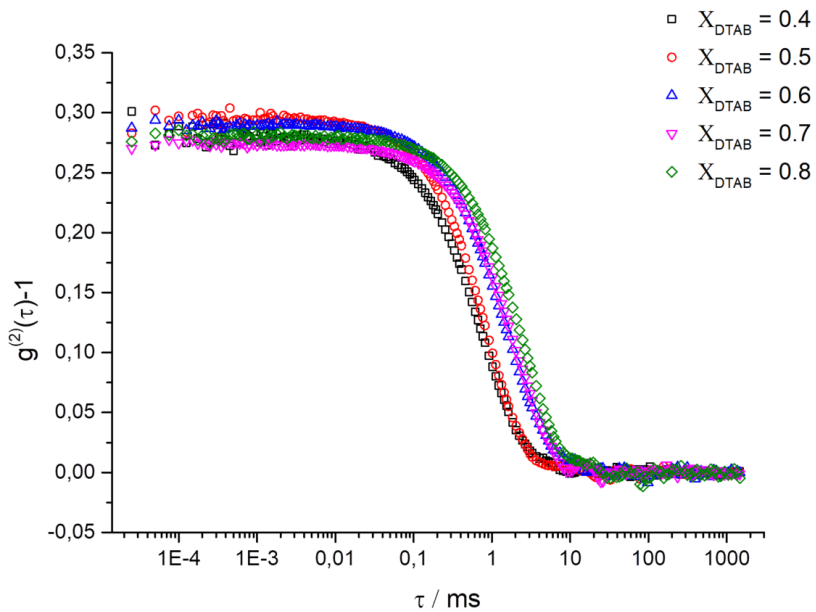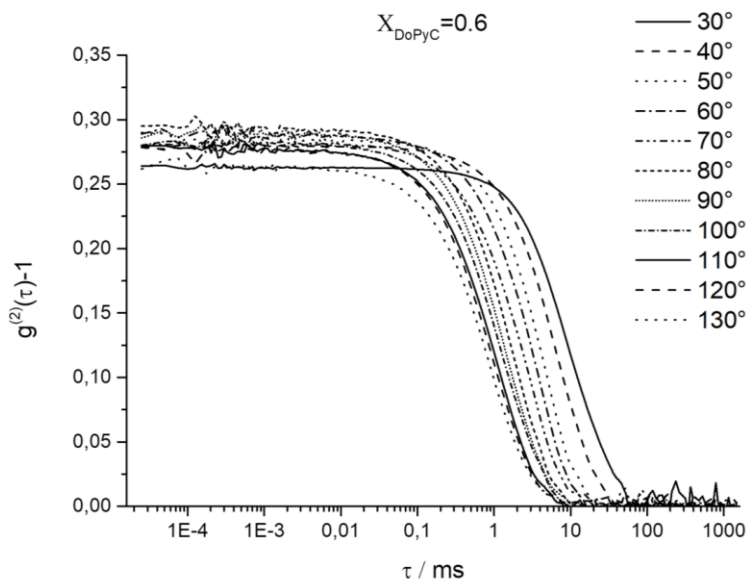
Figure 48. Autocorrelation function for **DTAB/C4TS** mixtures at 0.1 wt% at different molar fractions at a scattering angle θ=90°
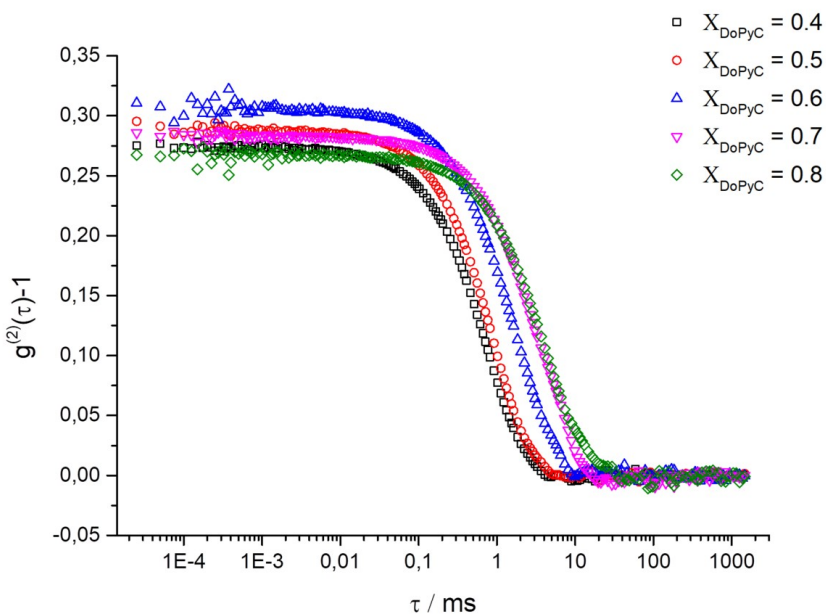
Figure 49 Autocorrelation function for **DoPyC/C4TS** mixtures at 0.1 wt% at different molar fractions at a scattering angle θ=90°
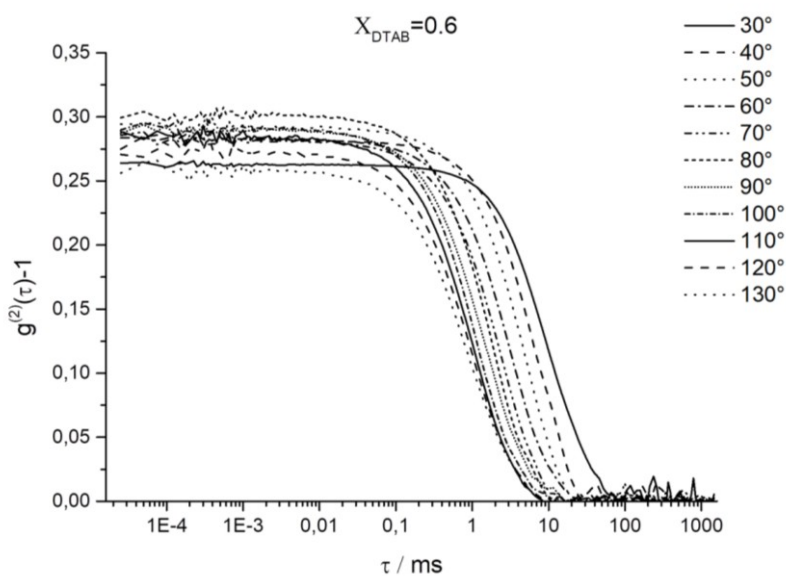
Figure 50. Autocorrelation functions for **DTAB/C4TS** mixtures at 0.1 wt% at X_{DTAB}=0.6 at all scattering angle investigated.


Figure 51. Autocorrelation functions for **DoPyC/C4TS** mixtures at 0.1 wt% at X_{DoPyC}=0.6 at all scattering angle investigated.

From the above data we may estimate the size of aggregates; in turn, the apparent translational diffusion coefficient (D) at finite concentration can be calculated from the relaxation rate, Γ, for $q \to 0$:

$$D = \left(\frac{\Gamma}{q^2}\right)_{q \to 0} \quad (24)$$

where q is the magnitude of the scattering vector.

D is obtained from the slope of $\Gamma = f(q^2)$ (**Figure 52** and **Figure 53**).
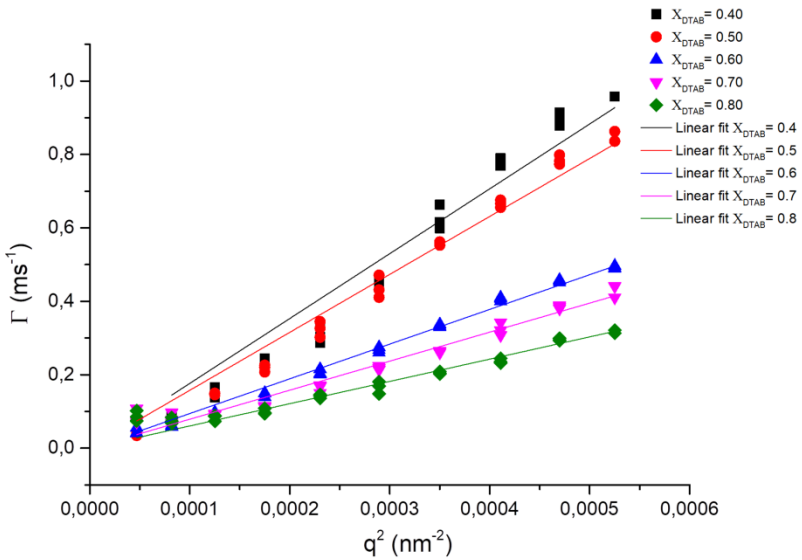
Figure 52. Relaxation rate Γ as a function of the scattering vector q for the **DTAB/C4TS** system.
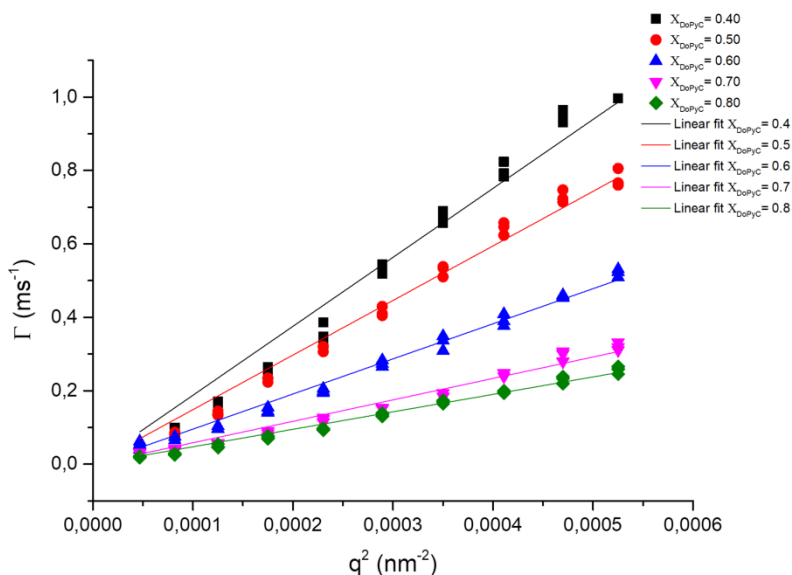
Figure 53. Relaxation rate Γ as a function of the scattering vector q for the **DoPyC/C4TS** system

The hydrodynamic radii for all samples investigated were calculated using Stokes-Einstein equation:

$$R_h = \frac{k_B T}{6\pi\eta D} \quad (25)$$

Figure 52 and **Figure 53** show that we are in the presence of well separated sets of data with different slopes and hence that we are dealing with aggregates with apparently different size. More precisely a decrease in the slope values is observed by increasing the molar fraction or in other words the cationic surfactant amount. Noteworthy, different slope values indicate different diffusion coefficient values that relate to the hydrodynamic radius of the aggregates. Larger aggregates form at higher molar fractions of **DTAB** and **DoPyC**. All parameters are reported in **Table 6**.

Usually, from the dependence of the mean decay time $\bar{\Gamma}$ on q, power law behaviour (i.e., $\bar{\Gamma} \propto q^{\gamma}$) is observed and for a diffusive mode, $\gamma = 2$.

One has to keep in mind that one has real R_h values only when a diffusive mode is observed (i.e., when $\gamma = 2$).

It was found that for molar fraction value $X_{surf.} = 0.4$ and to a lesser extent for $X_{surf.}$, exponents values are around 2.7. and 2.5, respectively. On the other hand, for the other molar fractions the exponents have values around 2. However, in **Table 6** the apparent values for R_h for the mixtures at $X_{surf.} = 0.4$ and $X_{surf.} = 0.5$, are reported even though $\gamma \neq 2$.

In order to further evaluate the polydispersity of these systems, linear fits of each relaxation rate curve were carried out; the R^2 values obtained are also reported in **Table 6**.

**Table 6.** DLS results for catanionic supramolecular aggregates at different molar fractions at 25 °C.

System	Molar fraction $(X_{surf.})$	R_h (nm)	D $(\mu m^2/s)$	PDI	R^2 value from linear fit
DTAB/C4TS	0.4	139 (3)	1.76 (4)	0.51 (3)	0.986
	0.5	155 (2)	1.58 (2)	0.24 (2)	0.993
	0.6	260 (2)	0.94 (1)	0.41 (3)	0.998
	0.7	311 (4)	0.79 (1)	0.46 (3)	0.991
	0.8	396 (8)	0.62 (1)	0.42 (4)	0.986
DoPyC/C4TS	0.4	130 (2)	1.88 (4)	0.30 (2)	0.990
	0.5	165 (2)	1.49 (2)	0.21 (2)	0.995
	0.6	255 (2)	0.96 (1)	0.38 (2)	0.997
	0.7	411(6)	0.60 (1)	0.49 (7)	0.993
	0.8	503 (6)	0.49 (1)	0.3 (1)	0.996

Static light scattering provides additional information on the structure of aggregates. The radius of gyration, obtained from a Guinier plot of the corrected intensity excess I(q) of the mixture solutions as a function of the magnitude of the scattering vector q (**Figure 54** and **Figure 55**), and I_0 values are listed in **Table 7**.
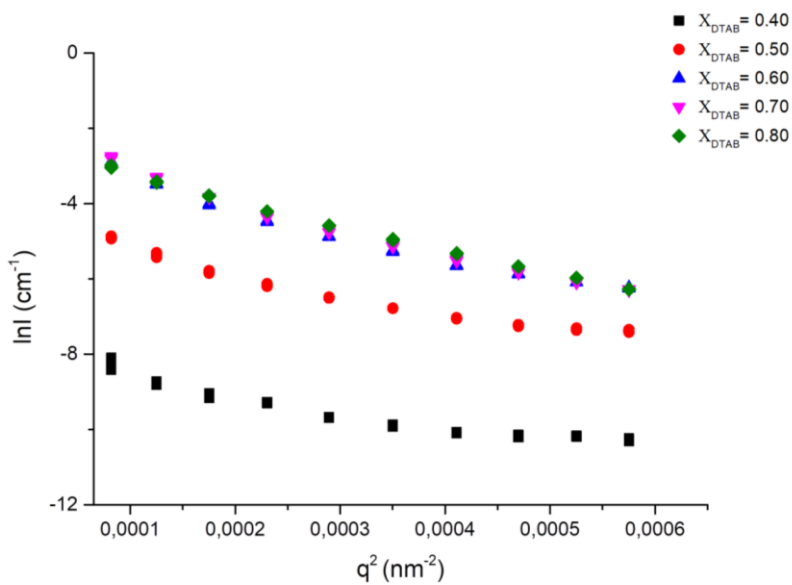
Figure 54. Guinier plot for the **DTAB/C4TS** system
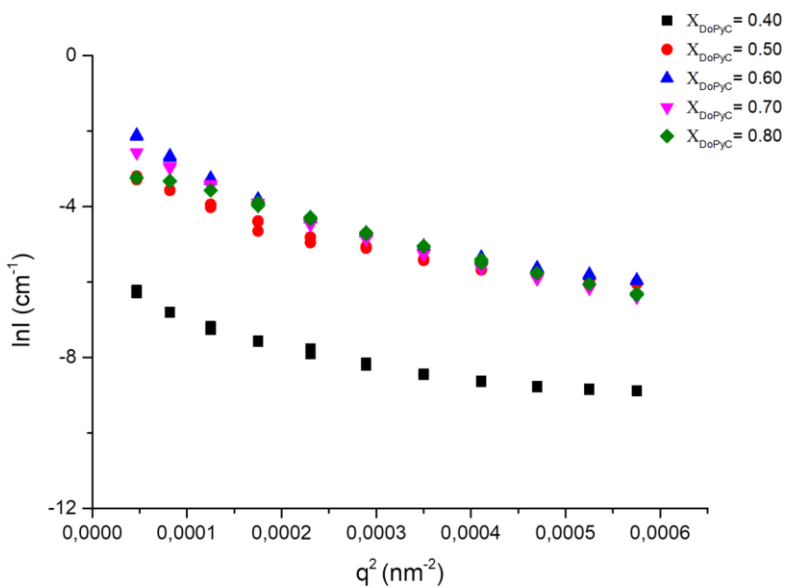
Figure 55. Guinier plot for the **DoPyC/C4TS** system.

Since the plot reported in **Figure 54** and **Figure 55** are not perfectly linear, presumably due to a rather high polydispersity in size, the R_g and I_0 calculation were performed also by taking the first data points (i. e. scattering angles in the range between 30° and 60°). Thus, two different values are reported for R_g and I_0, which come from *i.* a linear fit of the data points corresponding to the scattering angle values between 30° and 60° of the Guinier plot (SLS Initial slope) and from *ii.* a fit of all data points of the Guinier plot in **Table 7** .

Table 7. SLS results for catanionic supramolecular aggregates at different molar fractions at 25 °C.

System	Molar fraction $(X_{surf.})$	SLS Initial slope			
		R_g (nm)	I_0 (cm^{-1})	R_g (nm)	I_0 (cm^{-1})
DTAB/C4TS	0.4	114 (4)	0.0008 (1)	189 (19)	0.00030 (3)
	0.5	126 (3)	0.020 (4)	183 (14)	0.0092 (7)
	0.6	146 (3)	0.16 (2)	192 (9)	0.081 (8)
	0.7	149 (2)	0.18 (2)	193 (8)	0.094 (7)
	0.8	141 (1)	0.10 (1)	171 (8)	0.077 (2)
DoPyC/C4TS	0.4	119 (3)	0.0030 (5)	177 (12)	0.0014 (1)
	0.5	125 (3)	0.072 (9)	179 (9)	0.035 (3)
	0.6	145 (3)	0.18 (2)	192 (8)	0,096 (8)
	0.7	146 (2)	0.12 (1)	176 (7)	0.078 (5)
	0.8	135 (1)	0.047 (3)	125 (8)	0.0055 (1)

Evaluating the data reported in **Table 7**, one may immediately observe that the I_0 values increase of two orders of magnitude from $X_{surf.} = 0.4$ to $X_{surf.} = 0.6$. This shows that a relevant change in the aggregates formed occurs in the presence of an excess of free surfactant, once again highlighting the effective formation of the catanionic mixture. The I_0 values have allowed to determine the apparent molecular weight values for these systems, which may be useful

for suggesting the structure of the aggregates. Indeed, theoretical molecular weight values were calculated by using both the experimentally determined hydrodynamic radius and radius of gyration, assuming a particular shape for the aggregates. In this case, both values were used as the radius of an unilamellar vesicle with a bilayer of 3 nm, in line with literature reports for comparable systems.[58-62] The volume values calculated were then used for the molecular weight calculation. These parameters are reported in **Table 8** together with the aggregation number values. As the theoretical building block for these systems is formed by the supramphiphile, the molecular weights used in the aggregation numbers calculation are 1141 and 1116 g/mol for **DTAB/C4TS** and **DoPyC/C4TS**, respectivey.

Table 8. Experimental and theoretical molecular weight values calculated for catanionic supramolecular aggregates at different molar fractions at 25 °C.

System	Molar fraction $(X_{surf.})$	M_w (g/mol)	M_w (theoretical using R_g) (g/mol)	$N_{agg.}$	M_w (theoretical using R_H) (g/mol)	$N_{agg.}$
DTAB/C4TS	0.4	$5.1*10^6$ (2)	$8.0*10^8$	$4.7*10^5$	$4.3*10^8$	$7.0*10^5$
	0.5	$1.2*10^8$ (3)	$7.5*10^8$	$5.4*10^5$	$5.4*10^8$	$6.6*10^5$
	0.6	$9.8*10^8$ (1)	$8.2*10^8$	$1.7*10^6$	$1.5*10^9$	$7.2*10^5$
	0.7	$1.1*10^9$ (1)	$8.3*10^8$	$1.9*10^6$	$2.2*10^9$	$7.3*10^5$
	0.8	$6.3*10^8$ (8)	$6.5*10^8$	$3.1*10^6$	$3.5*10^9$	$5.7*10^5$
DoPyC/C4TS	0.4	$1.9*10^7$ (3)	$7.0*10^8$	$3.1*10^5$	$3.8*10^8$	$6.2*10^5$
	0.5	$4.4*10^8$ (6)	$7.2*10^8$	$5.2*10^5$	$6.1*10^8$	$6.4*10^5$
	0.6	$1.1*10^9$ (1)	$8.2*10^8$	$1.3*10^6$	$1.5*10^9$	$7.4*10^5$
	0.7	$7.7*10^8$ (7)	$6.9*10^8$	$3.2*10^6$	$3.8*10^9$	$6.2*10^5$
	0.8	$2.9*10^8$ (2)	$3.4*10^8$	$4.7*10^6$	$5.7*10^9$	$3.1*10^5$

The molecular weight values theoretical and experimental determined for both **DTAB/C4TS** and **DoPyC/C4TS** as a function of surfactant molar fraction are presented in **Figure 56** and **Figure 57**.
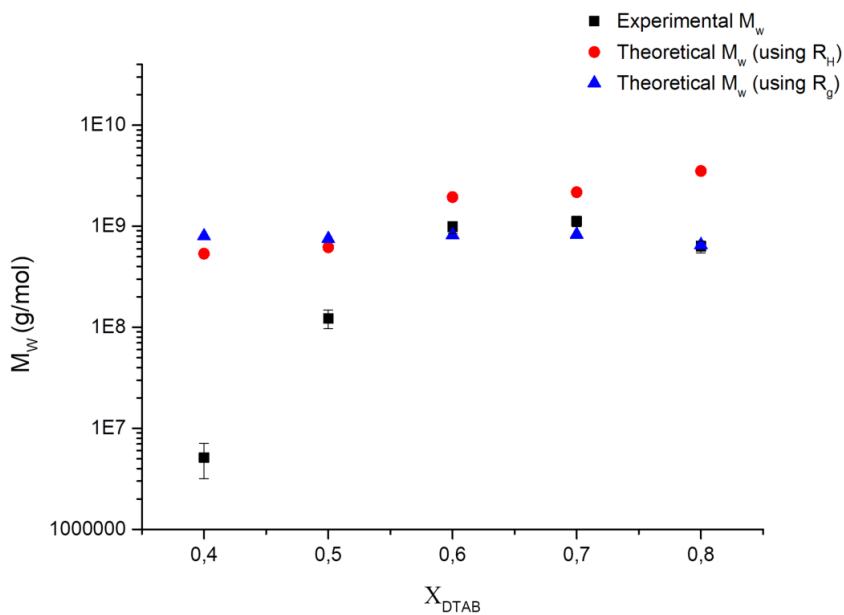
Figure 56. Apparent and theoretical molecular weight values as a function of molar fractions of **DTAB.**
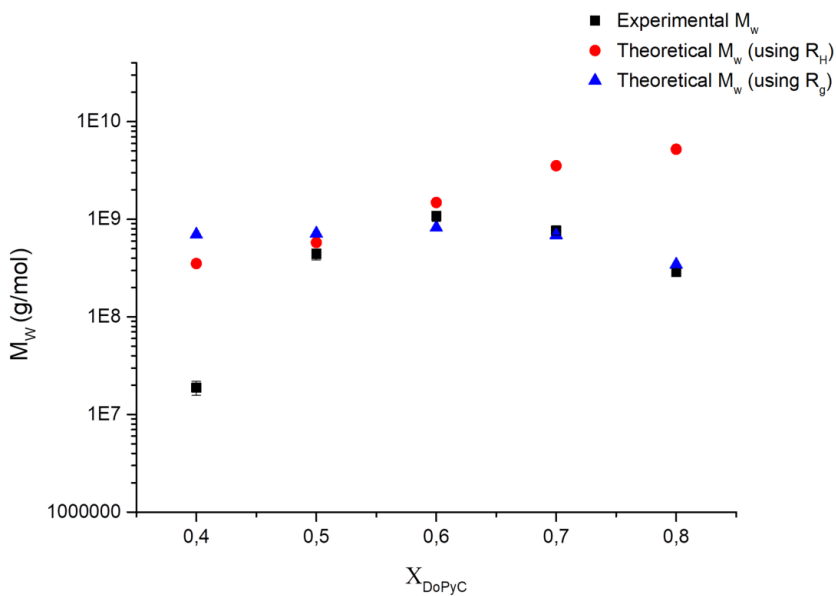

Figure 57 Apparent and theoretical molecular weight values as a function of molar fractions of **DoPyC.**

As graphically shown, no overlap is observed between experimentally and theoretically calculated molecular weight values at lower molar fraction (i.e X<0.6 and X<0.5 for **DTAB/C4TS** and **DoPyC/C4TS**, respectively), suggesting that vesicles formation does not occur under these conditions. On the other hand, one or both theoretical molecular weights are comparable to the experimental ones at higher molar fractions, indicating that structures present here are well-described as vesicles.

The hydrodynamic radius and the radius of gyration as a function of molar fractions of **DTAB** and **DoPyC** are shown in **Figure 58**.

The radius of gyration of the aggregates is not significantly altered by the amount of cationic surfactant (higher molar fractions), in both systems. By contrast, the molar fraction increase has a striking effect on the hydrodynamic radius of these supramolecular aggregates. The pronounced rise indicates a change of the shape. An explanation of the present results is that the supramolecular vesicles organize themselves into clusters at high molar fractions.[146] It may be assumed that DLS is dominated by the diffusive motion of the whole clusters resulting in a strong increase of hydrodynamic radius values.
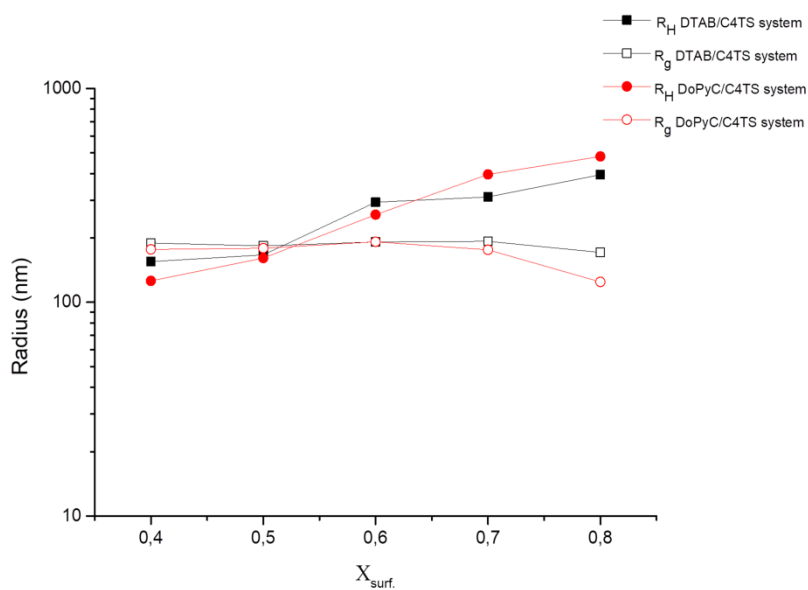
Figure 58. Hydrodynamic radius and radius of gyration values as a function of molar fractions of **DTAB** or **DoPyC**, respectively.

Since precipitation phenomena were observed for these systems, the samples stability was monitored over time. All the values reported above were calculated by measuring the samples in different times. The results obtained are reported in **Figures A33-A38**. Missing data at higher molar fractions for **DTAB/C4TS** system are due to precipitation.

Experimental

Materials

As to guests and host providers please see Experimental Section, Chapter 3. Both **C4TS** and the guests were dissolved in 25 mM phosphate buffer (pH 7.2). The buffer was chosen to keep the host in the penta-anionic form. All samples were prepared by mixing a proper amount of **DTAB** or **DoPyC** stock solutions with a proper amount of a **C4TS** stock solution.

Light Scattering Measurements

Light scattering is a powerful non-destructive technique for material characterization covering size and shape of particles, molecular weight of polymeric chains up to the structure of aggregates resulting from the aggregation process The technique is based on the scattering of light by the dispersed particles and, depending on the applied set up, we refer to dynamic light scattering (DLS) or static light scattering (SLS).

SLS measures the dependence of the average intensity of the scattered light at different scattering angles. Structural information about the particles, including size, shape and molar mass, can be obtained using SLS.

DLS measures the time autocorrelation of the scattered light intensity as a function of the delay time. The results obtained from DLS provide dynamic information about the diffusion coefficient(s) of the particles and, indirectly, about their size. This difference is schematically shown in **Figure 59**. A fundamental application of light-scattering techniques is the accurate measurement of the size distribution of particles in the dispersion.[147-150]
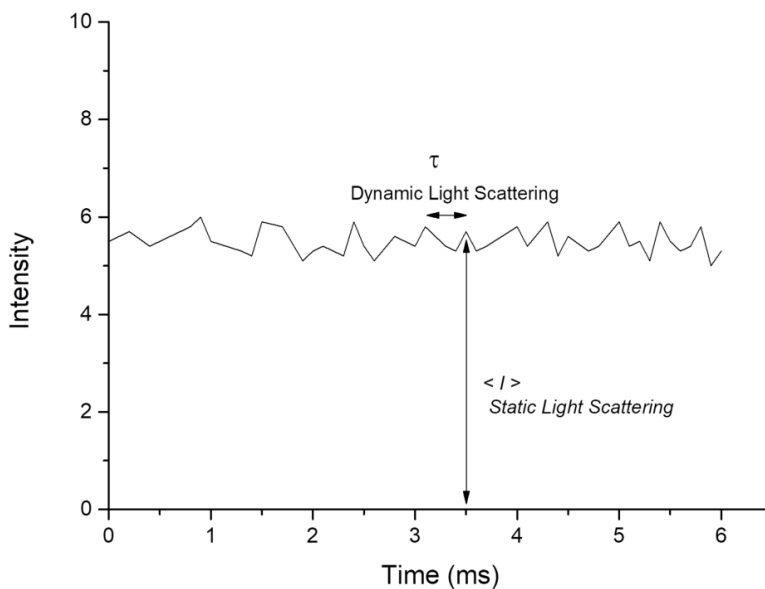
Figure 59. Light scattered from a solution containing particles has a mean intensity <*I*> that reflects the molecular weight of the particles while the fluctuations in the intensity have a characteristic fluctuation time, τ, that reflects the diffusion coefficient of the particles.

Dynamic Light Scattering

In a colloidal dispersion, suspended particles undergo Brownian motion. The motion results in fluctuations of the distances between particles and hence also in fluctuations of the phase relations of the scattered light. Additionally, the number of particles within the scattering volume varies over time. The end result is a fluctuating scattered intensity $I_s(q; t)$, in which q is the scattering vector directly related to the scattering angle θ, as follows:

$$q = \frac{4\pi}{\lambda \sin\left(\frac{\theta}{2}\right)} \quad (26)$$

where λ is the wavelength

The corresponding measured intensity correlation function may be expressed as:

$$g^2(q, \tau) = \frac{\langle I_s(q,t)I_s(q,t+\tau) \rangle}{\langle |I_s(q,t)|^2 \rangle} \quad (27)$$

where τ is the time delay. $g^2(q; \tau)$ can be related to the field correlation function $g^1(q; \tau)$ by means of the Siegert relation:

$$g^2(q, \tau) = 1 + \beta |g^1(q,t)|^2 \quad (28)$$

where β is the intercept. The field correlation function may be used to determine the diffusion coefficient D of the scatterers. The field correlation function $g^1(q; \tau)$ can be described by the following relation:

$$ln[g^1(q, \tau)] = -Dq^2\tau + \frac{c_v}{2}(Dq^2\tau)^2 + \cdots \quad (29)$$

where D is the intensity weighted diffusion coefficient, c_v is the coefficient of variation related to the sample polydispersity. Using the Stokes-Einstein equation and the viscosity of the surrounding medium, the radius R_h may be obtained:[151-153]

Static Light Scattering

In static light scattering experiments the intensity of light scattered due to the presence of objects (scatterers) with refractive index different from the surrounding medium is measured as a function of the scattering angle, θ.

In the simplest case, i.e. for monodispersed spherical particles, the average scattered intensity $I_s(q)$ is proportional to the particle form factor $P(q)$

$$I(q) = I_0 CNV_P^2 P(q) \quad (30)$$

where:

I_0 is the incident light intensity

C is the instrument constant that is a function of the experimental setup

N is the number of the particles

V_p is the volume of the particles.

In the case of monodispersed particles with diameter substantially smaller than the laser wavelength, $P(q)$ can be calculated analytically as follows:

$$P(q) = \left\{ \frac{3[\sin(qR_P) - qR_P \cos(qR_P)]}{(qR_P)^3} \right\}^2 \quad (31)$$

where R_p is the particle radius.

Since the size of particles is not known *a priory*, commonly a Guinier plot is used to extract the particles size. The Guinier plot allows for the determination of the Radius of Gyration (R_g) from the measured scattered intensity $I_s(q)$ as a function of the scattering angle θ. Using a logarithmic plot of the Guinier equation

$$\ln I_s(q) = \ln I(0) - R_g^2 \frac{q^2}{3} \quad (32)$$

R_g can be simply obtained from the slope of the linear fit of the $\ln I_s(q)$ *vs.* q^2.[154] The molecular weight M_w is estimated using the following equation:[155]

$$M_w = \frac{I(q \to 0)}{Kc} \quad (33)$$

where K is the optical constant and c is the concentration of the sample.

All measurements were carried out at scattering angles ranging from 30° to 130° at 25 °C using an ALV/CGS-3 instrument (ALV, Langen, Germany). The light scattering setup consists of a 22 mW He−Ne laser, an ALV CGS/8F goniometer, an ALV High QE APD detector, and an ALV 5000/EPP multibit, multitau autocorrelator.

All samples were prepared by dissolving both cationic surfactant and **C4TS** in 25 mM phosphate buffer, in order to have a concentration that is roughly three times above the critical aggregation/micellization concentration, previously determined by surface tension measurements.

Furthermore, in order to exclude the presence of aggregates below the CAC/CMC, samples prepared below these concentration values were also investigated. Measurements were performed at angles ranging from 30° to 130° with increments of 10°. Each measurement was run at least in triplicate.

Static light scattering (SLS) measurements of the corrected excess scattering intensity of the surfactant solutions (I(q)) as a function of the magnitude of the scattering vector q were treated by fitting the data using the Guinier plot to obtain the forward scattering intensity I(0), that allows to obtain the molecular weight of the aggregates, and the radius of gyration, R_g.

Dynamic light scattering measurements were analyzed by fitting the measured normalized time autocorrelation function of the scattered light intensity, $g^{(2)}(t)$, related to the second order cumulant expansion[156]

$$ln g^{(1)}(t, q) = \Gamma_1(q)t^2 + \frac{\Gamma_2(q)}{2}t^2 \quad (34)$$

CHAPTER 5 - ADSORPTION OF SUPRAMOLECULAR CATANIONIC MIXTURES AT THE SOLID/LIQUID INTERFACE

Adsorption of surfactants on a surface can modify its characteristics such as hydrophobicity, surface charge, and other key properties that are the basis of interfacial processes like flocculation, flotation, wetting, detergency, enhanced oil recovery and corrosion inhibition.

Adsorption is governed by a certain number of forces such as covalent bonding, electrostatic interactions, hydrogen bonding or non-polar interactions between the adsorbed species, lateral associative interactions, solvation and desolvation processes. The overall adsorption process results from some or all of these forces.

Adsorption can be considered as a partitioning of the surfactant molecules between the interface and the bulk, and it may occur if the interface is energetically favoured by the presence of the surfactant compared to the bulk solution.

The standard free energy of the adsorption process $\Delta \bar{G}_{ads}^0$ is the result of a number of contributing forces and can be defined as:

$$\Delta \bar{G}_{ads}^0 = \Delta G_{elec}^0 + \Delta G_{chem}^0 + \Delta G_{C-C}^0 + \Delta G_{C-S}^0 + \Delta G_H^0 + \Delta G_{H_2O}^0 + \cdots \quad (35)$$

where ΔG_{elec}^0 is the free energy contribution due to the electrostatic interaction, ΔG_{chem}^0 the chemical term due to covalent bonding, ΔG_{C-C}^0 the free energy gained upon interaction between methyl groups in the hydrocarbon chain, ΔG_{C-S}^0 the free energy due to interactions between the

hydrocarbon chains and the surface, ΔG_H^0 the hydrogen bonding term and $\Delta G_{H_2O}^0$ is the term resulting from dissolution or solvation of the adsorbate species or any species displaced from the interface due to adsorption.

For each surfactant/solid system, the number of terms in equation 34 depends on the solid and the surfactant nature, surfactant concentration, electrolytes and ionic strength, pH, temperature, etc.

Gu and Zhu[157] have developed two models, namely "one-step" and "two-step" model, that treat the adsorption process as reactions between unoccupied sites of a surface and surfactant molecules.

In the "one-step" model, the surfactant monomer interacts with the active site to form a hemi-micelle:

Site + Monomer $\rightleftarrows$ Hemi-micelle
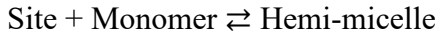
and the equilibrium constant of which is given by:

$$K = \frac{a_{hm}}{a_s a} \quad (36)$$

Where a_{hm}, a_s and a are the activities of the adsorbed hemi-micelle, surface site and surfactant monomer, respectively. At low concentration, a is equal to the surfactant concentration C.

By converting the activity to adsorption density (Γ) values through the mass action law, the final equation is:

$$\frac{\Gamma}{\Gamma_\infty - \Gamma} = KC^n \quad (37)$$

in which:

Γ_∞ is the maximum adsorption density at large solution concentrations

C is the surfactant concentration in solution

n is the aggregation number.

The "two-step" model originates from a modified one-step model in which the adsorption processis assumed to occur in two successive steps.

In the first step, surfactant monomers adsorb on the solid surface at concentrations below the critical aggregation concentration (cac) and yet no aggregates form.

Site + Monomer $\rightleftarrows$ Adsorbed Monomer
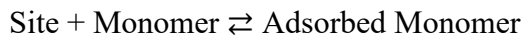
In the second step, the adsorbed surfactant monomers act as anchoring points for the formation of hemi-micelles:

$(n-1)$ Monomers + Adsorbed Monomer $\rightleftarrows$ Hemi-micelle

The general expression for the two-step model is:

$$\Gamma = \frac{\Gamma_\infty K_1 C(\frac{1}{n}+K_2 C^{n-1})}{1+K_1 C(1+K_2 C^{n-1})} \quad (38)$$

in which K_1 and K_2 are the equilibrium constants for the first and second reaction steps, respectively.[158]

While equilibrium adsorption isotherms of surfactants have been widely reported in the literature, less is known about the kinetics of adsorption. This lack of information is due to the relatively fast adsorption of surfactants and since adsorption isotherms are often measured by depletion measurements in systems that contain solid materials of relatively large surface area. Studies carried out using optical reflectometry, ellipsometry and quartz crystal microbalances (QCM) are filling this gap.

Atkin *et al*.[159-161] have reported about the use of optical reflectometry to monitor the kinetics of adsorption of CTAB to the silica-water interface and to investigate the role of micelles in this process. This research group found evidences of cooperative adsorption processes and suggested that, micelles directly adsorb on the surface, at bulk concentrations above the CMC. This type of cooperative adsorption was observed for other cationic surfactants as well. However, for a narrow concentration range, evidence suggests that surfactant adsorption can be extremely slow (for example, CTAB adsorption on silica from a bulk concentration of 0.66(CMC) requires a period of

several hours to be completed). This "slow adsorption region" was interpreted as a consequence of a stochastic process that determines how surfactants fill the available surface adsorption sites coupled with the fact that the structures on the surface have morphological order. These findings suggest that surfactants that aggregate onto a surface, may in some cases be kinetically trapped in local minima of the free-energy landscape.

Tiberg *et al.*[162] have studied adsorption and desorption kinetics of various polyethylene glycol monoalkyl ethers at the silica−water interface using ellipsometry. Their results show that the rate of adsorption increases as the bulk surfactant concentration increases, even above the bulk cmc. At all concentrations, the adsorption rate was fast at low observation times (attributed to the diffusion of monomers and micelles from the bulk to the surface) followed by slower adsorption rates at longer observation times (presumably reflecting saturation of the surface).

Eskilsson and Yaminsky[163] have reported on the adsorption of CTAB at the silica−water interface by using ellipsometry. Characteristic times of adsorption at the silica−water interface were found to be of the order of seconds near and above the critical micelle concentration but control adsorption times were larger at smaller concentrations due to diffusion phenomena. Interestingly, desorption by substitution of pure water for the solution proceeded rapidly (less than a minute at all concentrations).

Striolo *et al.*[164-166] have employed the quartz crystal microbalance with dissipation monitoring (QCM-D) to measure both the "apparent equilibrium" and the kinetics of surfactant adsorption from liquid systems onto solid surfaces. The term apparent equilibrium was introduced by the above authors to indicate results obtained when the bulk surfactant concentration is increased gradually. Indeed, they have demonstrated that the total amount of surfactant adsorption obtained as the bulk concentration increases from zero

to values above the CMC through small multiple steps is different than that observed when the bulk concentration is increased suddenly from zero to values above the bulk CMC.

The surfactants investigated were the non-ionic hexaethylene glycol monododecyl ether $CH_3(CH_2)_{11}(OCH_2CH_2)_6OH$ ($C_{12}E_6$) and the cationic cetyltrimethylammonium bromide $CH_3(CH_2)_{15}N(CH_3)_3Br$ (CTAB); while silicon dioxide and gold chips were the adsorbing surfaces.

The dynamics of adsorption was studied by plotting the percentage of the amount adsorbed compared to the equilibrium adsorption amount as a function of time. To assess the effect of micelles on the adsorption kinetics, adsorption from a solution well below the CMC was compared to that above the CMC. By fitting the kinetics data, two sequential steps were identified that characterize the adsorption of CTAB. The first, fast, first-order step is followed by a slower one that was ascribes to the reorganization of the surfactant molecules on the surfaces. Differences in the first step for the different surfaces were consistent with differences in the amount adsorbed below the CMC. For $C_{12}E_6$, the kinetics of adsorption on gold slows down significantly when the bulk concentration increases from below to above the critical micelle concentration, indicating that the presence of the micelles decreases adsorption. The adsorption of $C_{12}E_6$ on silica was identical for both the concentrations. The different adsorption kinetics could also be correlated to the structure of the surface aggregates suggesting that $C_{12}E_6$ forms monolayer-like aggregates on both gold and silica while CTAB yields bilayer-like structures on both gold and silica.

The adsorption process was also studied for mixed systems. Naderi e Claesson[167] have employed QCM-D to investigate the adsorption properties of a polyelectrolyte-surfactant mixture formed by the cationic polyelectrolyte poly(vinylamine), PVAm, and the anionic surfactant, sodium dodecyl

sulfate, SDS. The polyelectrolyte and the surfactant readily associate in bulk solution, resulting in increased solution turbidity once large aggregates are formed. Solutions were placed in contact with a polystyrene surface, and the adsorption process was monitored by following the changes in the resonance frequency and dissipation factor. Data obtained were analysed mostly using the Sauerbrey relation. It was found that PVAm adsorbs onto polystyrene in the absence of SDS; conversely, at high SDS concentrations, the surfactant dominates in the adsorbed layer.

Aim of the work

In the present thesis work, supramolecular systems formed by the anionic *p*-sulfonatocalix[4]arene and cationic surfactants have proved to act as effective anionic supramphiphile/cationic surfactant mixed systems in bulk conditions. In this chapter, the adsorption properties at the solid-liquid interface of two cationic surfactants, **DTAB** or **DoPyC**, in combination with the anionic calixarene **C4TS**, have been investigated at different compositions and concentrations by QCM-D experiments. Significant variations of the adsorbed amounts were found depending on compositions/concentrations of the mixtures; moreover, suitable changes in the shape of the kinetics curves were analysed and associated to possible adsorption mechanisms.

Study of the adsorption processes by quartz crystal microbalance with dissipation monitoring (QCM-D)

The QCM-D technique allows for the evaluation of the adsorption features of surfactants by measuring/monitoring the variations in frequency and dissipation (**Figures A39 – A54)** of suitable amphiphilic solutions flowing onto a gold surface. The adsorption processes involving the **DTAB/C4TS** and **DoPyC/C4TS** mixed systems have been studied at molar fractions $X_{surf.}$= 0; 0.2; 0.4; 0.5; 0.6; 0.8; 1 at two different concentrations, 0.01 wt% and 0.1 wt%, that are below and above CMC, respectively. All experimental data have been treated by using Sauerbrey equation, that allows to calculate the mass change corresponding to the frequency variation. This equation enables to properly estimate the mass adsorbed at the interface when the dissipation variation is negligible (rigid film). On the other hand, a large dissipation change due to the presence of a softer film at the interface, requires the use of other models (e.g., Voigt model).

For the main purpose of this work, Sauerbrey equation may be used also in the presence of large dissipation variations. Indeed, the mass values obtained when significant increases in dissipation occur might be underestimated by Sauerbrey equation; however, larger mass values (such as those likely obtained by using other models) would not change the main picture and the conclusions of this work.[168]

The plots of the adsorbed mass as a function of time, obtained at all molar fractions investigated at 0.01 wt% and 0.1 wt%, for both the **DTAB/C4TS** and **DoPyC/C4TS** systems, are reported in **Figures 60 – 63**.
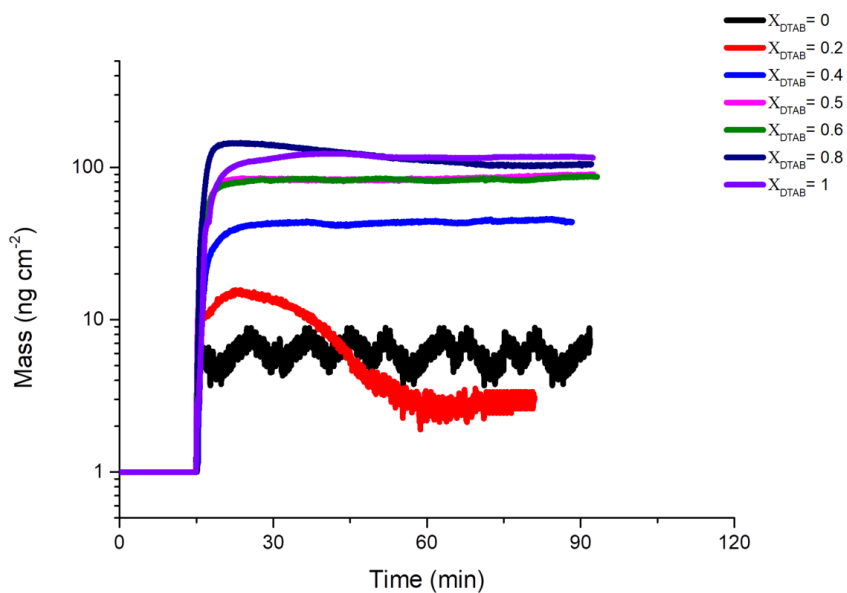
Figure 60. Adsorbed mass versus time at different molar fractions for the
DTAB/C4TS system at 0.01 wt%.
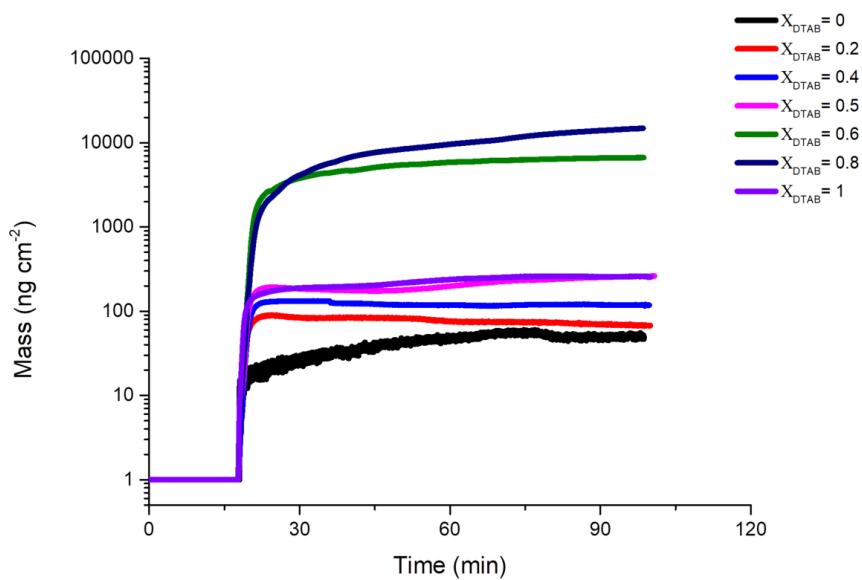
Figure 61. Adsorbed mass versus time at different molar fractions for the
DTAB/C4TS system at 0.1 wt%.
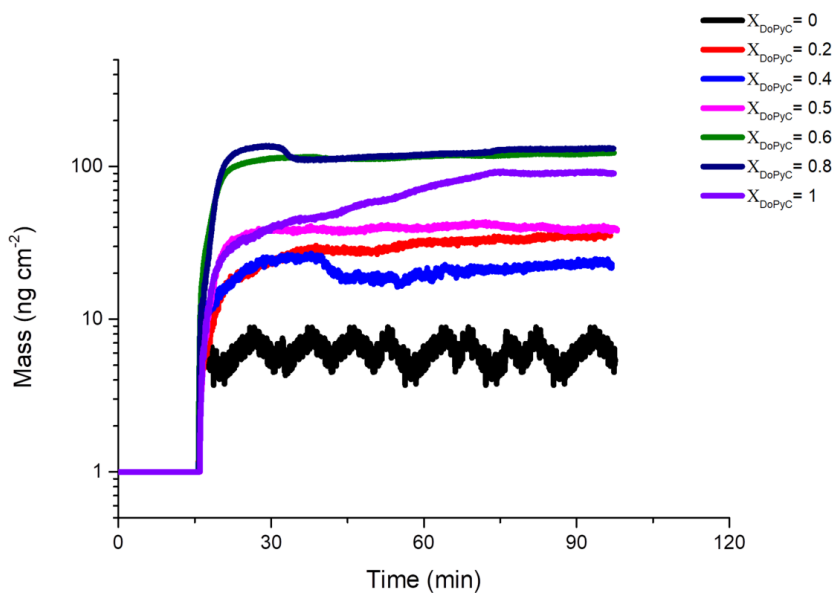
Figure 62. Adsorbed mass versus time at different molar fractions for the **DoPyC/C4TS** system at 0.01 wt%.
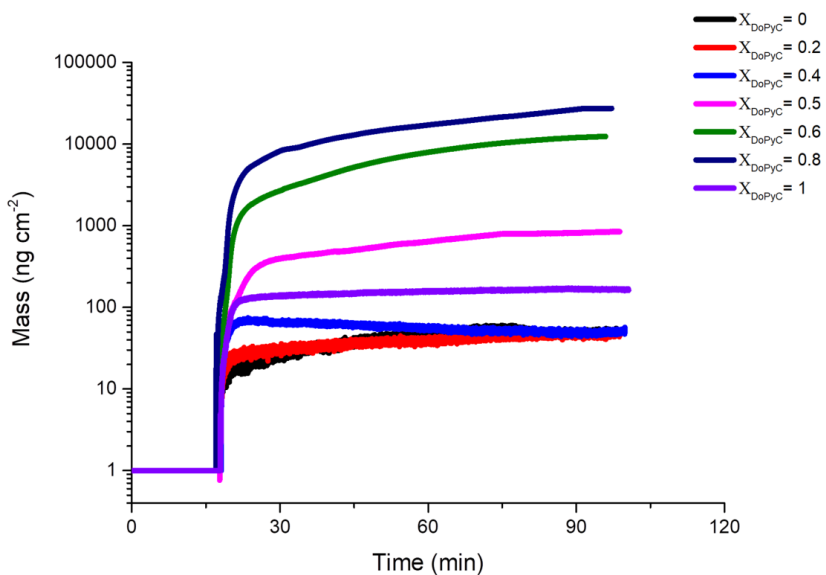
Figure 63. Adsorbed mass versus time at different molar fractions for the **DoPyC/C4TS** system at 0.1 wt%.

The values of mass adsorbed at each composition and concentration are reported in **Table 9**. These values are also shown in the plots of **Figure 64** and **Figure 65**.

Table 9. Mass adsorbed at different molar fraction values and different concentrations for the **DTAB/C4TS** and **DoPyC/C4TS** systems at 25 °C and pH 7.2.

	Mass adsorbed* (ng cm^{-2}) DTAB/C4TS		Mass adsorbed* (ng cm^{-2}) DoPyC/C4TS	
$X_{surf.}$**	0.01 wt%	0.1 wt%	0.01 wt%	0.1 wt%
0	6 (1)	50 (1)	6 (1)	50 (1)
0.2	2.8 (2)	62 (1)	35.3 (6)	47 (1)
0.4	44.0 (2)	119 (1)	23.1 (6)	49 (2)
0.5	89.1 (7)	286 (1)	39.0 (6)	1098 (5)
0.6	85.7 (4)	7413 (9)	122 (1)	12950 (9)
0.8	104.5 (8)	23201 (46)	131.0 (6)	35335 (50)
1	116.9 (8)	257 (1)	91 (1)	161 (2)

*Mass is calculated by using Saurebrey equation; σ in parenthesis.

** $X_{surf.}$ is calculated as $\dfrac{C_{surf}}{C_{surf}+C_{C4TS}}$
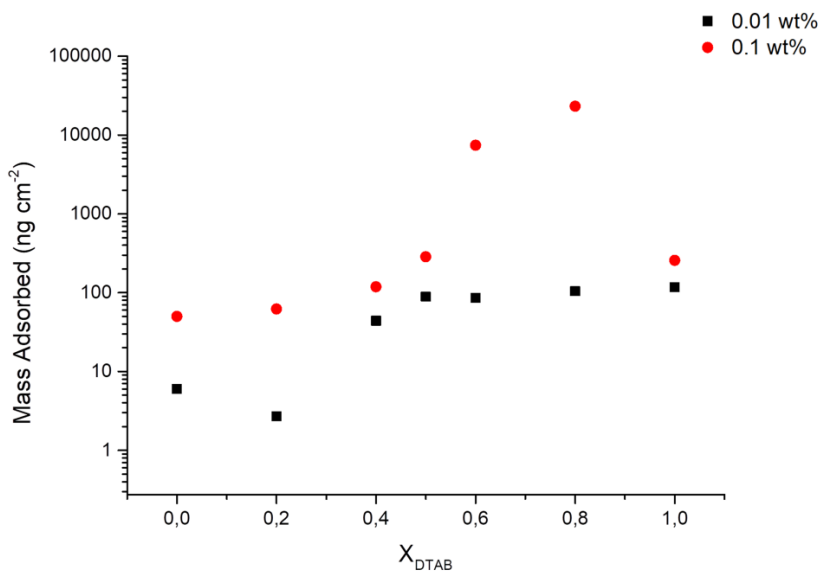
Figure 64. Mass adsorbed at 0.01 wt% (black squares) and 0.1 wt% (red circles) at different molar fractions for the **DTAB/C4TS** system.
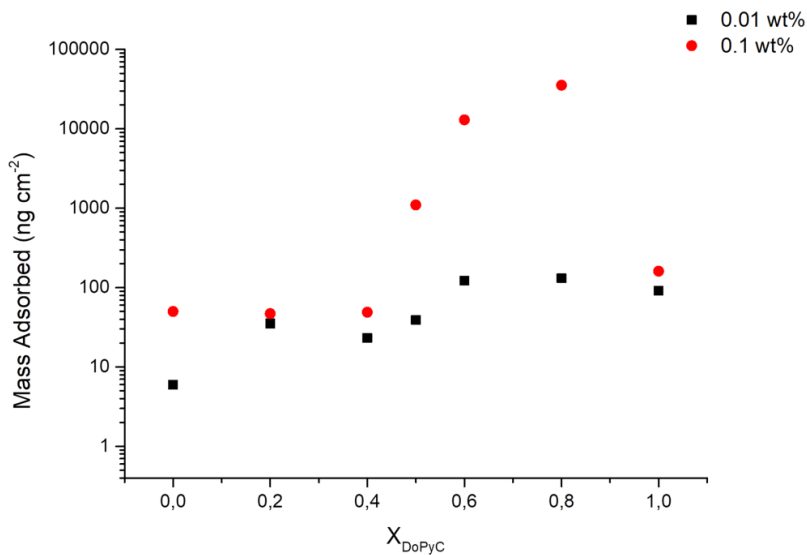
Figure 65. Mass adsorbed at 0.01 wt% (black squares) and 0.1 wt% (red circles) at different molar fractions for the **DoPyC/C4TS** system.

At 0.01 wt% the mass adsorbed increases as the molar fraction increases, suggesting that the cationic surfactant drives the adsorption process and the presence of calixarene does not basically affect this process. At all molar fractions, the total amount adsorbed never exceeds 130 ng cm^{-2}.

At higher concentrations (0.1 wt%) a totally different picture appears and three different behaviours can be identified at different molar fraction intervals (**Figure 61** and **Figure 63**).

- $0 < X_{surf.} < 0.5$: adsorption mass values are comparable to those obtained at lower concentration (0.01 wt%). Within this molar fraction range, the main species is the supramphiphile (since the excess of calixarene causes the complexation of almost all the surfactant molecules – see previous chapters) that acts as an actual surfactant.

- $0.5 \leq X_{surf.} \leq 0.8$: under this conditions, an increase of the adsorbed mass as the molar fraction increases was also found; however, these values are up to three orders of magnitude larger than those obtained at lower concentration. The systems are acting as effective catanionic mixtures, forming bigger aggregates that influence the adsorption process and consequently the total amount adsorbed.

- $X_{surf.} = 1$: under these conditions, in which there are only free surfactant molecules, the amount of adsorbed mass decreases and becomes comparable to that found at $X_{surf.} < 0.5$. Again we are dealing with a system containing only one active component.

All the above observations are schematically represented in **Figure 66**.
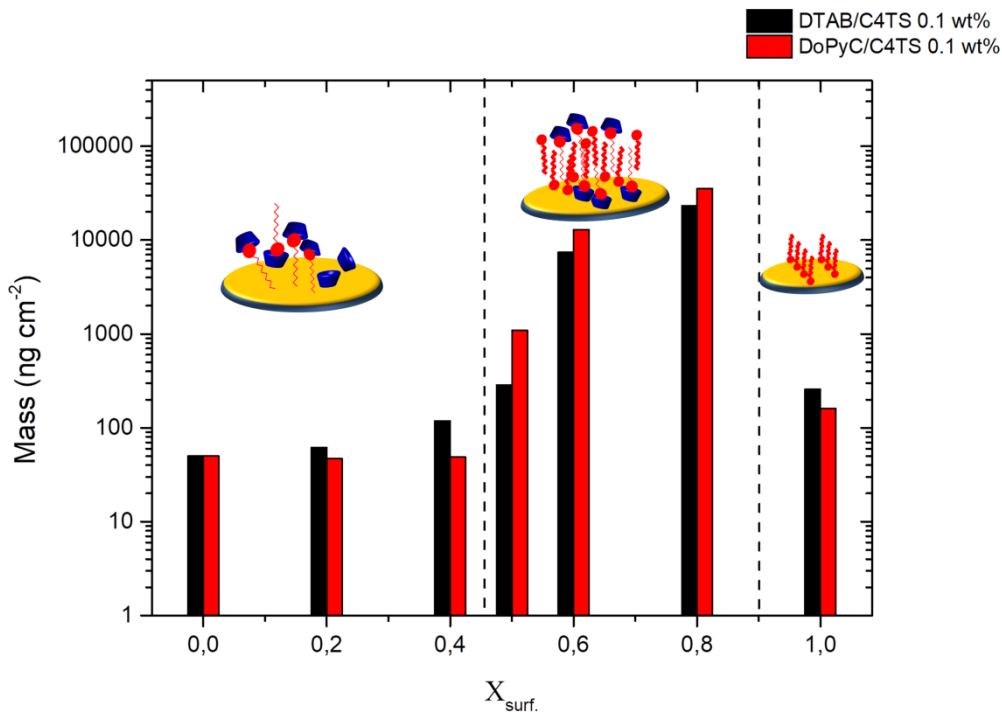
Figure 66. Schematic representation of the adsorption process at different molar fraction ranges at 0.1 wt% for the **DTAB/C4TS** (black bars) and **DoPyC/C4TS** (red bars) systems.

The dynamics of the adsorption processes can be examined by plotting the percentage of the amount adsorbed at the interface (compared to the equilibrium adsorption amount) as a function of time. In **Figure 67** and **68** experimental results expressed as a percentage of the equilibrium adsorbed amount ($\Gamma\%$) at each bulk concentration (0.01 wt% and 0.1 wt%) for some selected molar fraction values are reported for the **DTAB/C4TS** and **DoPyC/C4TS** systems, respectively. 100% adsorption corresponds to the maximum (equilibrium) adsorption amount with respect to the bulk surfactant concentrations used in the experiments.
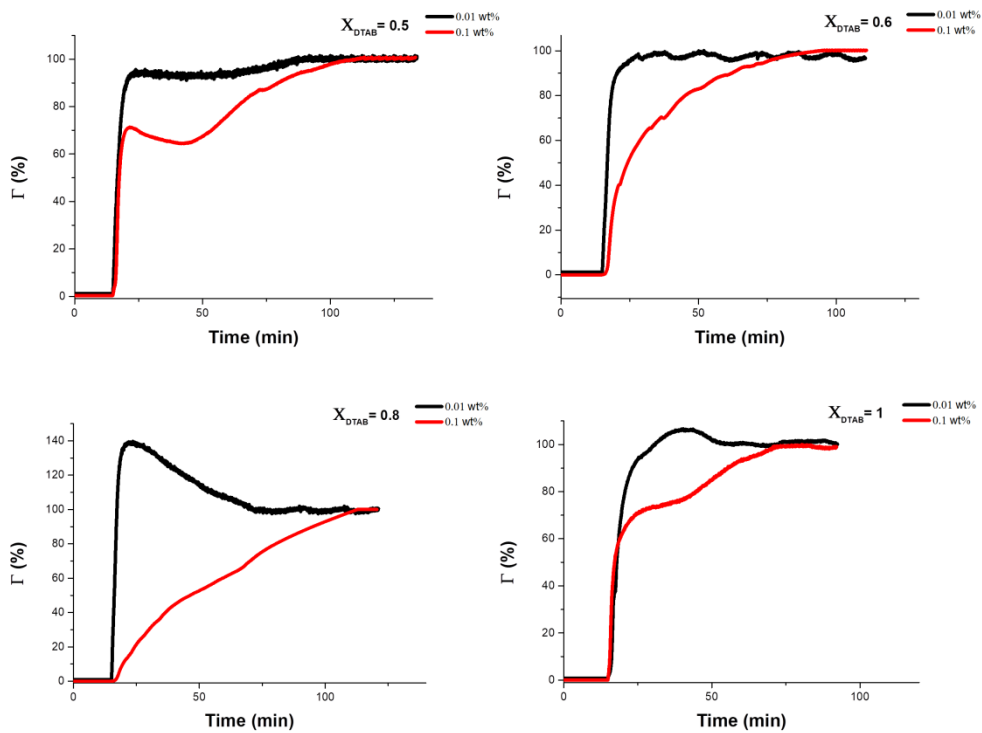
Figure 67. Percentage of the surfactant adsorbed on gold surface as a function of time for the **DTAB/C4TS** system at different molar fractions and at concentrations below (black line) and above (red line) the CMC.
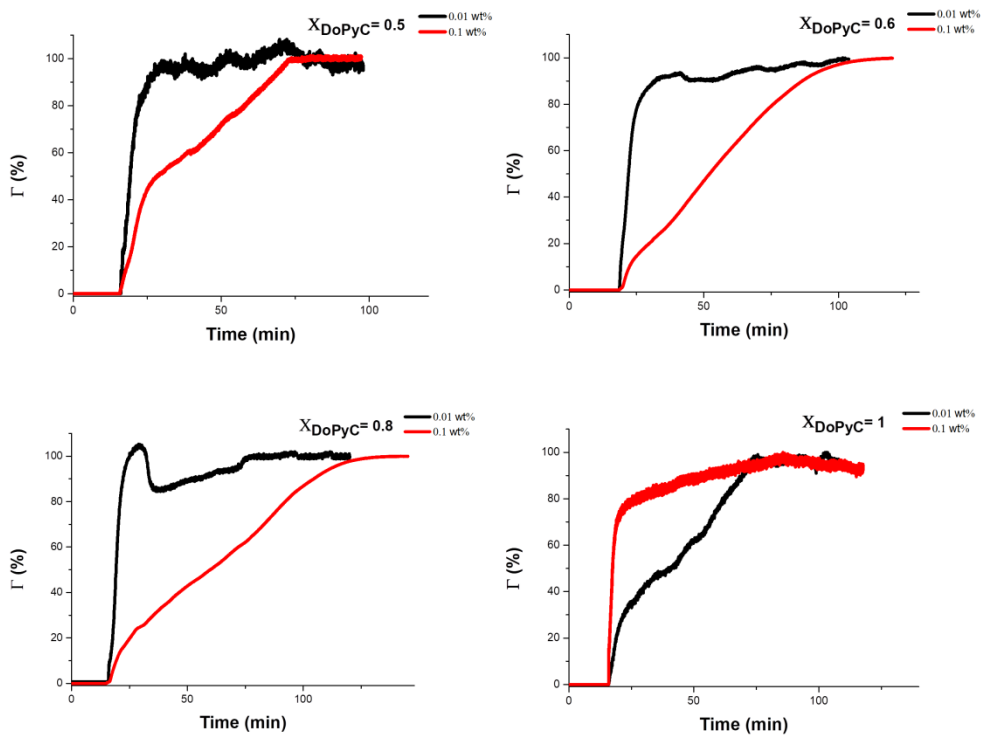
Figure 68. Percentage of the surfactant adsorbed on gold surface as a function of time for **DoPyC/C4TS** system at different molar fractions and at concentrations below (black line) and above (red line) the CMC.

The curves indicate that in the case of samples with 0.01 wt% concentration the mechanism of adsorption is similar regardless of the composition and the system examined: a fast increase in the mass adsorbed is followed by the achievement of a plateau. Since no aggregates are formed under these conditions, the adsorption process is driven by the monomeric species. An exception is pure **DoPyC** that surprisingly exhibits this one step behaviour at 0.1 wt% while at lower concentration a two steps mechanism was observed. Experimental curves recorded at higher concentration (0.1 wt%, red curves) clearly show two different regions/events: one in which the amount of

surfactant adsorbed quickly increases followed by a slower adsorption event until a plateau is reached. As demonstrated in the bulk studies, at 0.1 wt% and at $X_{surf} > 0.6$, these systems self-assemble forming vesicles-like aggregates that would need longer time intervals for deposition as bilayers on the surface. One may suppose that closed vesicles initially interact with the sensor surface and that this process occurs as soon as the solution reaches the sensor. Then, these aggregates rearrange at the interface forming multiple layer structures, as typically observed for catanionic mixtures.[167]

The percentages of the amount adsorbed on gold surfaces for both the investigated systems in the $0.5 \leq X_{surf} \leq 1$ range and at 0.1 wt% are displayed in **Figure 69** and **Figure 70.** A decrease of the rate of the second step of the adsorption process is observed as the molar fraction increases up to $X_{surf.}=0.8$, confirming that vesicles formation influences the adsorption. At $X_{surf.} = 1$, the adsorption process follows a one step mechanism, as commonly observed for cationic surfactants.

These systems behave as neutral catanionic mixtures (that usually aggregate into vesicles and may also form precipitate) at $X_{surf.}=0.8333$. When working at a slightly lower molar fraction (such as at $X_{surf.}=0.8$) to avoid precipitation, conditions for optimal vesicles formation are achieved, resulting in a very slow two step adsorption process.
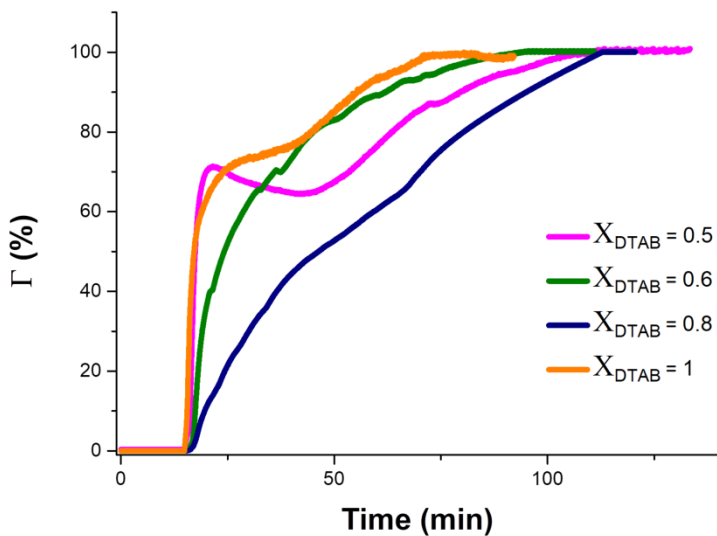
Figure 69. Percentage of the amount adsorbed on gold surfaces as a function of time for **DTAB/C4TS** system at different molar fractions at 0.1 wt%
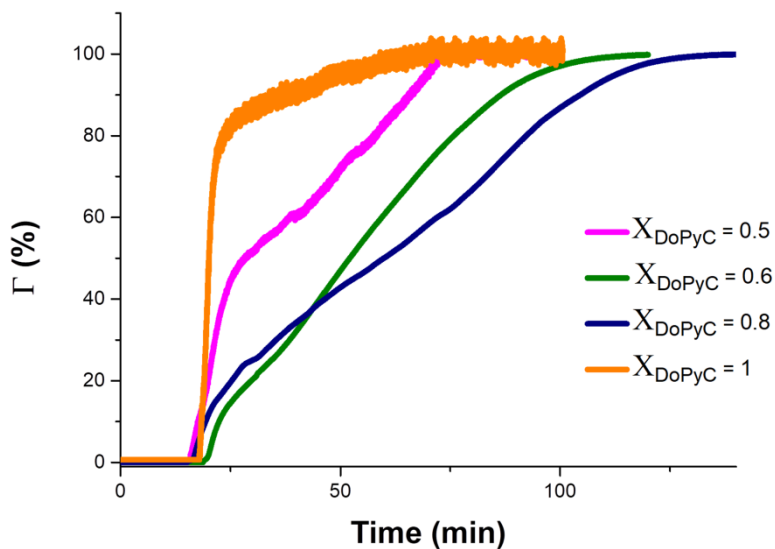
Figure 70. Percentage of the amount adsorbed on gold surfaces as a function of time for **DoPyC/C4TS** system at different molar fractions at 0.1 wt%

Experimental

Materials

As to guests and host providers please see Experimental Section, Chapter 3. Both **C4TS** and the guests were dissolved in 25 mM phosphate buffer (pH 7.2). The buffer was chosen to keep the host in the penta-anionic form. All samples were prepared by mixing a proper amount of **DTAB** or **DoPyC** stock solutions with a proper amount of a **C4TS** stock solution.

Samples preparation

Since the QCM-D instrument measures the variation of the frequency that is directly correlated to the mass adsorbed, each sample was prepared at the same total concentration (wt %) by varying the relative amount of the two components in order to have the desired molar fraction (see Chapter 3). Accordingly, any variation in the mass estimated may be attributed only to the different nature of the mixture since the total mass of the material flowing in the instrument chamber is kept constant. More precisely, two different total concentration values have been chosen, 0.01 wt% and 0.1 wt%, in order to have samples at concentrations below and above CMC, respectively. Under these conditions all mixtures are below (0.01 wt%) or above (0.1 wt%) CMC except for: free **DTAB** and **DoPyC** (that have higher CMC than 0.1 wt%), free **C4TS** (that is not a surfactant) and at molar fraction $X_{surf} = 0.2$. Higher concentrations cannot be explored for two main reasons: *i.* they would overlap with the CMC values of the free surfactants (indeed, the main advantage of using supramphiphiles is the lower CMC values compared to the free surfactants); *ii.* at higher concentration some samples do not show a satisfactory phase stability (see Chapter 3). Thus, while keeping the total concentrations constant, different molar fractions

have been investigated in the range from $X_{surf} = 0$ (free **C4TS**) to $X_{surf} = 1$ (free cationic surfactant) with an increment of 0.2. The molar fraction $X_{surf} = 0.5$ (equimolar condition) was also investigated. The experimental conditions employed are reported in **Scheme 5**.
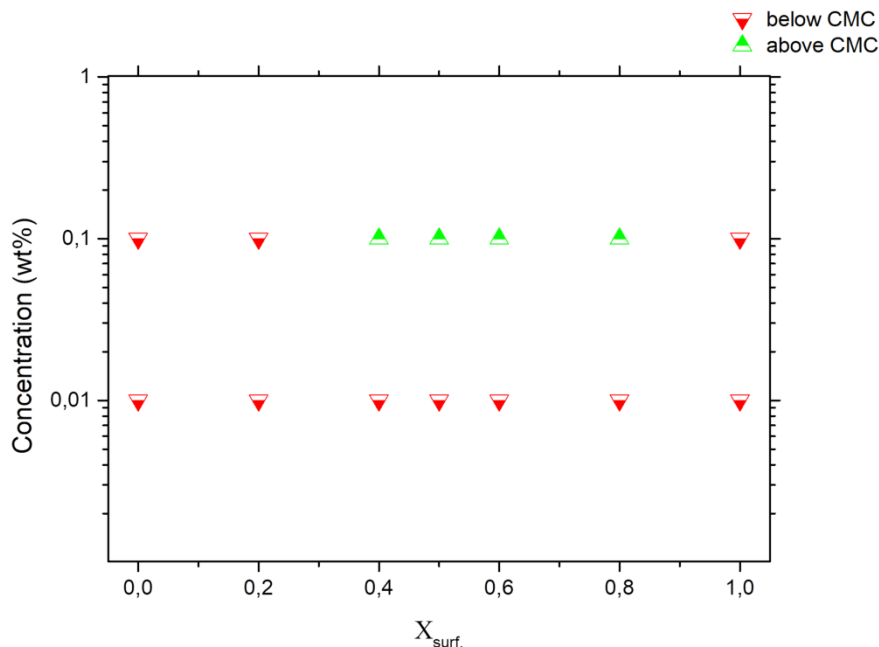
Scheme 5. Schematic representation of the relationship between the concentration values investigated (wt%) and the CMC values at different molar fractions.

QCM-D technique

Quartz crystal microbalance (QCM or QCM-D) is a fashionable and up-to-date technique for the study of soft and solvated interfaces. The dynamics of the interfaces between solid surfaces and bulk liquids is extremely important in fundamental research and technology. Examples of soft and solvated interfaces include biointerfaces that arise when biological systems interact

with inorganic materials (i.e. implants, biosensors, food processing and marine technologies). Another example is functional polymer coatings that control the binding or release of target molecules and provide lubrication or stabilization.

Since the organization of these interfaces is often determined by the interactions with the solvent, their study is challenging and hence calling for methods that can do so with as little modification as possible and that can zoom in on the role of solvent in these systems is of paramount importance. The interfaces organization changes also in response to external (chemical or physical) stimuli, and this requires methods that can monitor these changes in real time. Finally, these methods need to be quantitative.

QCM (and QCM-D) is able to meet these requirements. Indeed, this technique works in liquid phase, is able to monitor changes of the interface organization *in situ*, with a reasonable time resolution and without requiring labels, and can also provide information about the solvent inside interfacial films. [169-173]

QCM is based on the inverse piezoelectric effect discovered by the Curies in the late 19th century: application of voltage results in mechanical deformation of crystalline materials with certain symmetry properties. Alternating the applied voltage leads to a cyclical deformation, resulting in an oscillatory motion. If the frequency of the applied voltage matches the crystal resonance frequency (or multiples thereof called overtones), a standing wave is generated within the crystal (**Figure 71**).[174,175]
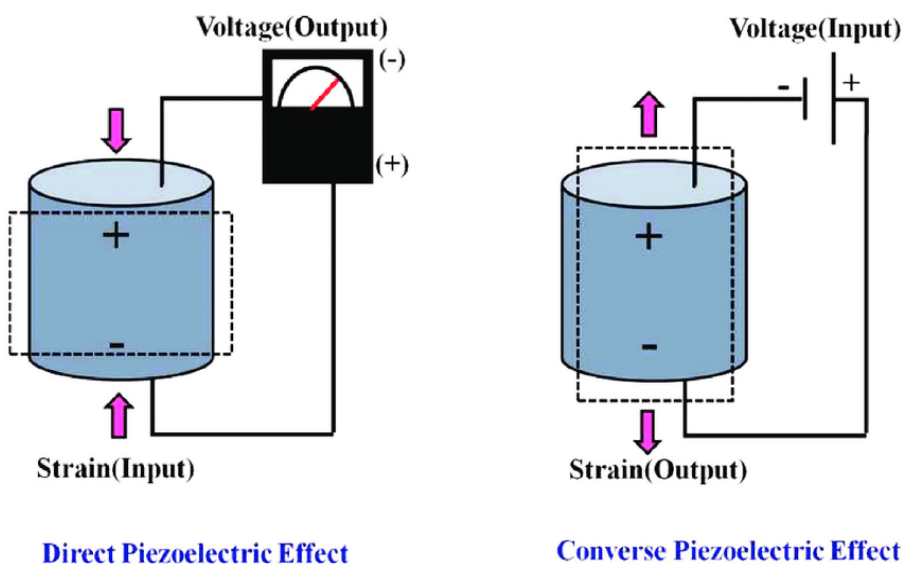
Figure 71. Direct and converse piezoelectric effect.

The cut of the crystal relative to its crystallographic axes may generate different kinds of oscillations. AT-cut crystal, such as that used in QCM (**Figure 72 a**), vibrates in the so-called thickness-shear mode, where the two surfaces move in an antiparallel fashion (**Figure 72 b**). In resonance, crystal surfaces are located at the antinodes of a standing wave with the wavelength:

$$\lambda = \frac{2d}{n} \quad (39)$$

in which d is the crystal thickness and n is the overtone order (odd), leading to the resonance frequency:

$$f_n = \frac{nc}{2d} \quad (40)$$

where c is the speed of sound in quartz. In liquids and gases, shear-waves decay rapidly, making QCM an interface-specific technique.

There are several ways to perform QCM measurements. One can examine the polarization at the crystal surface as a function of the frequency of the applied voltage, the so-called impedance analysis.[176] This yields two

parameters per overtone: the resonance frequency f_n and the bandwidth Γ_n (**Figure 72 c**). An alternative is the "ring-down" scheme developed by Rodahl *et al.*,[170] referred to as QCM-D, where the external driving voltage is turned off intermittently and the oscillations are left to decay freely. Given that quartz is piezoelectric, a voltage is generated during these decaying mechanical oscillations. This signal is recorded, also yielding two parameters per overtone: the resonance frequency f_n and the dissipation D_n (**Figure 72 d**). Bandwidth and dissipation are equivalent, with

$$D_n = \frac{2\Gamma_n}{f_n} \quad (41)$$

The third way to perform QCM measurements is with oscillator circuits. These can be quite cheap but usually operate on one harmonic only and provide only indirect access to the bandwidth via the oscillation amplitude. This limits data interpretation severely. All these approaches require that the quartz crystal is coated with electrodes (typically gold as showed in **Figure 72 a**).

The ubiquitous application of quartz crystals in oscillator circuits is based on their exceptional stability and very low energy dissipation. Their use as microbalances is based on the linear relationship between changes in the resonator mass and in the resonance frequency, derived by Sauerbrey's equation:

$$\Delta f_n = -\frac{n}{C}m_f = -\frac{n}{C}\rho_f h_f \quad (42)$$

where m_f is the areal mass density of the adsorbed film (mass per unit area), and ρ_f and h_f are the density and the thickness of the adsorbed film. The mass sensitivity constant C depends exclusively on the fundamental resonance frequency and the material properties of the quartz crystal.

The above is schematically reported in **Figure 72**.[177]
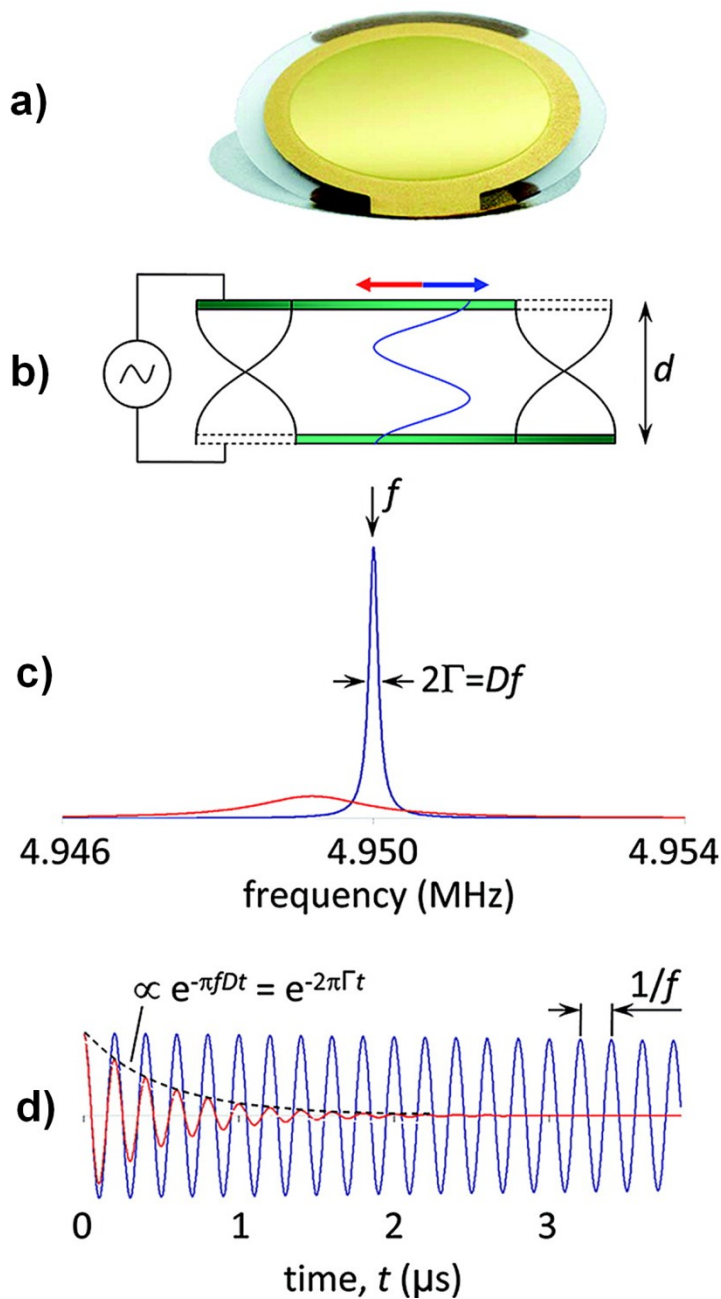
Figure 72. a) Picture of a T-cut crystal; **b), c)** and **d)** main phenomena involved in the QCM and QCM-D technique.[177]

In most applications, the adsorbed film is not rigid and the Sauerbrey relation becomes invalid. A film that is "soft" (viscoelastic) will not fully couple to the oscillation of the crystal and, hence, Sauerbrey relation will underestimate the mass at the surface. A soft film dampens the sensor oscillation. The damping or energy dissipation (D) of the sensor oscillation mirrors the film softness (viscoelasticity).
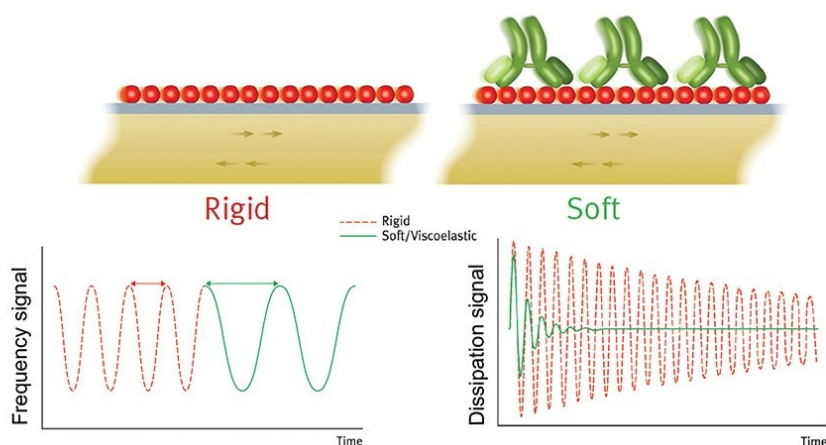
Figure 73. Frequency of the oscillating sensor crystal (gold) changes as the mass is increased by addition of a molecular layer (left diagram). Antibodies (green) are added to a layer of protein (red); difference in dissipation signal generated by a rigid (red) and soft (green) molecular layer on the sensor crystal (right diagram).

The energy dissipation D is defined as:

$$D = \frac{E_{lost}}{2\pi E_{stored}} \quad (43)$$

where:

E_{lost} is the energy lost during one oscillation cycle

E_{stored} is the total energy stored in the oscillator.

The energy dissipation of the sensor is measured by recording the response of a freely oscillating sensor that vibrates at its resonance frequency. This also allows to jump between the fundamental frequency and overtones (e.g. 15, 25 and 35 MHz), which provides additional information on the system under study. Indeed, the adhering film can be characterized in detail by carrying out measurements at multiple frequencies and analysing data by applying a viscoelastic model (e.g. the so called Voigt model).

Instrumentation

Measurements were performed using a Q-Sense E1 instrument composed of three parts: the flow module, which contains the sensor crystal and is connected to a peristaltic pump that forces the surfactant solution through the chamber, the chamber platform, which holds the module, and the electronics unit. These parts are all connected to a computer that monitors the different signals (resonance, oscillation frequency, and temperature) (**Figure 74**).

Figure 74. Q-Sense E1 instrument

The chamber platform is equipped with a precise temperature control. All measurements were carried out at 25±0.05 °C. All parts are connected with Teflon tubing. All crystals were purchased from Q-Sense AB and were coated with a 50 nm gold layer (QSX 301).

Cleaning procedures

Before starting an experiment, the solid surfaces on the sensing elements must be thoroughly cleaned. Surface treatment can influence the surface composition and consequently the adsorption of surfactants from the solution. Reproducible results can be obtained only when solid surfaces have been "conditioned" following strictly controlled procedures. The following cleaning procedure was employed:

1. UV/ozone treatment for 10 minutes;
2. the sensor is placed in a 5:1:1 mixture of milliQ water, ammonia (25 %) and hydrogen peroxide (30 %) at 75 °C for 5 minutes;
3. the sensor is rinsed with milliQ water and dried with nitrogen gas;
4. UV/ozone treatment for 10 minutes.

After conditioning, the crystal was inserted into the flow module. A cleaning procedure is necessary also for the chamber before each experiment:

1. a "sacrificial" sensor is mounted into the flow module;
2. 20 ml of a 2% Hellmanex II solution are pumped through the system, while heating up to 30 °C;
3. 100 ml of milliQ water are pumped through the system and then all the visible parts are dried with nitrogen gas.

Measurements

Measurements were carried out after obtaining a stable baseline by flowing 25 mM phosphate buffer over the crystal sensor. The baseline was assumed

to be stable when the drift observed was smaller than ±0.2 Hz for at least 15-20 min. Sometimes the crystal had to be left in the module under flux overnight before the baseline was sufficiently stable.

Each solution containing the surfactant mixture flowed through the flow module (which contains the crystal sensor) at a constant flow rate of 0.100 mL/min for 1 h, during which surfactants/mixtures are adsorbed on the crystal. After the pump was stopped, the signal was recorded until a plateau was reached. The waiting time can be either as short as 20 min or as long as 2 to 3 h, depending on the surfactant concentration and the amount adsorbed on the crystals. Frequency data were converted into adsorbed mass values by using Sauerbrey equation.

CONCLUSIONS

In this thesis work, a comprehensive characterization of calix[4]arene-based supramolecular amphiphiles has been reported, moving from the thermodynamics of the formation of these unconventional surfactants to the properties at the solid/liquid interface of suitably mixed catanionic systems. Each part of this work represents a fundamental starting point for the next one, since the thermodynamic characterization has allowed to establish the composition of the aggregates formed by the mixed systems and the aggregation features have offered insights on the phenomena that occur at the solid/liquid interface.

The results obtained enable to draw the following conclusions:

- *p*-sulfonato-calix[4]arene (**C4TS**) and cationic surfactants form very stable host-guest complexes in neutral aqueous solution, and this process is always enthalpically driven. The stability of the host-guest complexes, that is not affected by either the length of the alkyl chain or the nature of the head the surfactants, makes these adducts promising candidates as supramphiphiles;

- Cationic surfactants in the presence of **C4TS** self-aggregate at a much lower concentration than their parent free uncomplexed surfactants; the CMC values of supramphiphiles containing a homogeneous series of guests decreases as the tail length increases. Supramphiphiles having longer alkyl chains have more favourable ΔH^0_{mic} values resulting from stronger hydrophobic interactions. The ΔS^0_{mic} is always positive due to the large desolvation of the alkyl chains of the supramphiphiles upon micellization;

- Mixtures of anionic and cationic surfactants offer an attractive approach for the construction of complex self-assembled nanostructures and the formation of host–guest complexes between macrocyclic hosts and surfactant monomers is a different and appealing strategy to modulate the physicochemical properties of these systems. Thus, mixed systems formed by the calixarene host **C4TS** with selected cationic guests have been studied in order to assess whether these host-guest based systems still behave as conventional surfactant mixtures.

- The binding constant values have allowed to accurately establish the amount of each component at every composition and, since one is dealing with a mixture, a thorough phase behaviour examination has been carried out in order to fix the phase boundaries for each system.

- Surface tension measurements have allowed to determine the change of the critical aggregation concentration values with varying the composition of the mixtures. The synergistic behaviour of these mixtures has been evaluated and critical parameters such as surface excess concentration and area per molecule have been also determined;

- Light scattering measurements have allowed for the determination of the dimensions of the aggregates as a function of the mixture composition; interesting structural changes, corresponding to variations in size and shape of the aggregates, have been also identified. Under the proper conditions, the structures investigated may be correctly described as vesicles;

- These mixed systems have shown different thermodynamic stability over time that depends on their composition; thus suitable light

scattering experiments over time also unveiled relevant insights of the aggregates characteristics;

- The adsorption properties at the solid-liquid interface of selected surfactants in the presence of the anionic calixarene (**C4TS**) have been investigated at different compositions and concentrations by QCM-D experiments;

- At lower concentration, the mass adsorbed on a gold surface increases as the molar fraction increases, suggesting that the cationic surfactant drives the adsorption process and the presence of the calixarene does not basically affect the adsorption process;

- At higher concentrations, three different behaviours have been identified at specific molar fraction intervals: the increase in the molar fraction causes the switch from a system containing only one active component (i.e., the supramphiphile) to an effective catanionic mixture which forms bigger aggregates that influence the adsorption process and consequently the total amount adsorbed (that is maximum under these conditions). Finally, in the presence of free surfactants only, the amount of adsorbed mass decreases and becomes comparable to that found for the supramphiphiles;

- The dynamics of the adsorption processes has been also examined. For samples at lower concentration, a "one step" mechanism of adsorption driven by monomers has been always found, regardless of the composition and the system examined. At higher concentration, a "two step" process occurs, one in which the amount of surfactant adsorbed on the surface quickly increases followed by a slower adsorption event until a plateau is reached.

- This thesis work on sulfonatocalixarene-based supramphiphiles has offered a quantitative standpoint on the main properties of these

amphiphilic systems, providing the basis for their potential use in various fields. The applications of nanosystems resulting from the self-assembly of supramolecular amphiphiles, such as liposomes, micelles, nanoparticles and hybrid materials in cancer diagnostics and therapeutics are expected to attract growing attention in the next few decades. Through suitable noncovalent functionalization, these supramolecular nanosystems may be employed as functional vehicles to deliver drugs, to enhance water solubility of poorly soluble therapeutic agents as well as to alter and control drug release rate and bioavailability *in vitro* and, hopefully, also *in vivo*.

APPENDIX – SUPPLEMENTARY MATERIALS
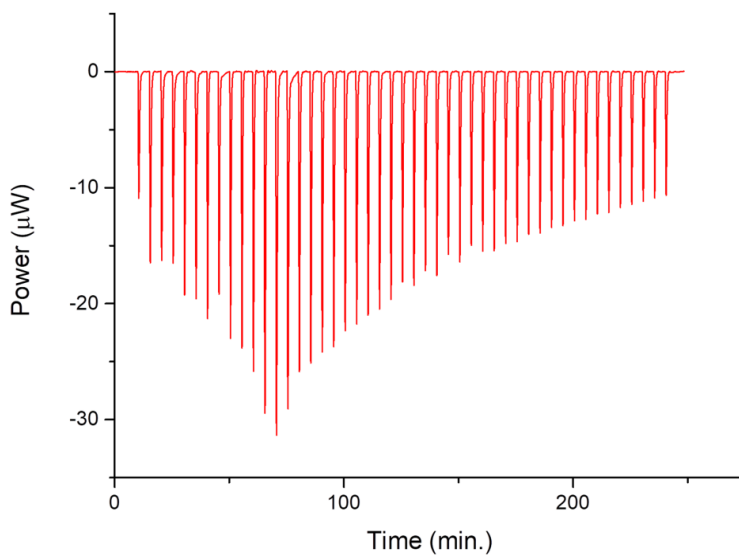
Figure A1. Titration of sodium dodecylsulphate (**SDS**, 100 mM) at 25 °C in plain water
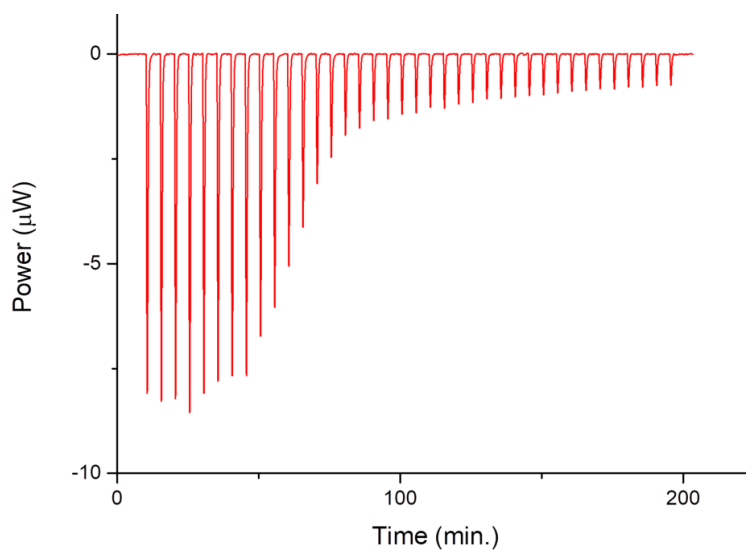
Figure A2. Titration of sodium dodecylbenzensulphonate (**SDBS**, 25 mM) at 25 °C in plain water
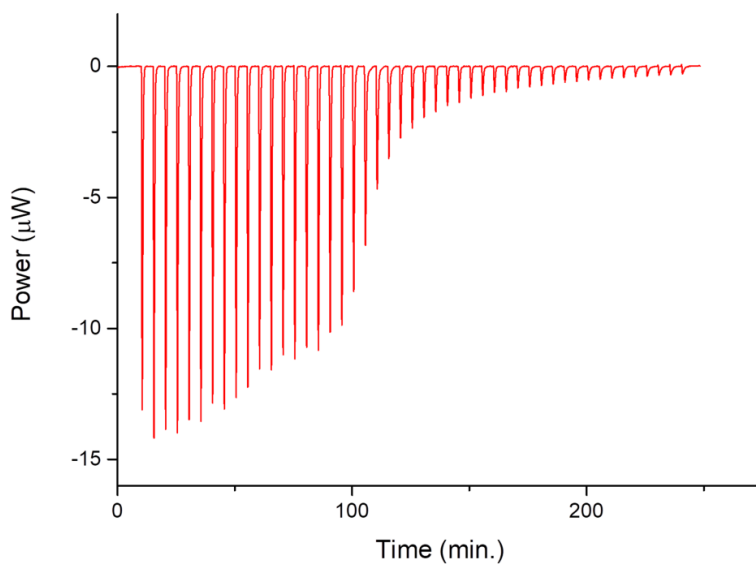
Figure A3. Titration of cetyltrimethylammonium bromide (**CTAB**, 10 mM) at 25 °C in plain water
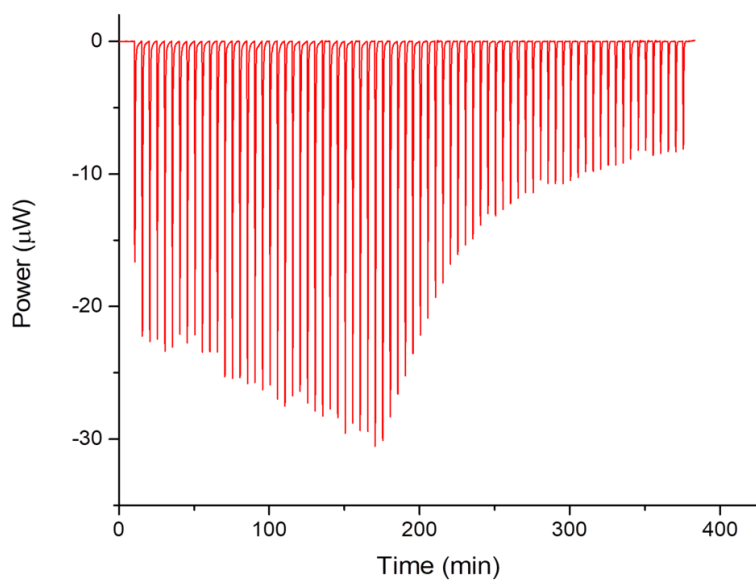
Figure A4. Titration of dodecyltrimethylammonium bromide (**DTAB**, 150 mM) at 25 °C in plain water
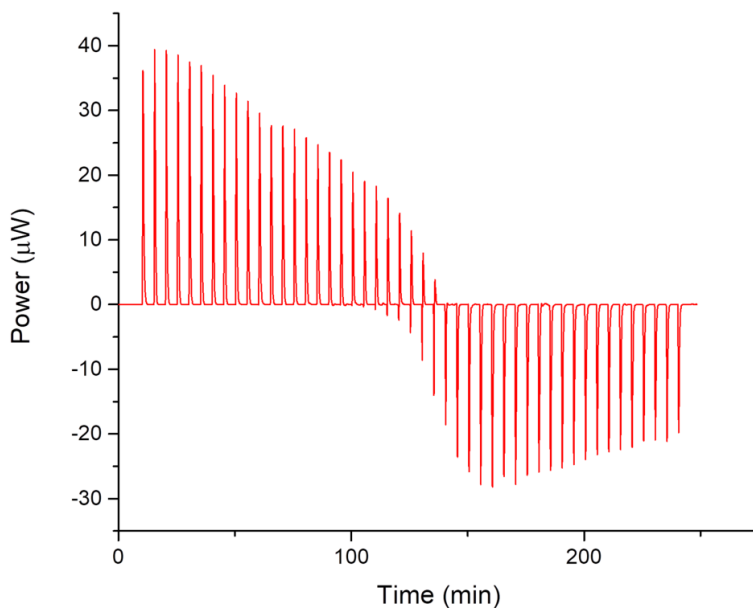
Figure A5. Titration of dodecylpyridinium chloride (**DoPyC**, 150 mM) at 25 °C in plain water

Table A1. Thermodynamic parameters for micelle formation at 25 ° C in plain water

Surfactant	CMC (M)	ΔH_{mic} (kJ mol^{-1})
SDS	0.0076 (2)*	0.4 (1)
SDBS	0.0152 (2)	1.8 (2)
CTAB	0.00096 (3)	6.3 (1)
CetPyr	0.00065 (3)	9.3 (3)
DTAB	0.0152 (1)	1.4 (2)
DoPyC	0.0146 (1)	-4.3 (3)

*σ in parenthesis
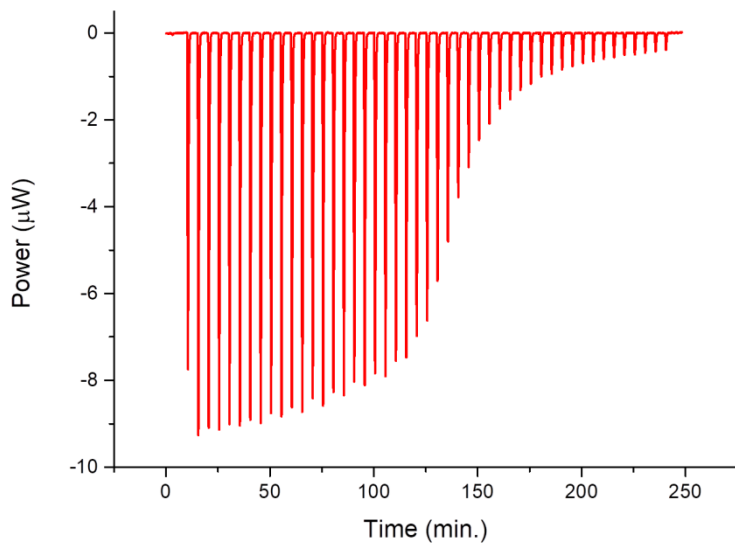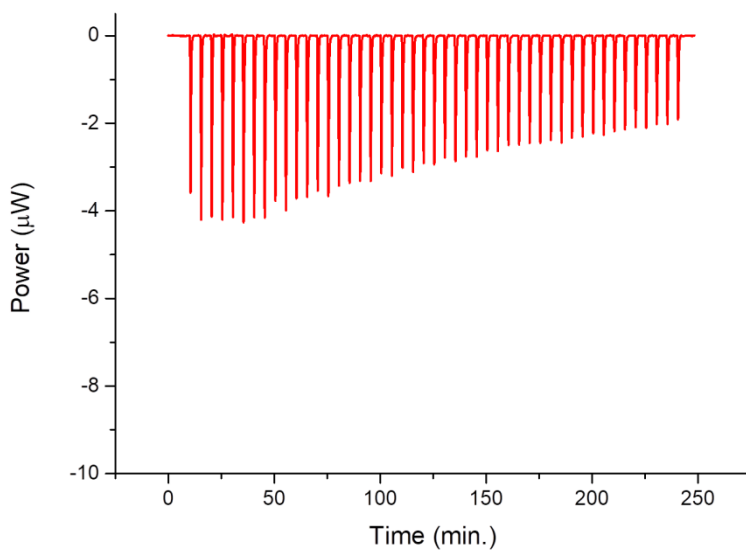
Figure A6. Titration of Cetyhlpyridinium chloride (5 mM) at 25 °C **a)** in plain water; **b)** in phosphate buffer 25 mM
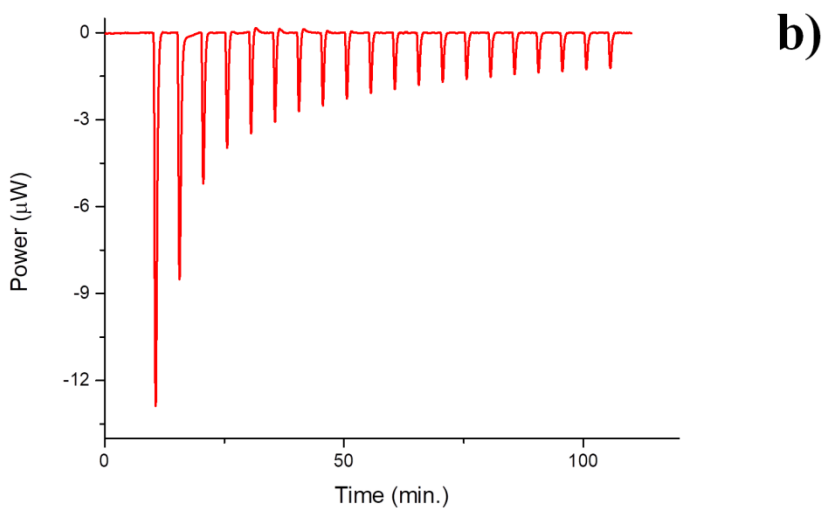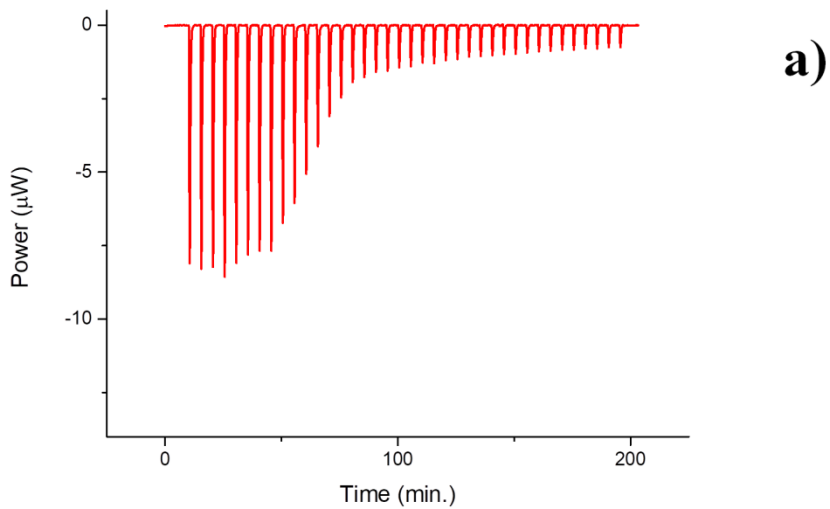
Figure A7. Titration of sodium dodecylbenzensulphonate (**SDBS**, 25 mM) at 25 °C **a)** in plain water; **b)** in phosphate buffer 25 mM
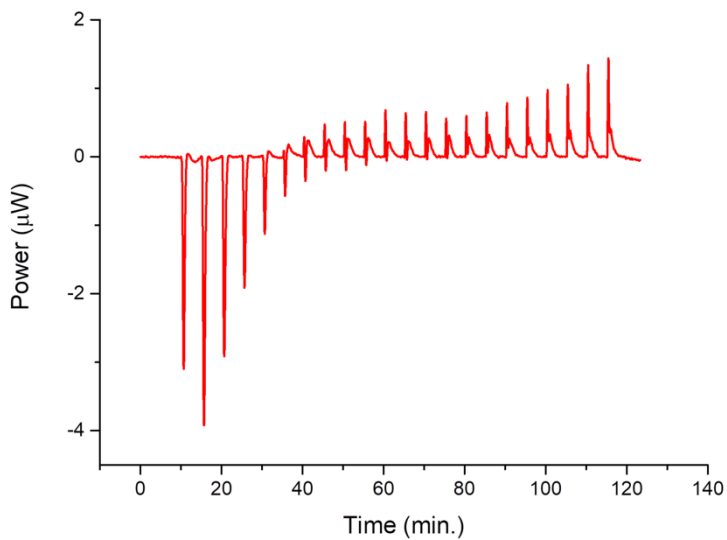
Figure A8. Titration of sodium dodecylbenzensulphonate (**SDBS**, 25 mM) at 25 °C in phosphate buffer 25 mM (pH 7.2).
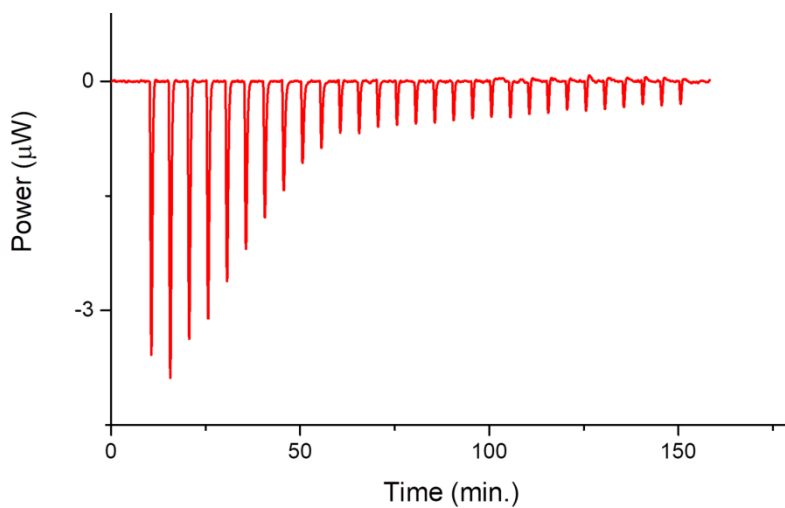
Figure A9. Titration of sodium dodecylbenzensulphonate (**SDBS**, 25 mM) at 25 °C in MOPS 50 mM (pH 7.2).
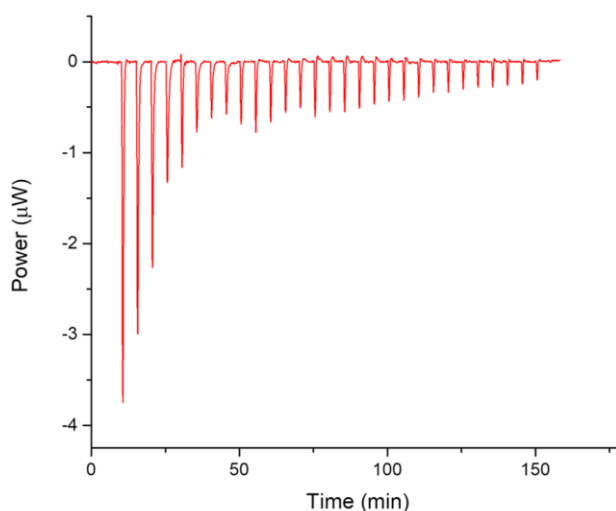
Figure A10. Titration of sodium dodecylbenzensulphonate (**SDBS**, 10 mM) at 25 °C NaCl 50 mM.

Table A2. Thermodynamic parameters at 25 ° C for **SDBS** in the presence of ionic background.

Ionic Background	CMC (M)	ΔH^0_{mic} (kJ mol^{-1})
Phosphate buffer (25 mM)	0.00040 (2)*	-2.0 (1)
MOPS (50 mM)	0.00049 (2)	-2.4 (1)
NaCl (50 mM)	0.00043 (3)	-2.1 (3)

*σ in parenthesis.
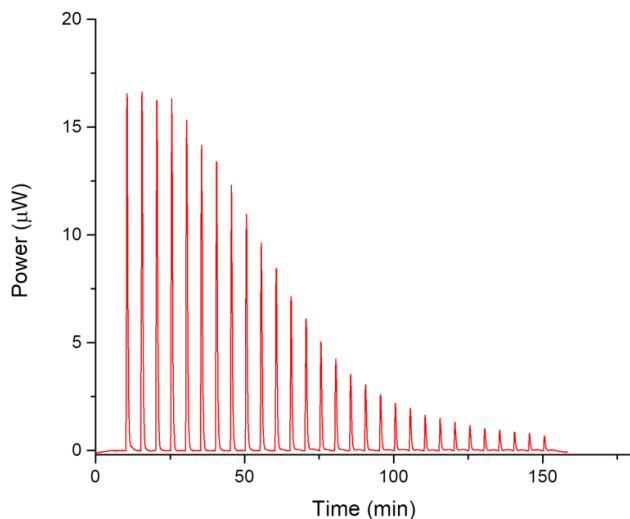
Figure A11. Titration of octyltrimethylammonium bromide 3 mM (**OTAB**) into **C4TS** 0.3 mM at 25 °C in buffered aqueous solution (pH 7.2, phosphate buffer).
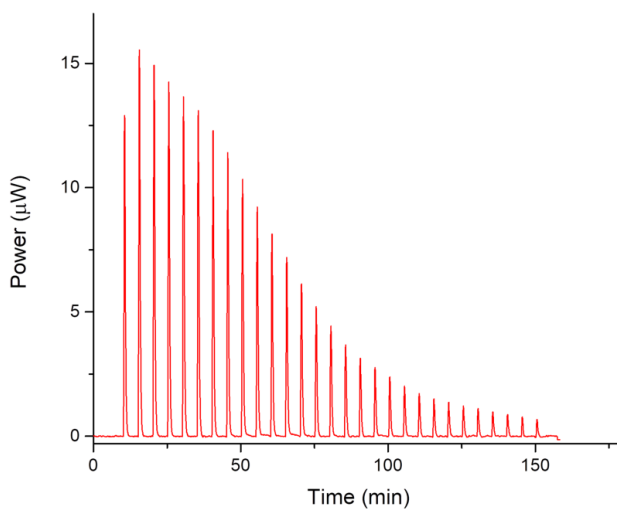
Figure A12. Titration of decyltrimethylammonium bromide 3 mM (**DeTAB**) into **C4TS** 0.3 mM at 25 °C in buffered aqueous solution (pH 7.2, phosphate buffer).
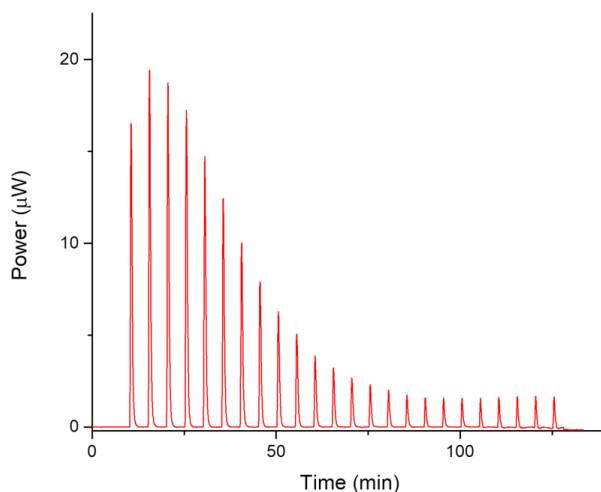
Figure A13. Titration of dodecyltrimethylammonium bromide 3 mM (**DTAB**) into **C4TS** 0.3 mM at 25 °C in buffered aqueous solution (pH 7.2, phosphate buffer).
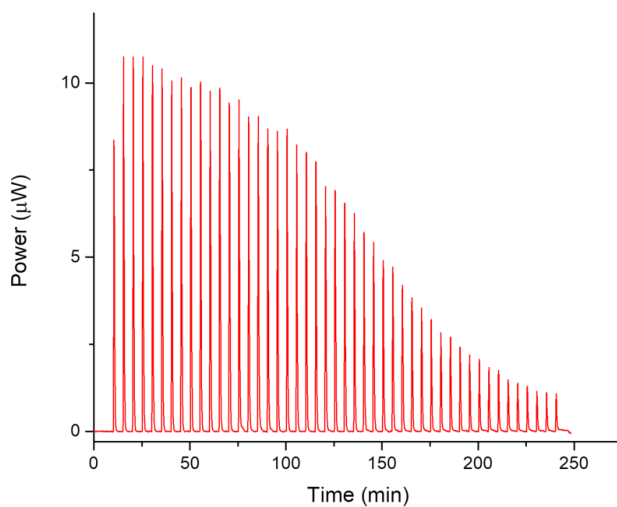
Figure A14. Titration of octylpyridinium chloride 3 mM (**OPyC**) into **C4TS** 0.3 mM at 25 °C in buffered aqueous solution (pH 7.2, phosphate buffer).
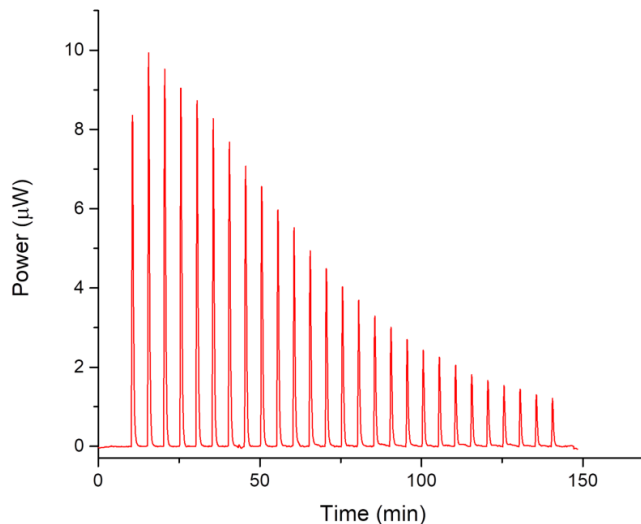
Figure A15. Titration of decyl-3methylimidazolium chloride 3 mM (**D3MIC**) into **C4TS** 0.3 mM at 25 °C in buffered aqueous solution (pH 7.2, phosphate buffer).
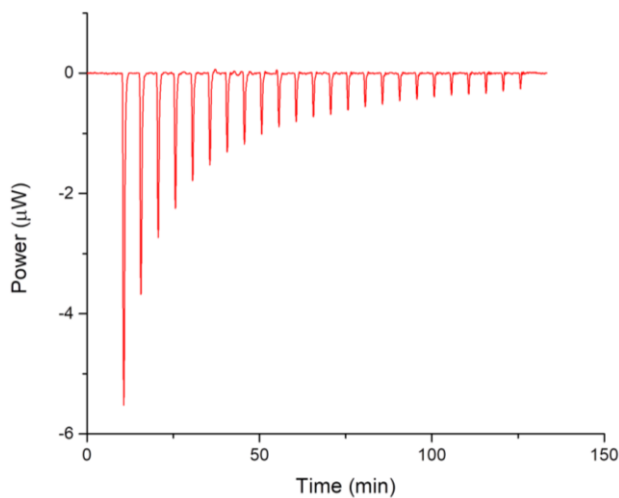
Figure A16. Titration of the supramphiphile (**C4TS**)(**OTAB**) 1 mM at 25 °C in buffered aqueous solution (pH 7.2, phosphate buffer).
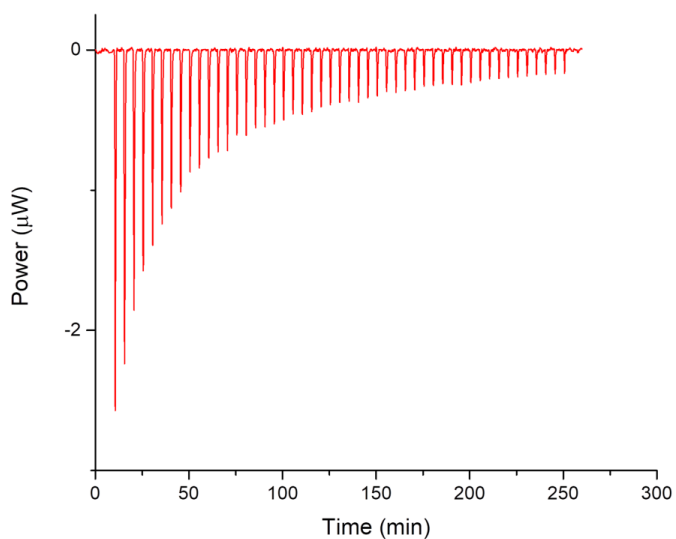
Figure A17. Titration of the supramphiphile (**C4TS**)(**DeTAB**) 1 mM at 25 °C in buffered aqueous solution (pH 7.2, phosphate buffer).
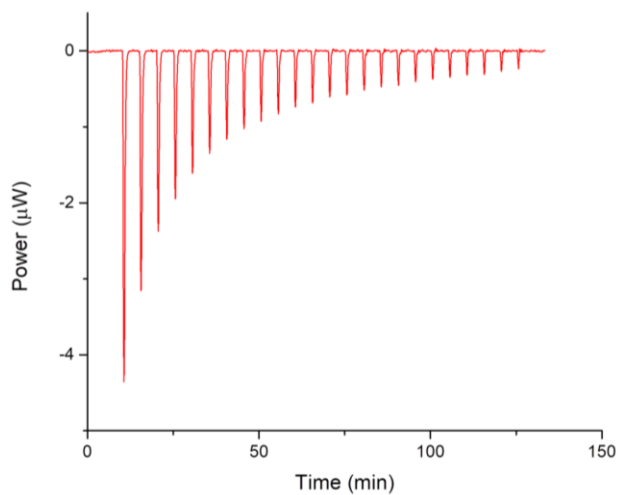
Figure A18. Titration of the supramphiphile (**C4TS**)(**DTAB**) 1 mM at 25 °C in buffered aqueous solution (pH 7.2, phosphate buffer).
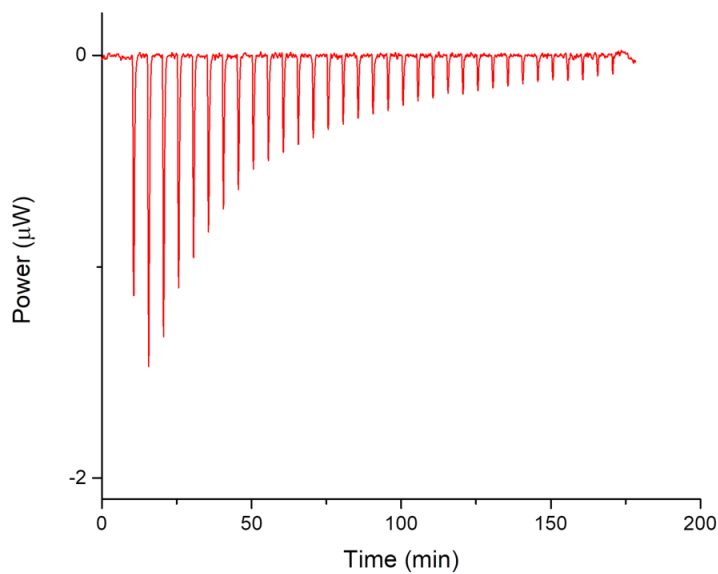
Figure A19. Titration of the supramphiphile (**C4TS**)(**OPyC**) 1 mM at 25 °C in buffered aqueous solution (pH 7.2, phosphate buffer).
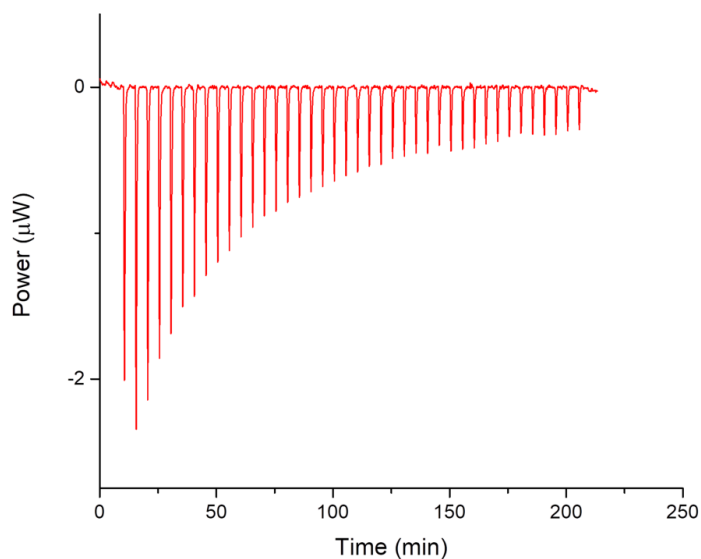
Figure A20. Titration of the supramphiphile (**C4TS**)(**D3MIC**) 1 mM at 25 °C in buffered aqueous solution (pH 7.2, phosphate buffer).
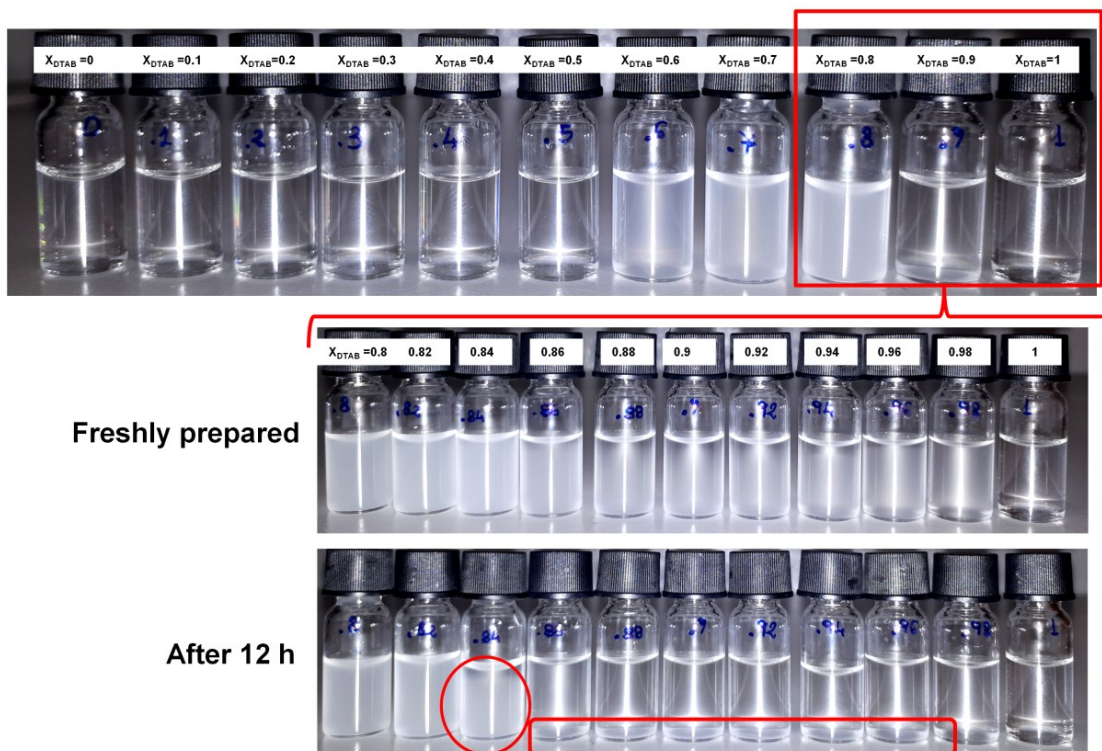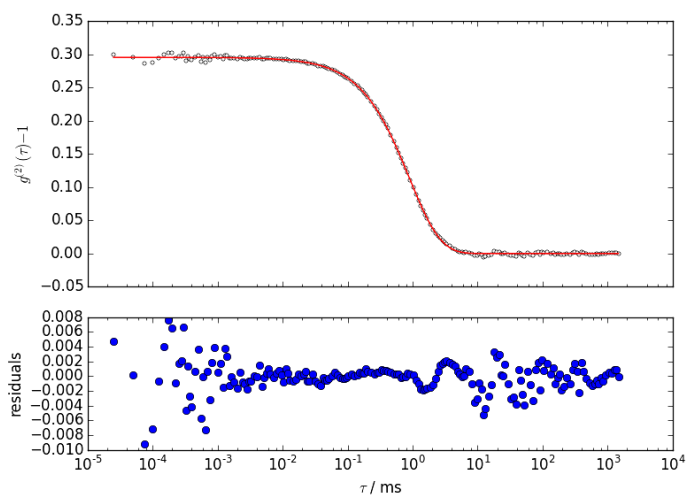
Figure A21. DTAB/C4TS samples at different molar fractions at 0.1 wt%.
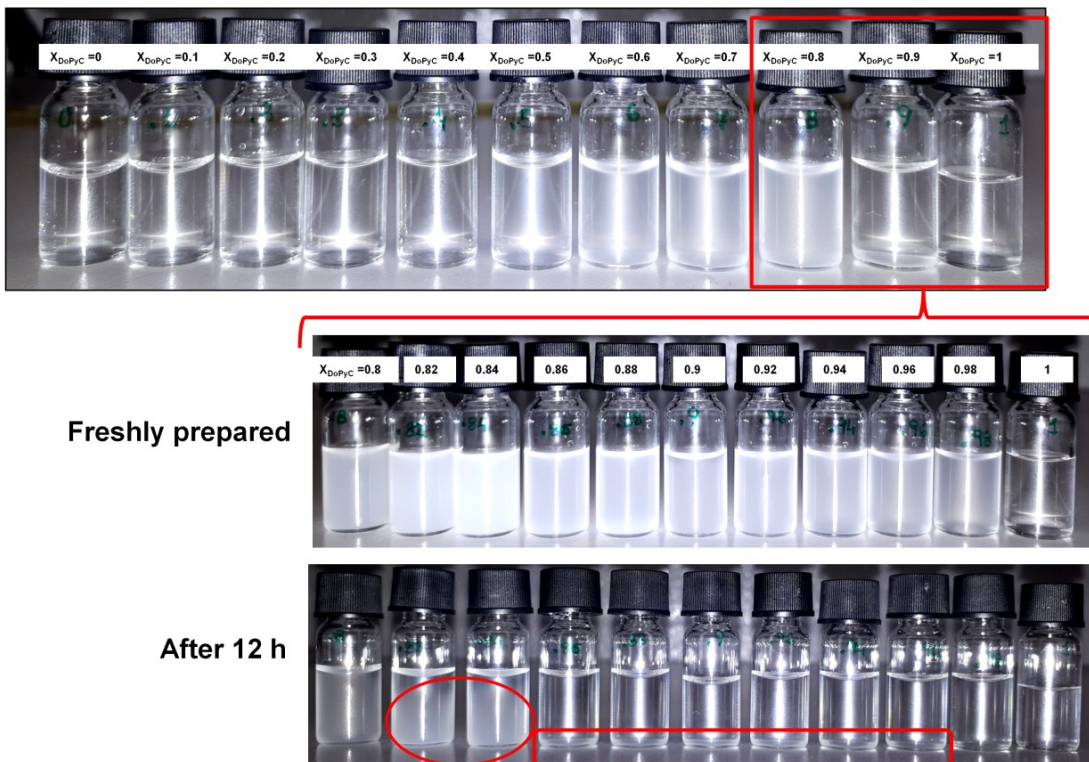
**Figure A22. DoPyC/C4TS** samples at different molar fractions at 0.1 wt%.
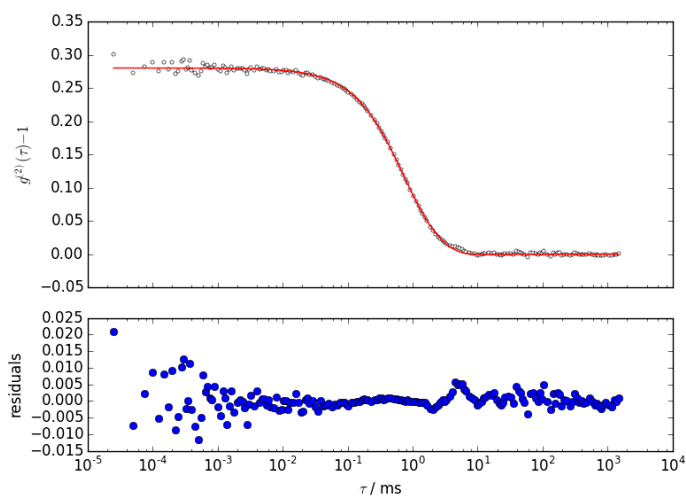
Figure A23. Autocorrelation function for **DTAB/C4TS** mixture (0.1 wt%) at X_{DTAB}=0.4 and at a scattering angle θ=90°, together with the fit curve (obtained using a bimodal stretched exponential function) and the corresponding residuals.
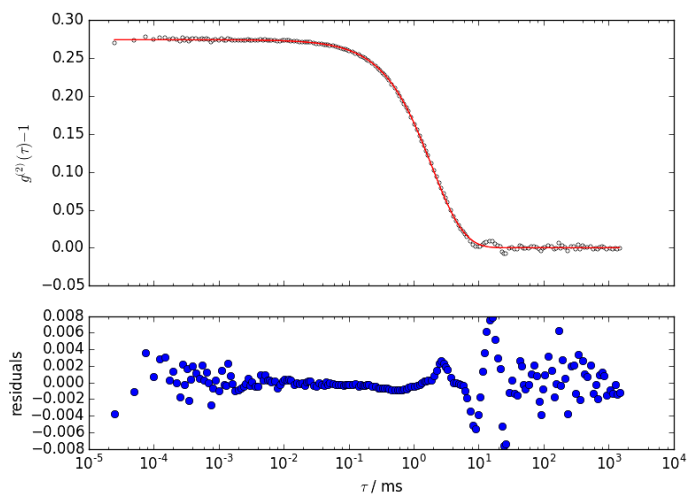

Figure A24. Autocorrelation function for **DTAB/C4TS** mixture (0.1 wt%) at X_{DTAB}=0.5 at a scattering angle θ=90°, together with the fit curve (obtained using a bimodal stretched exponential function) and the corresponding residuals.
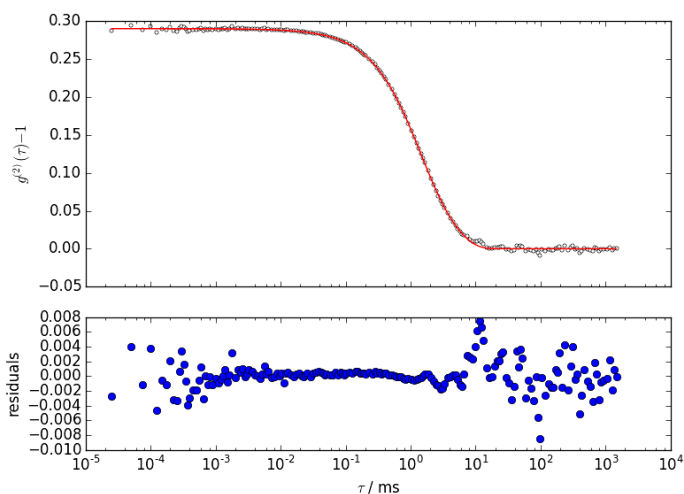
Figure A25. Autocorrelation function for **DTAB/C4TS** mixture (0.1 wt%) at X_{DTAB}=0.6 at a scattering angle θ=90°, together with the fit curve (obtained using a bimodal stretched exponential function) and the corresponding residuals.
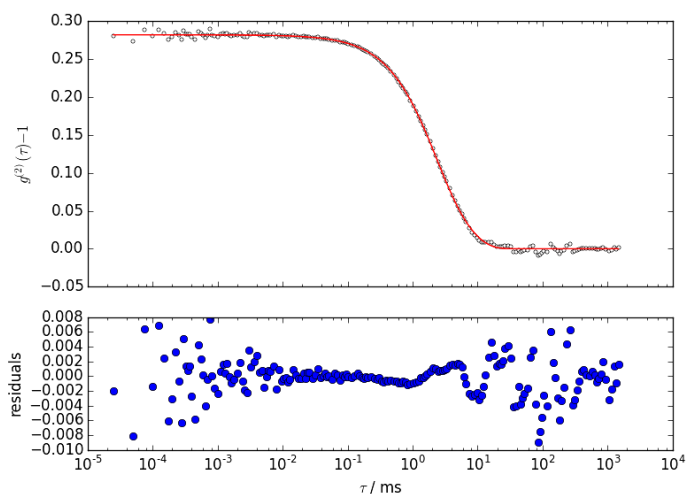

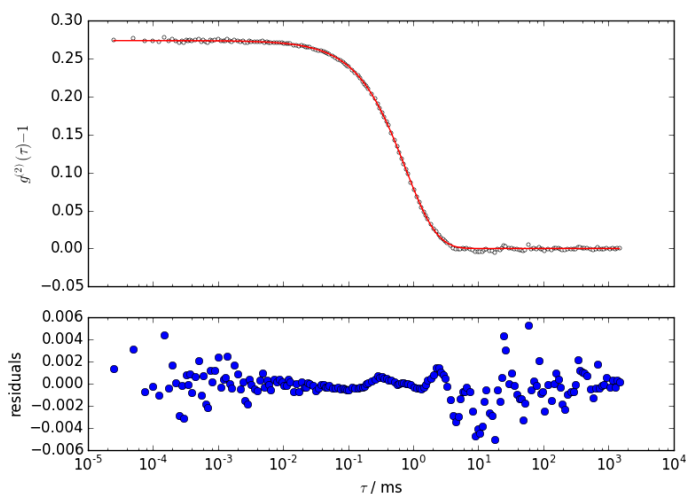**Figure A26.** Autocorrelation function for **DTAB/C4TS** mixture (0.1 wt%) at X_{DTAB}=0.7 at a scattering angle θ=90°, together with the fit curve (obtained using a bimodal stretched exponential function) and the corresponding residuals.

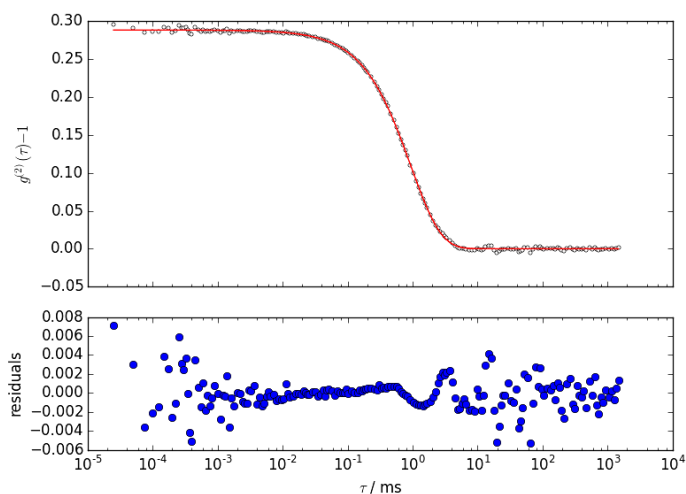**Figure A27.** Autocorrelation function for **DTAB/C4TS** mixture (0.1 wt%) at X_{DTAB}=0.8 at a scattering angle θ=90°, together with the fit curve (obtained using a bimodal stretched exponential function) and the corresponding residuals.

Figure A28. Autocorrelation function for **DTAB/C4TS** mixture (0.1 wt%) at X_{DoPyC}=0.4 at a scattering angle θ=90°, together with the fit curve (obtained using a bimodal stretched exponential function) and the corresponding residuals.

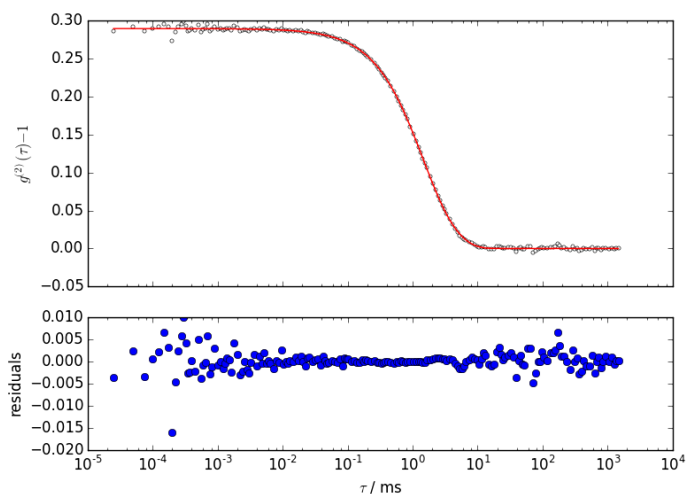**Figure A29.** Autocorrelation function for **DTAB/C4TS** mixture (0.1 wt%) at X_{DoPyC}=0.5 at a scattering angle θ=90°, together with the fit curve (obtained using a bimodal stretched exponential function) and the corresponding residuals.

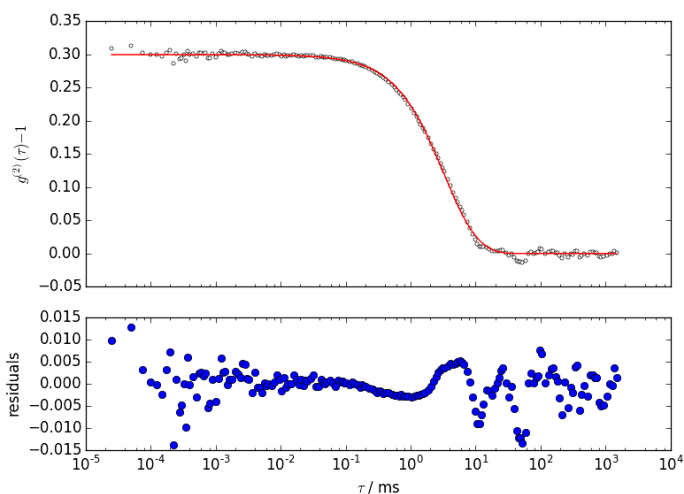**Figure A30.** Autocorrelation function for **DTAB/C4TS** mixture (0.1 wt%) at X_{DoPyC}=0.6 at a scattering angle θ=90°, together with the fit curve (obtained using a bimodal stretched exponential function) and the corresponding residuals.

182

Figure A31. Autocorrelation function for **DTAB/C4TS** mixture (0.1 wt%) at X_{DoPyC}=0.7 at a scattering angle θ=90°, together with the fit curve (obtained using a bimodal stretched exponential function) and the corresponding residuals.

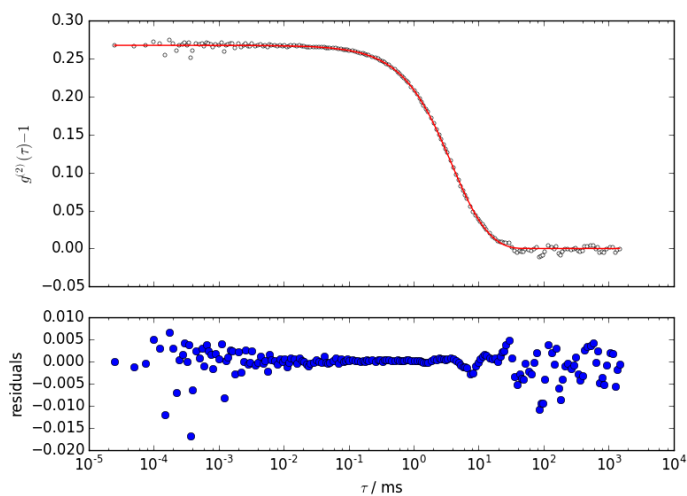**Figure A32.** Autocorrelation function for **DTAB/C4TS** mixture (0.1 wt%) at X_{DoPyC}=0.8 at a scattering angle θ=90°, together with the fit curve (obtained using a bimodal stretched exponential function) and the corresponding residuals.

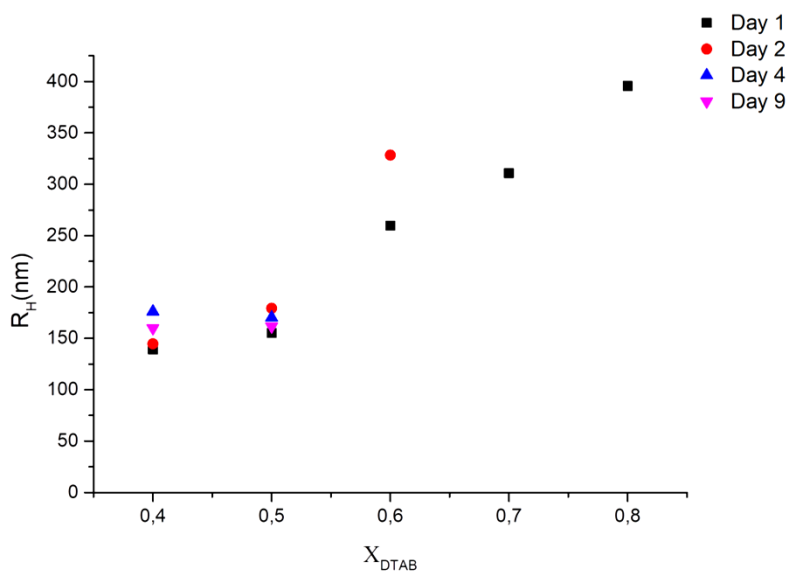**Figure A33.** Hydrodynamic radius values for the system **DTAB/C4TS** at different molar fractions by monitoring the samples stability over time.
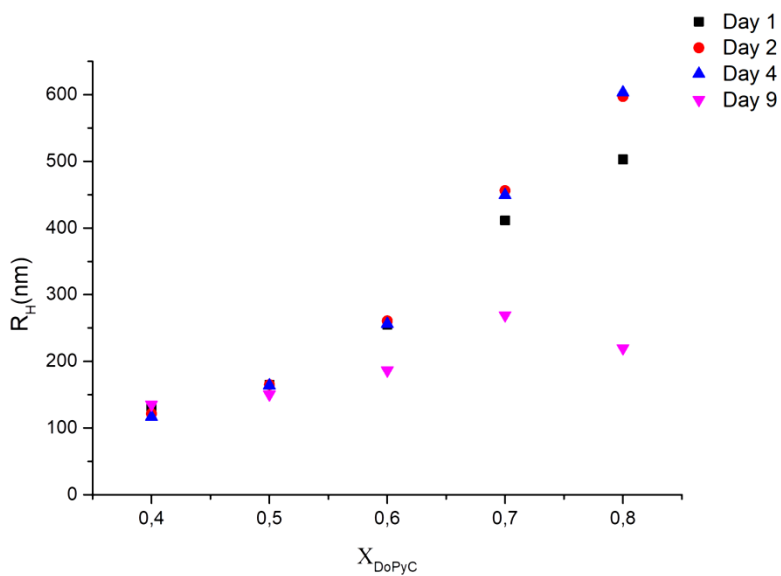
Figure A34. Hydrodynamic radius values for the system **DoPyC/C4TS** at different molar fractions by monitoring the samples stability over time.
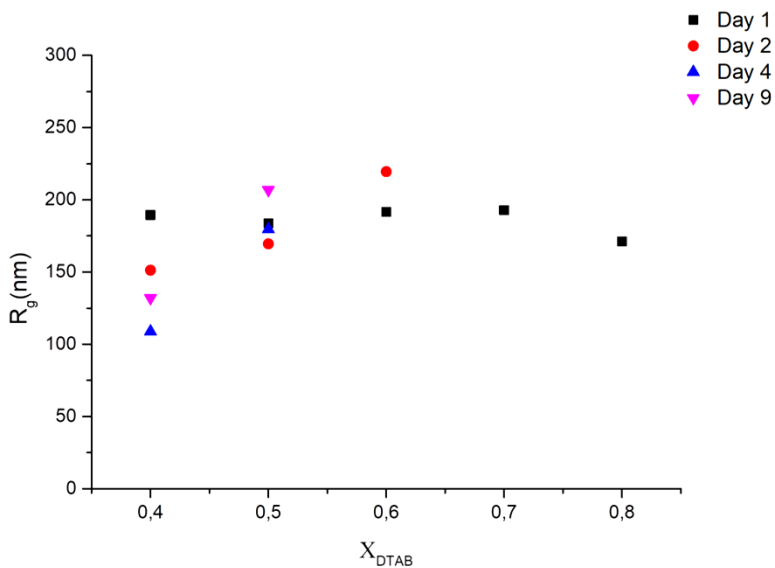
Figure A35. Radius of gyration values for the system **DTAB/C4TS** at different molar fractions by monitoring the samples stability over time.

Figure A36. Radius of gyration values for the system **DoPyC/C4TS** at different molar fractions by monitoring the samples stability over time.

Figure A37. I_0 values for the system **DTAB/C4TS** at different molar fractions by monitoring the samples stability over time.
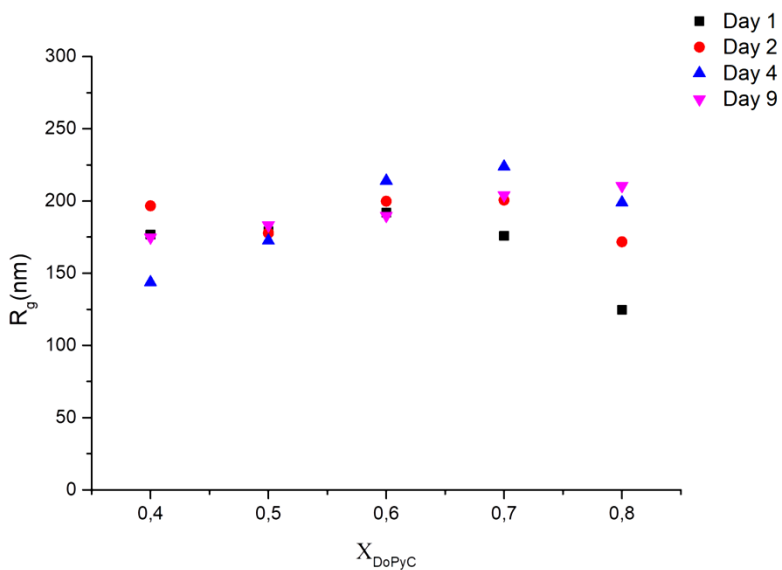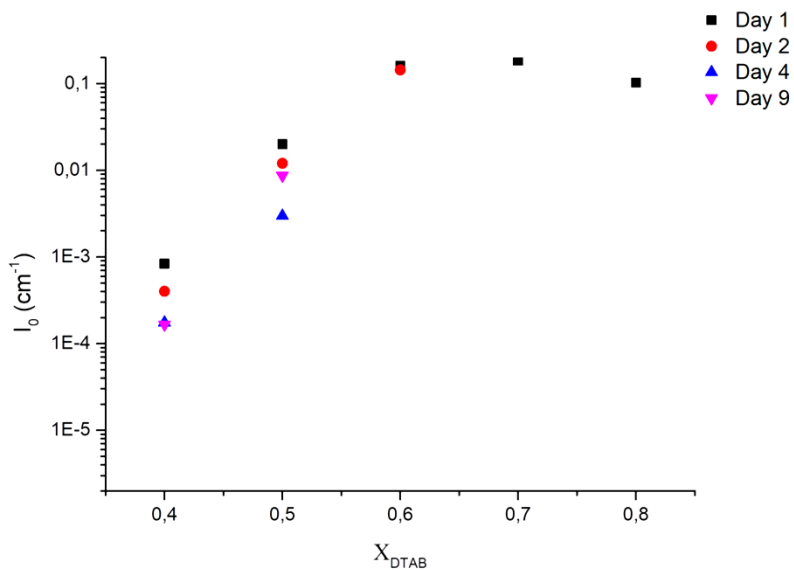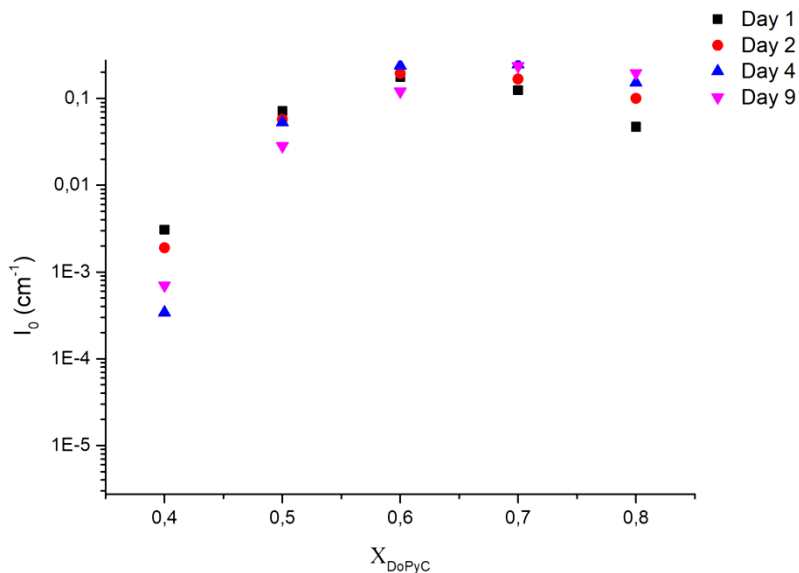

Figure A38. I_0 values for the system **DoPyC/C4TS** at different molar fractions by monitoring the samples stability over time.
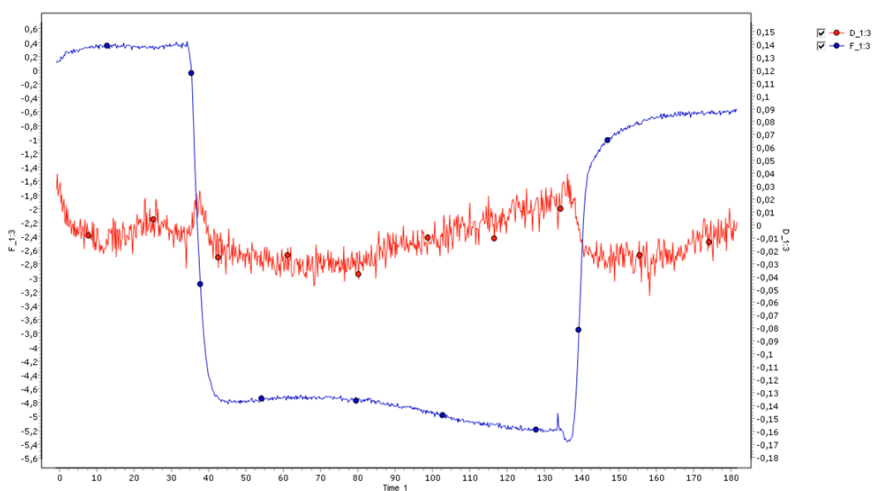
Figure A39. QCM-D measurement of **DTAB/C4TS** system at $X_{surf.}$=0.5 at 0.01 wt% at 25 °C (pH 7.2). The change in frequency (Δf, blue line) and dissipation (ΔD, red line) are monitored at the 3rd overtone of the fundamental frequency of oscillation.
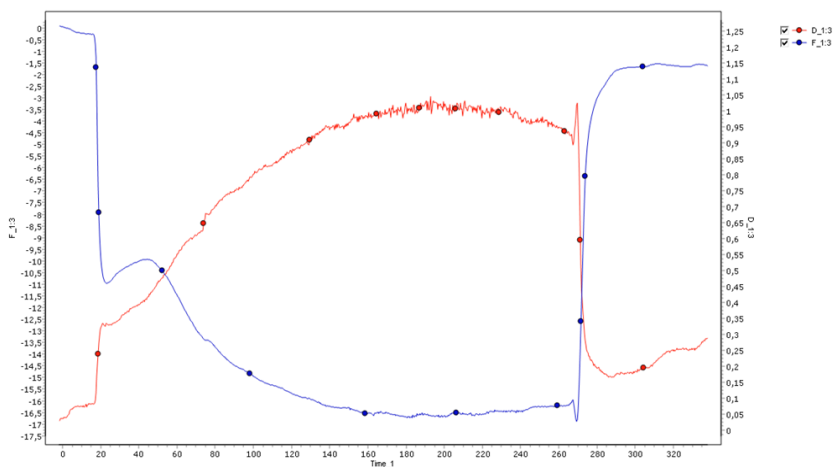
Figure A40. QCM-D measurement of **DTAB/C4TS** system at $X_{surf.}$=0.5 at 0.1 wt% at 25 °C (pH 7.2). The change in frequency (Δf, blue line) and dissipation (ΔD, red line) are monitored at the 3rd overtone of the fundamental frequency of oscillation.

Figure A41. QCM-D measurement of **DTAB/C4TS** system at $X_{surf.}$=0.6 at 0.01 wt% at 25 °C (pH 7.2). The change in frequency (Δf, blue line) and dissipation (ΔD, red line) are monitored at the 3rd overtone of the fundamental frequency of oscillation.

Figure A42. QCM-D measurement of **DTAB/C4TS** system at $X_{surf.}$=0.6 at 0.1 wt% at 25 °C (pH 7.2). The change in frequency (Δf, blue line) and dissipation (ΔD, red line) are monitored at the 3rd overtone of the fundamental frequency of oscillation.

Figure A43. QCM-D measurement of **DTAB/C4TS** system at $X_{surf.}$=0.8 at 0.01 wt% at 25 °C (pH 7.2). The change in frequency (Δf, blue line) and dissipation (ΔD, red line) are monitored at the 3rd overtone of the fundamental frequency of oscillation.
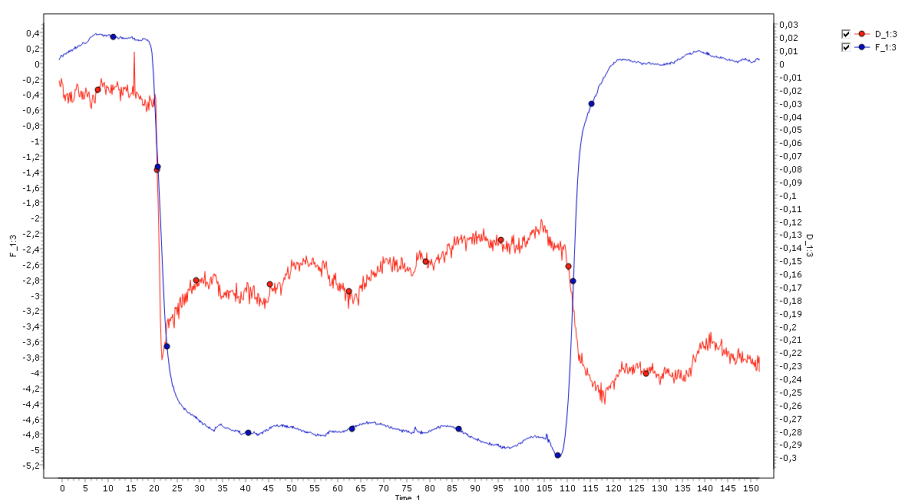

Figure A44. QCM-D measurement of **DTAB/C4TS** system at $X_{surf.}$=0.8 at 0.1 wt% at 25 °C (pH 7.2 The change in frequency (Δf, blue line) and dissipation (ΔD, red line) are monitored at the 3rd overtone of the fundamental frequency of oscillation.

Figure A45. QCM-D measurement of pure **DTAB** at 0.01 wt% at 25 °C (pH 7.2). The change in frequency (Δf, blue line) and dissipation (ΔD, red line) are monitored at the 3rd overtone of the fundamental frequency of oscillation.

Figure A46. QCM-D measurement of pure **DTAB** at 0.1 wt% at 25 °C (pH 7.2). The change in frequency (Δf, blue line) and dissipation (ΔD, red line) are monitored at the 3rd overtone of the fundamental frequency of oscillation.
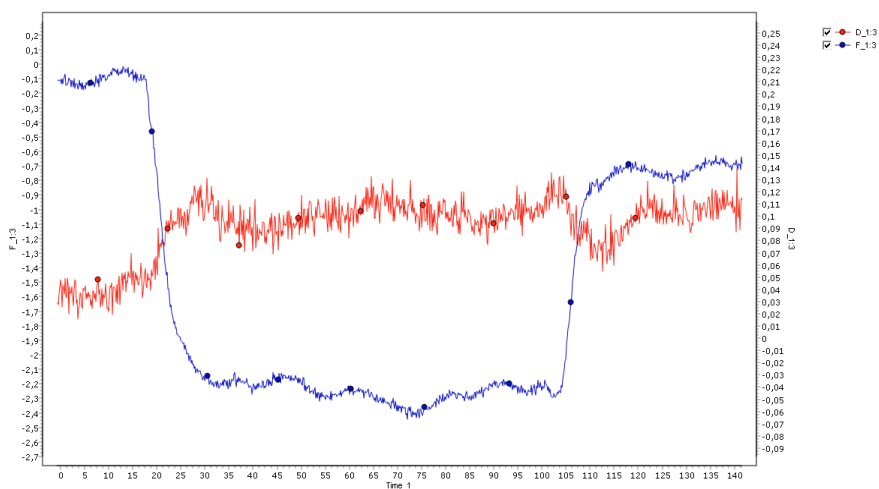
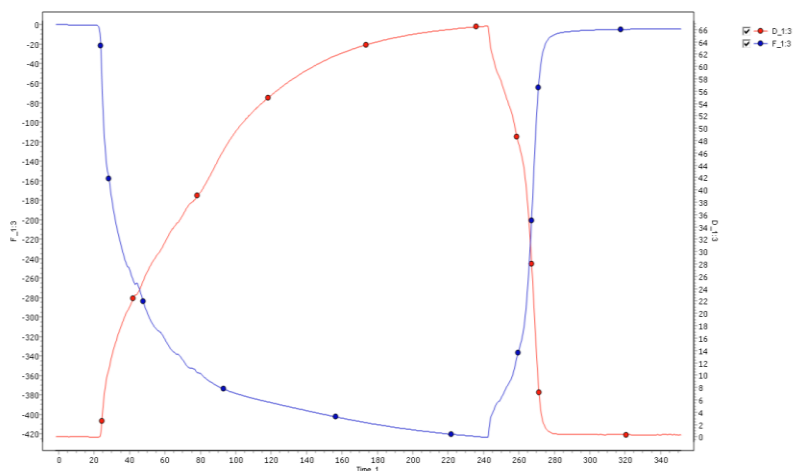**Figure A47.** QCM-D measurement of **DoPyC/C4TS** system at $X_{surf.}$=0.5 at 0.01 wt% at 25 °C (pH 7.2). The change in frequency (Δf, blue line) and dissipation (ΔD, red line) are monitored at the 3rd overtone of the fundamental frequency of oscillation.
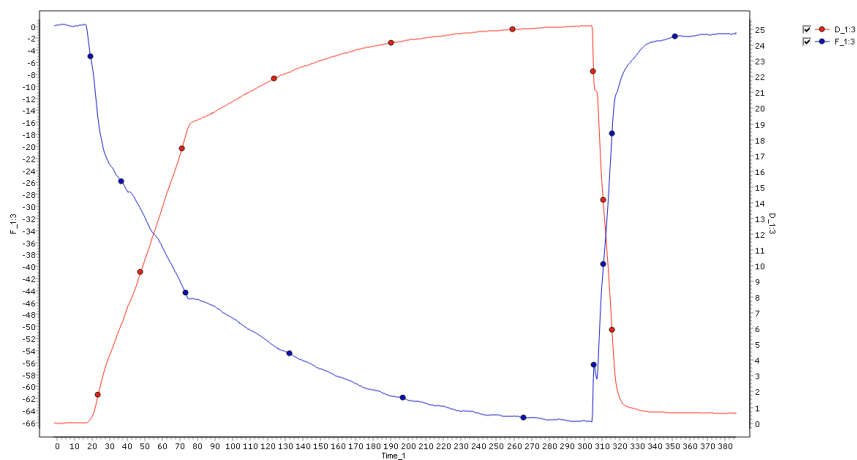
Figure A48. QCM-D measurement of **DoPyC/C4TS** system at $X_{surf.}$=0.5 at 0.1 wt% at 25 °C (pH 7.2 The change in frequency (Δf, blue line) and dissipation (ΔD, red line) are monitored at the 3rd overtone of the fundamental frequency of oscillation.
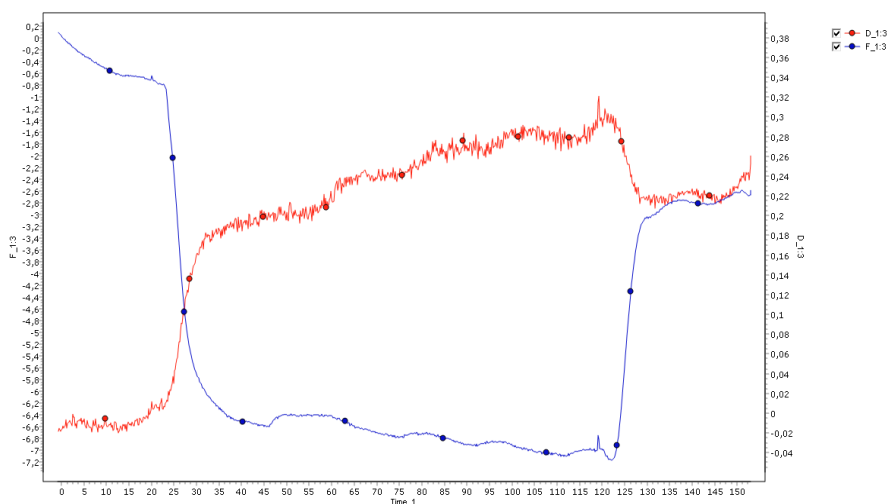
Figure A49. QCM-D measurement of **DoPyC/C4TS** system at $X_{surf.}$=0.6 at 0.01 wt% at 25 °C (pH 7.2 The change in frequency (Δf, blue line) and dissipation (ΔD, red line) are monitored at the 3rd overtone of the fundamental frequency of oscillation.
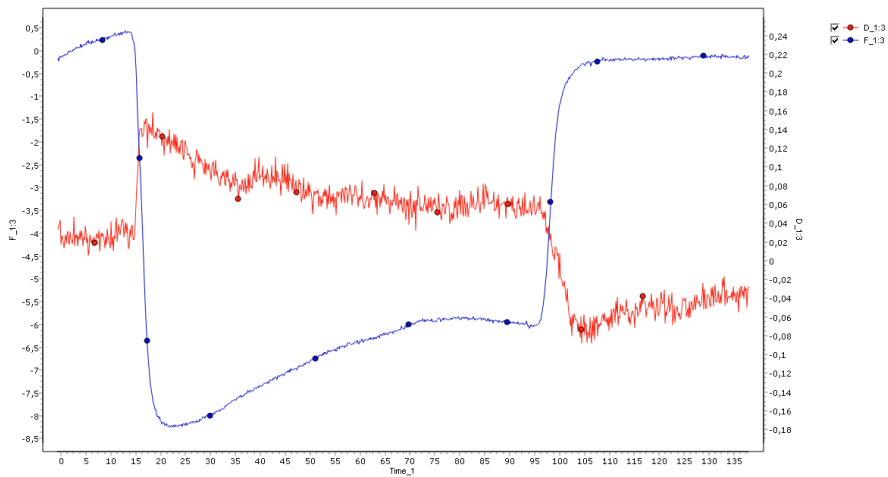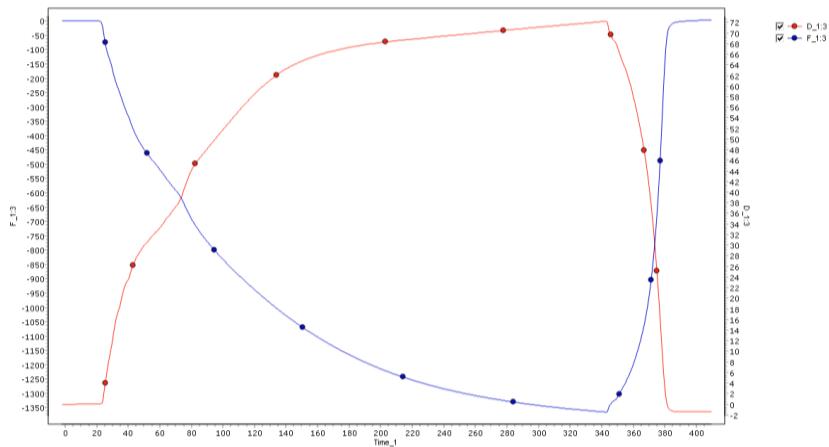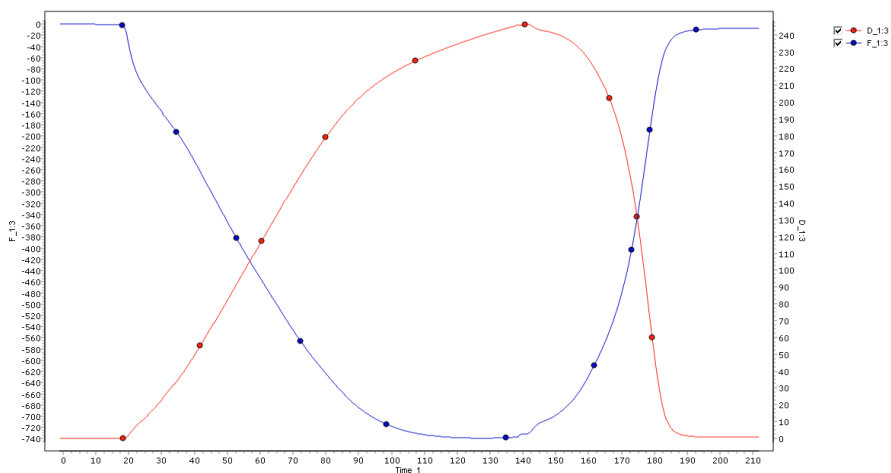

Figure A50. QCM-D measurement of **DoPyC/C4TS** system at $X_{surf.}$=0.6 at 0.1 wt% at 25 °C (pH 7.2). The change in frequency (Δf, blue line) and dissipation (ΔD, red line) are monitored at the 3rd overtone of the fundamental frequency of oscillation.
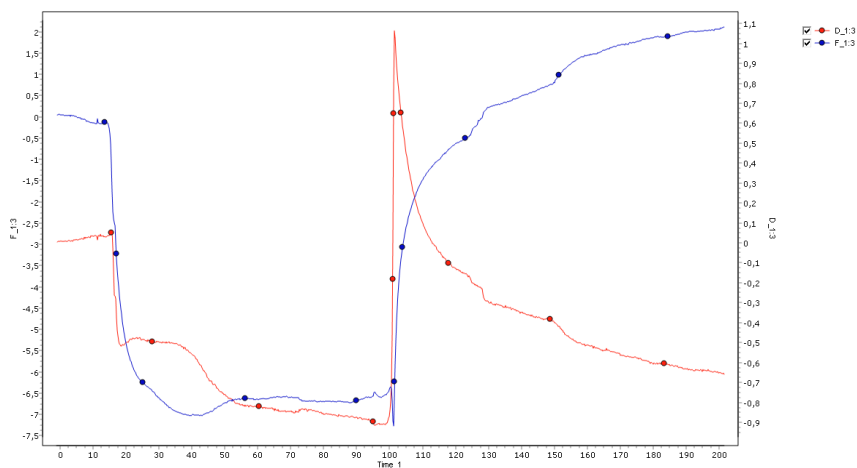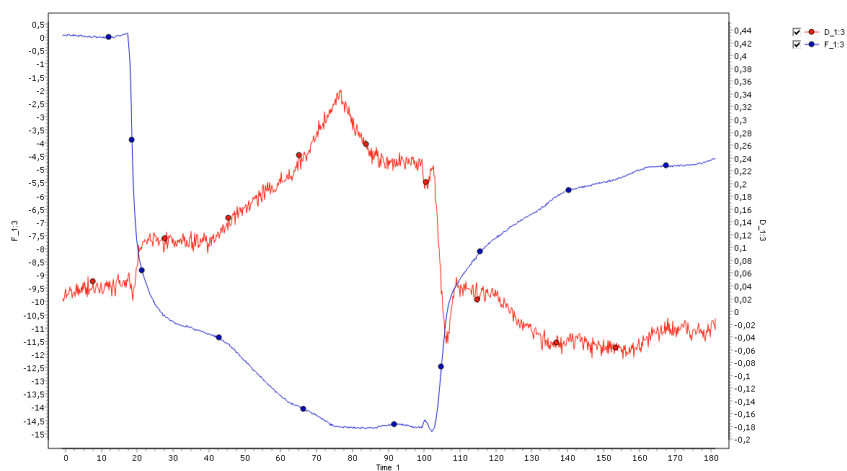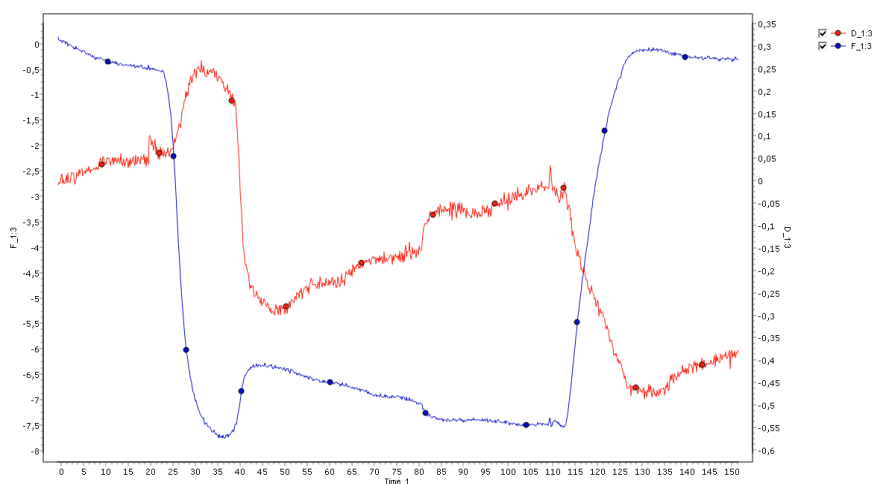
Figure A51. QCM-D measurement of **DoPyC/C4TS** system at $X_{surf.}$=0.8 at 0.01 wt% at 25 °C (pH 7.2 The change in frequency (Δf, blue line) and dissipation (ΔD, red line) are monitored at the 3rd overtone of the fundamental frequency of oscillation.
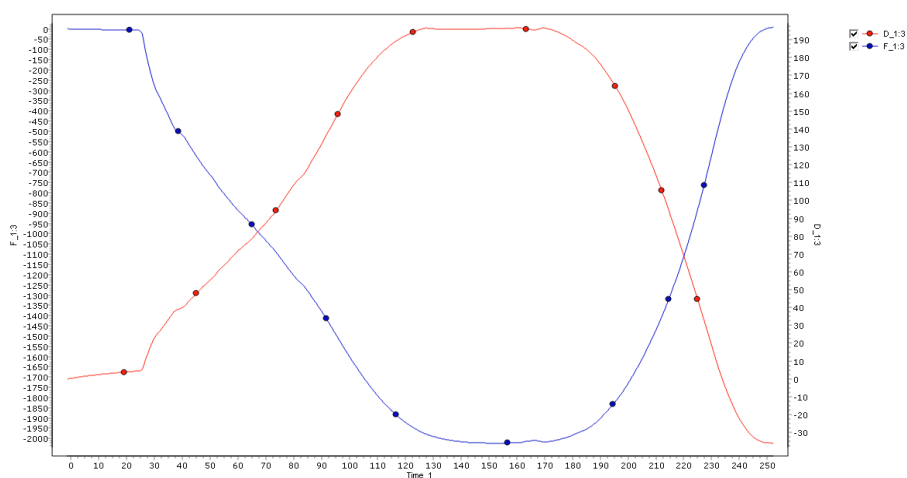
Figure A52. QCM-D measurement of **DoPyC/C4TS** system at $X_{surf.}$=0.8 at 0.1 wt% at 25 °C (pH 7.2 The change in frequency (Δf, blue line) and dissipation (ΔD, red line) are monitored at the 3rd overtone of the fundamental frequency of oscillation.
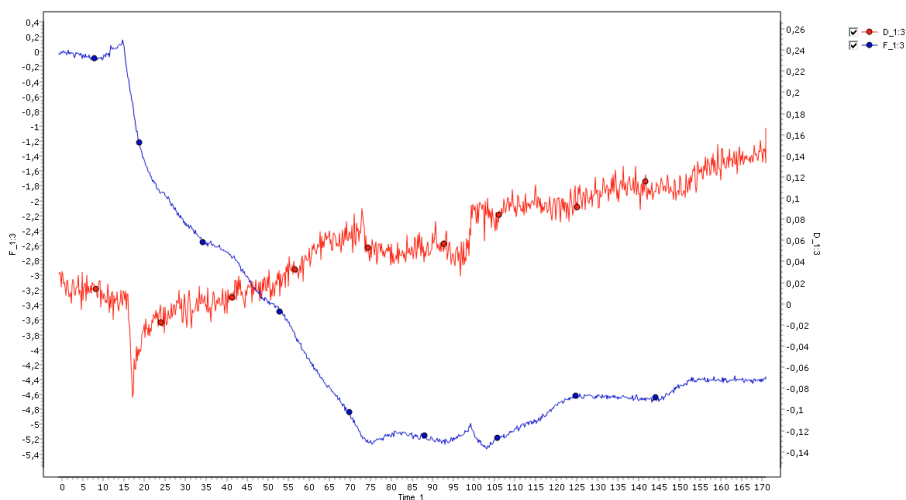
Figure A53. QCM-D measurement of pure **DoPyC** at 0.01 wt% at 25 °C (pH 7.2). The change in frequency (Δf, blue line) and dissipation (ΔD, red line) are monitored at the 3rd overtone of the fundamental frequency of oscillation.
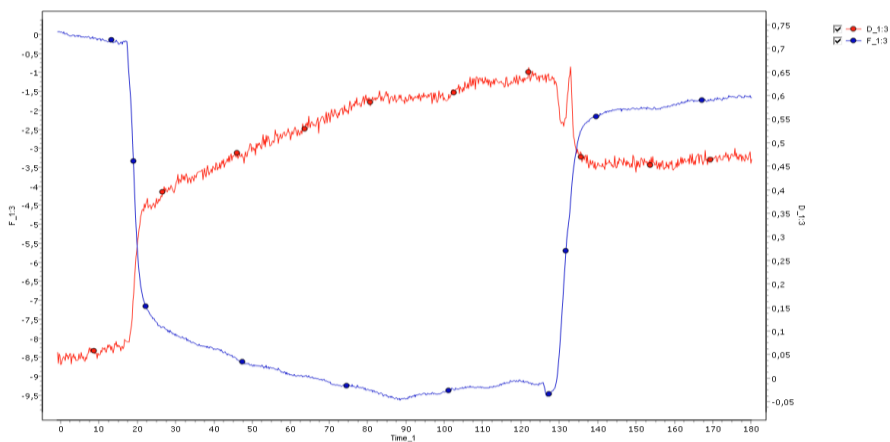
Figure A54. QCM-D measurement of pure **DoPyC** at 0.1 wt% at 25 °C (pH 7.2). The change in frequency (Δf, blue line) and dissipation (ΔD, red line) are monitored at the 3rd overtone of the fundamental frequency of oscillation.

REFERENCES

[1] Chaudhari, S. P., Dugar, R. P. (2017). Application of surfactants in solid dispersion technology for improving solubility of poorly water soluble drugs. *Journal of Drug Delivery Science and Technology*.

[2] J.-L. Salager, J., -L. Surfactants types and uses, Fire p booket-E300-attaching aid in surfactant science and engineering in English, Merida Venezuela 2 (2002) 3.

[3] Schramm, L. L., Stasiuk, E. N., Marangoni, D. G. (2003). 2 Surfactants and their applications. *Annual Reports Section" C"(Physical Chemistry)*, *99*, 3-48.

[4] Knepper, T. P., Berna, J. L. (2003). Surfactants: properties, production, and environmental aspects. *Comprehensive Analytical Chemistry*, *40*, 1-49.

[5] Shinoda, K., Nakagawa, T., Tamamushi, B. I. (2016). *Colloidal surfactants: some physicochemical properties* (Vol. 12). Elsevier.

[6] van Os, N. M., Haak, J. R., Rupert, L. A. M. (2012). *Physico-chemical properties of selected anionic, cationic and non-ionic surfactants*. Elsevier.

[7] Rosen, M. J., Kunjappu, J. T. (2012). *Surfactants and interfacial phenomena*. John Wiley & Sons.

[8] Moulik, S. P., Haque, M. E., Jana, P. K., Das, A. R. (1996). Micellar properties of cationic surfactants in pure and mixed states. *The Journal of physical chemistry*, *100*(2), 701-708.

[9] Maibaum, L., Dinner, A. R., Chandler, D. (2004). Micelle formation and the hydrophobic effect. *The Journal of Physical Chemistry B*, *108*(21), 6778-6781.

[10] Holland, P. M., Rubingh, D. N. (1992). Mixed surfactant systems. *ACS symposium series* (Vol. 501, p. 1). American Chemical Society Washington, DC.

[11]Khan, A., Marques, E. F. (1999). Synergism and polymorphism in mixed surfactant systems. *Current opinion in colloid & interface science*, *4*(6), 402-410.

[12]Bergström, M., Eriksson, J. C. (2000). A theoretical analysis of synergistic effects in mixed surfactant systems. *Langmuir*, *16*(18), 7173-7181.

[13]Raghavan, S. R., Fritz, G., Kaler, E. W. (2002). Wormlike micelles formed by synergistic self-assembly in mixtures of anionic and cationic surfactants. *Langmuir*, *18*(10), 3797-3803.

[14]Kanoje, B., Padshala, S., Parikh, J., Sahoo, S. K., Kuperkar, K., Bahadur, P. (2018). Synergism and aggregation behaviour in an aqueous binary mixture of cationic–zwitterionic surfactants: physico-chemical characterization with molecular simulation approach. *Physical Chemistry Chemical Physics*, *20*(1), 670-681.

[15]Parekh, P., Varade, D., Parikh, J., Bahadur, P. (2011). Anionic–cationic mixed surfactant systems: micellar interaction of sodium dodecyl trioxyethylene sulfate with cationic gemini surfactants. *Colloids and Surfaces A: Physicochemical and Engineering Aspects*, *385*(1-3), 111-120.

[16]Li, Y., Puerto, M., Bao, X., Zhang, W., Jin, J., Su, Z., Shen, S., Hirasaki, G., Miller, C. (2017). Synergism and performance for systems containing binary mixtures of anionic/cationic surfactants for enhanced oil recovery. *Journal of Surfactants and Detergents*, *20*(1), 21-34.

[17]Zhou, Q., Rosen, M. J. (2003). Molecular interactions of surfactants in mixed monolayers at the air/aqueous solution interface and in mixed micelles in aqueous media: the regular solution approach. *Langmuir*, *19*(11), 4555-4562.

[18]Rosen, M. J., Hua, X. Y. (1982). Synergism in binary mixtures of surfactants: II. Some experimental data. *Journal of the American Oil Chemists' Society*, *59*(12), 582-585.

[19] James-Smith, M. A., Hellner, B., Annunziato, N., Mitragotri, S. (2011). Effect of surfactant mixtures on skin structure and barrier properties. *Annals of biomedical engineering, 39*(4), 1215-1223.

[20] Jadidi, N., Adib, B., Malihi, F. B. (2013). Synergism and performance optimization in liquid detergents containing binary mixtures of anionic–non-ionic, and anionic–cationic surfactants. *Journal of Surfactants and Detergents, 16*(1), 115-121.

[21] Pedro, R., Walters, K. A. (2019). Surfactants in Cosmetic Products. *Cosmetic Formulation: Principles and Practice*, 129.

[22] Ghosh, S., Ray, A., Pramanik, N., & Ambade, B. (2016). Can a catanionic surfactant mixture act as a drug delivery vehicle?. *Comptes Rendus Chimie, 19*(8), 951-954.

[23] Rosa, M., del Carmen Morán, M., da Graça Miguel, M., & Lindman, B. (2007). The association of DNA and stable catanionic amino acid-based vesicles. *Colloids and Surfaces A: Physicochemical and Engineering Aspects, 301*(1-3), 361-375.

[24] Zhang, X., & Wang, C. (2011). Supramolecular amphiphiles. *Chemical Society Reviews, 40*(1), 94-101.

[25] Kimizuka, N., Kawasaki, T., Kunitake, T. (1993). Self-organization of bilayer membranes from amphiphilic networks of complementary hydrogen bonds. *Journal of the American Chemical Society*, *115*(10), 4387-4388.

[26] Gohy, J. F., Lohmeijer, B. G., Schubert, U. S. (2002). Metallo-supramolecular block copolymer micelles. *Macromolecules*, *35*(12), 4560-4563.

[27] Kabanov, A. V., Bronich, T. K., Kabanov, V. A., Yu, K., Eisenberg, A. (1998). Spontaneous formation of vesicles from complexes of block ionomers and surfactants. *Journal of the American Chemical Society*, *120*(38), 9941-9942.

[28] Oda, R., Huc, Y., Schmutz, M., Candeau, S., Mackintosh, F. (1999). Tuning bilayer twist using chiral counterious. *Nature*, *399*, 566-569.

[29] Liu, K., Wang, C., Li, Z., Zhang, X. (2011). Superamphiphiles Based on Directional Charge-Transfer Interactions: From Supramolecular Engineering to Well-Defined Nanostructures. *Angewandte Chemie*, *123*(21), 5054-5058.

[30] Bojinova, T., Coppel, Y., Lauth-de Viguerie, N., Milius, A., Rico-Lattes, I., Lattes, A. (2003). Complexes between β-cyclodextrin and aliphatic guests as new noncovalent amphiphiles: formation and physicochemical studies. *Langmuir*, *19*(13), 5233-5239.

[31] Jeon, Y. J., Bharadwaj, P. K., Choi, S., Lee, J. W., Kim, K. (2002). Supramolecular amphiphiles: spontaneous formation of vesicles triggered by formation of a charge-transfer complex in a host. *Angewandte Chemie International Edition, 41*(23), 4474-4476.

[32] Gutsche, C. D. (1983). Calixarenes. *Accounts of Chemical Research*, *16*(5), 161-170.

[33] Gutsche, C. D., Bauer, L. J. (1985). Calixarenes. 13. The conformational properties of calix [4] arenes, calix [6] arenes, calix [8] arenes, and oxacalixarenes. *Journal of the American Chemical Society*, *107*(21), 6052-6059.

[34] Park, C., Chun, S., Bartsch, R. A. (2010). Effect of conformation on metal ion extraction by calix [4] arene dicarboxylic acids. Journal of Inclusion Phenomena and Macrocyclic Chemistry, 66(1-2), 95-105.

[35] Böhmer, V. (1995). Calixarenes, macrocycles with (almost) unlimited possibilities. *Angewandte Chemie International Edition*, *34*(7), 713-745.

[36] Shinkai, S., Mori, S., Tsubaki, T., Sone, T., Manabe, O. (1984). New water-soluble host molecules derived from calix [6] arene. *Tetrahedron letters*, *25*(46), 5315-5318.

[37] Guo, D. S., Wang, K., Liu, Y. (2008). Selective binding behaviors of p-sulfonatocalixarenes in aqueous solution. *Journal of Inclusion Phenomena and Macrocyclic Chemistry*, *62*(1-2), 1-21.

[38] Guo, D. S., Liu, Y. (2014). Supramolecular chemistry of p-sulfonatocalix [n] arenes and its biological applications. *Accounts of chemical research*, *47*(7), 1925-1934.

[39] Liu, Y., Guo, D. S., Zhang, H. Y., Ma, Y. H., Yang, E. C. (2006). The structure and thermodynamics of calix [n] arene complexes with dipyridines and phenanthroline in aqueous solution studied by microcalorimetry and NMR spectroscopy. *The Journal of Physical Chemistry B*, *110*(7), 3428-3434.

[40] Sgarlata, C., Arena, G., Fortuna, C. G., Sciotto, D., Bonaccorso, C. (2016). Cationic gemini guests promote the efficient self-assembly of capsular entities in water at neutral pH. *Supramolecular Chemistry*, *28*(5-6), 544-550.

[41] Bonaccorso, C., Migliore, R., Volkova, M. A., Arena, G., Sgarlata, C. (2017). Self-assembling of supramolecular adducts by sulfonato-calix [4] arene and pyridinium gemini guests in neutral aqueous solution. Thermochimica Acta, 656, 47-52.

[42] Perret, F., Lazar, A. N., Coleman, A. W. (2006). Biochemistry of the para-sulfonato-calix [n] arenes. *Chemical Communications*, (23), 2425-2438.

[43] Perret, F., Coleman, A. W. (2011). Biochemistry of anionic calix [n] arenes. *Chemical Communications*, *47*(26), 7303-7319.

[44] Coleman, A. W., Jebors, S., Cecillon, S., Perret, P., Garin, D., Marti-Battle, D., Moulin, M. (2008). Toxicity and biodistribution of para-sulfonato-calix [4] arene in mice. *New Journal of Chemistry*, *32*(5), 780-782.

[45]Menger, F. M., Keiper, J. S. (2000). Gemini surfactants. *Angewandte Chemie International Edition*, *39*(11), 1906-1920.

[46] Zana, R. (2002). Dimeric and oligomeric surfactants. Behavior at interfaces and in aqueous solution: a review. *Advances in colloid and interface science*, *97*(1-3), 205-253.

[47] Laschewsky, A., Wattebled, L., Arotçaréna, M., Habib-Jiwan, J. L., Rakotoaly, R. H. (2005). Synthesis and properties of cationic oligomeric surfactants. *Langmuir*, *21*(16), 7170-7179.

[48] Murguía, M. C., Cabrera, M. I., Guastavino, J. F., Grau, R. J. (2005). New oligomeric surfactants with multiple-ring spacers: Synthesis and tensioactive properties. *Colloids and Surfaces A: Physicochemical and Engineering Aspects*, *262*(1-3), 1-7.

[49] Shinkai, S., Mori, S., Tsubaki, T., Sone, T., & Manabe, O. (1984). New water-soluble host molecules derived from calix [6] arene. *Tetrahedron letters*, *25*(46), 5315-5318.

[50] Shinkai, S., Mori, S., Koreishi, H., Tsubaki, T., & Manabe, O. (1986). Hexasulfonated calix [6] arene derivatives: a new class of catalysts, surfactants, and host molecules. *Journal of the American Chemical Society*, *108*(9), 2409-2416.

[51] Shinkai, S., Arimura, T., Araki, K., Kawabata, H., Satoh, H., Tsubaki, T., Manabe, O., Sunamoto, J. (1989). Syntheses and aggregation properties of new water-soluble calixarenes. *Journal of the Chemical Society, Perkin Transactions 1*, (11), 2039-2045.

[52] Basilio, N., García-Río, L., & Martín-Pastor, M. (2010). NMR evidence of slow monomer− micelle exchange in a calixarene-based surfactant. *The Journal of Physical Chemistry B*, *114*(14), 4816-4820.

[53] Basílio, N., Garcia-Rio, L., & Martín-Pastor, M. (2012). Calixarene-based surfactants: evidence of structural reorganization upon micellization. *Langmuir*, *28*(5), 2404-2414.

[54] Basílio, N., Garcia-Rio, L. (2012). Calixarene-Based Surfactants: Conformational-Dependent Solvation Shells for the Alkyl Chains. *ChemPhysChem*, *13*(9), 2368-2376.

[55] Basilio, N., García-Río, L. (2009). Sulfonated Calix [6] arene Host–Guest Complexes Induce Surfactant Self-Assembly. *Chemistry–A European Journal*, *15*(37), 9315-9319.

[56] Basilio, N., Martín-Pastor, M., García-Río, L. (2012). Insights into the structure of the supramolecular amphiphile formed by a sulfonated calix [6] arene and alkyltrimethylammonium surfactants. *Langmuir*, *28*(16), 6561-6568.

[57] Basílio, N., Spudeit, D. A., Bastos, J., Scorsin, L., Fiedler, H. D., Nome, F., García-Río, L. (2015). Exploring the charged nature of supramolecular micelles based on p-sulfonatocalix [6] arene and dodecyltrimethylammonium bromide. *Physical Chemistry Chemical Physics*, *17*(39), 26378-26385.

[58] Francisco, V., Basilio, N., Garcia-Rio, L., Leis, J. R., Maques, E. F., Vázquez-Vázquez, C. (2010). Novel catanionic vesicles from calixarene and single-chain surfactant. *Chemical Communications*, *46*(35), 6551-6553.

[59] Wang, K., Guo, D. S., Liu, Y. (2010). Temperature-Controlled Supramolecular Vesicles Modulated by p-Sulfonatocalix [5] arene with Pyrene. *Chemistry–A European Journal*, *16*(27), 8006-8011.

[60] Wang, K., Guo, D. S., Wang, X., & Liu, Y. (2011). Multistimuli responsive supramolecular vesicles based on the recognition of p-sulfonatocalixarene and its controllable release of doxorubicin. *Acs Nano*, *5*(4), 2880-2894.

[61] Guo, D. S., Wang, K., Wang, Y. X., & Liu, Y. (2012). Cholinesterase-responsive supramolecular vesicle. *Journal of the American Chemical Society*, *134*(24), 10244-10250.

[62] Li, Z., Hu, C., Cheng, Y., Xu, H., Cao, X., Song, X., Zhang, H., Liu, Y. (2012). Supramolecular vesicles of cationic gemini surfactants modulated by p-sulfonatocalix [4] arene. *Science China Chemistry*, *55*(10), 2063-2068.

[63] Wang, J., Ding, X., & Guo, X. (2019). Assembly behaviors of calixarene-based amphiphile and supra-amphiphile and the applications in drug delivery and protein recognition. *Advances in colloid and interface science, 269,* 187-202.

[64] Chatterjee, A. M. S. P., Moulik, S. P., Sanyal, S. K., Mishra, B. K., Puri, P. M. (2001). Thermodynamics of micelle formation of ionic surfactants: a critical assessment for sodium dodecyl sulfate, cetyl pyridinium chloride and dioctyl sulfosuccinate (Na salt) by microcalorimetric, conductometric, and tensiometric measurements. *The Journal of Physical Chemistry B*, *105*(51), 12823-12831.

[65] Zana, R. (1996). Critical micellization concentration of surfactants in aqueous solution and free energy of micellization. *Langmuir*, *12*(5), 1208-1211.

[66] Molyneux, P., Rhodes, C. T., Swarbrick, J. (1965). Thermodynamics of micellization of N-alkyl betaines. *Transactions of the Faraday Society*, *61*, 1043-1052.

[67] Mukerjee, P., Mysels, K. J. (1971). *Critical micelle concentrations of aqueous surfactant systems* (No. NSRDS-NBS-36). National Standard reference data system.

[68] Aranow, R. H., Witten, L. (1960). The environmental influence on the behavior of long chain molecules1. *The Journal of Physical Chemistry*, *64*(11), 1643-1648.

[69] Zdziennicka, A., Szymczyk, K., Krawczyk, J., Jańczuk, B. (2012). Critical micelle concentration of some surfactants and thermodynamic parameters of their micellization. *Fluid Phase Equilibria, 322*, 126-134.

[70] De Lisi, R., Milioto, S., Muratore, N. (2009). Thermodynamics of surfactants, block copolymers and their mixtures in water: the role of the isothermal calorimetry. *International journal of molecular sciences*, *10*(7), 2873-2895.

[71] Majhi, P. R.; Moulik, S. P. Energetics of Micellization: Reassessment by a High-Sensitivity Titration Microcalorimeter. *Langmuir* **1998**, *14* (15), 3986–3990.

[72] Moulik, S. P., Mitra, D. (2009). Amphiphile self-aggregation: An attempt to reconcile the agreement–disagreement between the enthalpies of micellization determined by the van't Hoff and Calorimetry methods. *Journal of colloid and interface science*, *337*(2), 569-578.

[73] Chauhan, S., Kumar, K., Rana, D. S., Kumar, R., Chauhan, M. S. (2016). A comparative study on the aggregation and thermodynamic properties of anionic sodium dodecylsulphate and cationic cetyltrimethylammonium bromide in aqueous medium: effect of the co-solvent n-methylacetamide. *Journal of Surfactants and Detergents*, *19*(1), 193-200.

[74] Causi, S., De Lisi, R., Milioto, S. (1991). Thermodynamic properties of N-octyl-, N-decyl-and N-dodecylpyridinium chlorides in water. *Journal of solution chemistry*, *20*(11), 1031-1058.

[75] Callaghan, A., Doyle, R., Alexander, E., Palepu, R. (1993). Thermodynamic properties of micellization and adsorption and electrochemical studies of hexadecylpyridinium bromide in binary mixtures of 1, 2-ethanediol with water. *Langmuir*, *9*(12), 3422-3426.

[76] Hait, S. K., Majhi, P. R., Blume, A., Moulik, S. P. (2003). A critical assessment of micellization of sodium dodecyl benzene sulfonate (SDBS) and its interaction with poly (vinyl pyrrolidone) and hydrophobically modified polymers, JR 400 and LM 200. *The Journal of Physical Chemistry B*, *107*(15), 3650-3658.

[77] Kroflič, A., Šarac, B., Bešter-Rogač, M. (2011). Influence of the alkyl chain length, temperature, and added salt on the thermodynamics of micellization: Alkyltrimethylammonium chlorides in NaCl aqueous solutions. *The Journal of Chemical Thermodynamics*, *43*(10), 1557-1563.

[78] Makowska, J., Wyrzykowski, D., Pilarski, B., Chmurzyński, L. (2015). Thermodynamics of sodium dodecyl sulphate (SDS) micellization in the presence of some biologically relevant pH buffers. *Journal of Thermal Analysis and Calorimetry*, *121*(1), 257-261.

[79] Arena, G., Casnati, A., Contino, A., Gulino, F. G., Sciotto, D., Ungaro, R. (2000). Entropic origin of the sulfonate groups' electrostatic assistance in the complexation of quaternary ammonium cations by water soluble calix [4] arenes. *Journal of the Chemical Society, Perkin Transactions 2*, (3), 419-423.

[80] Bonaccorso, C., Brancatelli, G., Forte, G., Arena, G., Geremia, S., Sciotto, D., Sgarlata, C. (2014). Factors driving the self-assembly of water-soluble

calix [4] arene and gemini guests: a combined solution, computational and solid-state study. *RSC Advances*, *4*(96), 53575-53587.

[81] Liu, Y., Guo, D. S., Zhang, H. Y., Ma, Y. H., Yang, E. C. (2006). The structure and thermodynamics of calix [n] arene complexes with dipyridines and phenanthroline in aqueous solution studied by microcalorimetry and NMR spectroscopy. *The Journal of Physical Chemistry B*, *110*(7), 3428-3434.

[82] Arena, G., Gans, P., Sgarlata, C. (2016). HypCal, a general-purpose computer program for the determination of standard reaction enthalpy and binding constant values by means of calorimetry. *Analytical and bioanalytical chemistry*, *408*(23), 6413-6422.

[83] Zieliński, R. (2001). Effect of temperature on micelle formation in aqueous NaBr solutions of octyltrimethylammonium bromide. *Journal of colloid and interface science*, *235*(2), 201-209.

[84] Perger, T. M., Bešter-Rogač, M. (2007). Thermodynamics of micelle formation of alkyltrimethylammonium chlorides from high performance electric conductivity measurements. *Journal of colloid and interface science*, *313*(1), 288-295.

[85] Jungnickel, C., Łuczak, J., Ranke, J., Fernández, J. F., Müller, A., Thöming, J. (2008). Micelle formation of imidazolium ionic liquids in aqueous solution. *Colloids and Surfaces A: Physicochemical and Engineering Aspects*, *316*(1-3), 278-284.

[86] Vanyúr, R., Biczók, L., Miskolczy, Z. (2007). Micelle formation of 1-alkyl-3-methylimidazolium bromide ionic liquids in aqueous solution. *Colloids and Surfaces A: Physicochemical and Engineering Aspects*, *299*(1-3), 256-261.R. Vanyúr, L.

[87] Portnaya, I., Cogan, U., Livney, Y. D., Ramon, O., Shimoni, K., Rosenberg, M., Danino, D. (2006). Micellization of bovine β-casein studied by isothermal titration microcalorimetry and cryogenic transmission electron microscopy. *Journal of agricultural and food chemistry*, *54*(15), 5555-5561.

[88] Bundle, D. R., Sigurskjold, B. W. (1994). Determination of accurate thermodynamics of binding by titration microcalorimetry. *Methods in enzymology*, *247*, 288-305.

[89] Hansen, L. D., Fellingham, G. W., Russell, D. J. (2011). Simultaneous determination of equilibrium constants and enthalpy changes by titration calorimetry: Methods, instruments, and uncertainties. *Analytical biochemistry*, *409*(2), 220-229.

[90] Sgarlata, C., Zito, V., Arena, G. (2013). Conditions for calibration of an isothermal titration calorimeter using chemical reactions. *Analytical and bioanalytical chemistry*, *405*(2-3), 1085-1094.

[91] Loh, W., Brinatti, C., Tam, K. C. (2016). Use of isothermal titration calorimetry to study surfactant aggregation in colloidal systems. *Biochimica et Biophysica Acta (BBA)-General Subjects*, *1860*(5), 999-1016.

[92] Bouchemal, K., Agnely, F., Koffi, A., Djabourov, M., Ponchel, G. (2010). What can isothermal titration microcalorimetry experiments tell us about the self-organization of surfactants into micelles?. *Journal of Molecular Recognition*, *23*(4), 335-342.

[93] Van Os, N. M., Daane, G. J., Haandrikman, G. (1991). The effect of chemical structure upon the thermodynamics of micellization of model alkylarenesulfonates: III. Determination of the critical micelle concentration and the enthalpy of demicellization by means of microcalorimetry and a comparison with the phase separation model. *Journal of colloid and interface science*, *141*(1), 199-217.

[94] Bouchemal, K., Agnely, F., Koffi, A., Ponchel, G. (2009). A concise analysis of the effect of temperature and propanediol-1, 2 on Pluronic F127 micellization using isothermal titration microcalorimetry. *Journal of colloid and interface science*, *338*(1), 169-176.

[95] Kamboj, R., Bharmoria, P., Chauhan, V., Singh, S., Kumar, A., Mithu, V. S., Kang, T. S. (2014). Micellization behavior of morpholinium-based amide-functionalized ionic liquids in aqueous media. *Langmuir*, *30*(33), 9920-9930.

[96] Tong, W., Zheng, Q., Shao, S., Lei, Q., Fang, W. (2010). Critical micellar concentrations of quaternary ammonium surfactants with hydroxyethyl substituents on head groups determined by isothermal titration calorimetry. *Journal of Chemical & Engineering Data*, *55*(9), 3766-3771.

[97] Graciaa, A., Ben Ghoulam, M., Marion, G., Lachaise, J. (1989). Critical concentrations and compositions of mixed micelles of sodium dodecylbenzenesulfonate, tetradecyltrimethylammonium bromide and polyoxyethylene octylphenols. *The Journal of Physical Chemistry*, *93*(10), 4167-4173.

[98] Yu, Z. J., Zhao, G. X. (1993). Micellar compositions in mixed surfactant solutions. *Journal of colloid and interface science*, *156*(2), 325-328.

[99] Brito, R. O., Marques, E. F., Gomes, P., Falcao, S., & Söderman, O. (2006). Self-assembly in a catanionic mixture with an aminoacid-derived surfactant: from mixed micelles to spontaneous vesicles. *The Journal of Physical Chemistry B*, *110*(37), 18158-18165.

[100] Tomašić, V., Štefanić, I., Filipović-Vinceković, N. (1999). Adsorption, association and precipitation in hexadecyltrimethylammonium bromide/sodium dodecyl sulfate mixtures. *Colloid and Polymer Science*, *277*(2-3), 153-163.

[101]Herrington, K. L., Kaler, E. W., Miller, D. D., Zasadzinski, J. A., Chiruvolu, S. (1993). Phase behavior of aqueous mixtures of dodecyltrimethylammonium bromide (DTAB) and sodium dodecyl sulfate (SDS). *The Journal of Physical Chemistry*, *97*(51), 13792-13802.

[102]Kume, G., Gallotti, M., Nunes, G. (2008). Review on anionic/cationic surfactant mixtures. *Journal of Surfactants and Detergents*, *11*(1), 1-11.

[103] Jurašin, D. D., Šegota, S., Čadež, V., Selmani, A., Sikirć, M. D. (2017). Recent Advances in Catanionic Mixtures. *Application and Characterization of Surfactants*, 33.

[104] Basílio, N., Spudeit, D. A., Bastos, J., Scorsin, L., Fiedler, H. D., Nome, F., García-Río, L. (2015). Exploring the charged nature of supramolecular micelles based on p-sulfonatocalix [6] arene and dodecyltrimethylammonium bromide. *Physical Chemistry Chemical Physics*, *17*(39), 26378-26385.

[105] Costa, C., Francisco, V., Silva, S. G., do Vale, M. L. C., García-Río, L., Marques, E. F. (2015). Supramolecular self-assembly between an amino acid-based surfactant and a sulfonatocalixarene driven by electrostatic interactions. *Colloids and Surfaces A: Physicochemical and Engineering Aspects*, *480*, 71-78.

[106]Holland, P. M., Rubingh, D. N. (1983). Nonideal multicomponent mixed micelle model. *The Journal of Physical Chemistry*, *87*(11), 1984-1990.

[107]Mittal, K. L. (Ed.). (2012). *Solution chemistry of surfactants* (Vol. 1). Springer Science & Business Media.

[108]Rosen, M. J., Hua, X. Y. (1982). Surface concentrations and molecular interactions in binary mixtures of surfactants. *Journal of Colloid and Interface Science*, *86*(1), 164-172.

[109]Rosen, M. J., Hua, X. Y. (1982). Synergism in binary mixtures of surfactants: II. Some experimental data. *Journal of the American Oil Chemists' Society*, *59*(12), 582-585.

[110]Rosen, M. J. (1975). Relationship of structure to properties in surfactants. III. Adsorption at the solid-liquid interface from aqueous solution. *Journal of the American Oil Chemists Society*, *52*(11), 431-435.

[111]Steffy, D. A., Nichols, A. C., Kiplagat, G. (2011). Investigating the effectiveness of the surfactant dioctyl sodium sulfosuccinate to disperse oil in a changing marine environment. *Ocean Science Journal*, *46*(4), 299-305.

[112]Lin, S. Y., Lin, Y. Y., Chen, E. M., Hsu, C. T., Kwan, C. C. (1999). A study of the equilibrium surface tension and the critical micelle concentration of mixed surfactant solutions. *Langmuir*, *15*(13), 4370-4376.

[113]Morita, A., Carastan, D., Demarquette, N. (2002). Influence of drop volume on surface tension evaluated using the pendant drop method. *Colloid and Polymer Science*, *280*(9), 857-864.

[114]Stauffer, C. E. (1965). The measurement of surface tension by the pendant drop technique. *The journal of physical chemistry*, *69*(6), 1933-1938.

[115]https://www.dataphysics-instruments.com/products/oca/software/

[116]Koller, T. M., Rausch, M. H., Pohako-Esko, K., Wasserscheid, P., Fröba, A. P. (2015). Surface tension of tricyanomethanide-and tetracyanoborate-based imidazolium ionic liquids by using the pendant drop method. *Journal of Chemical & Engineering Data*, *60*(9), 2665-2673.

[117]Winkel, D. (1965). Theoretical refinement of the pendant drop method for measuring surface tensions. *The Journal of Physical Chemistry*, *69*(1), 348-350.

[118] Long, J. A., Rankin, B. M., & Ben-Amotz, D. (2015). Micelle structure and hydrophobic hydration. *Journal of the American Chemical Society*, *137*(33), 10809-10815.

[119] Chevalier, Y., Zemb, T. (1990). The structure of micelles and microemulsions. *Reports on Progress in Physics*, *53*(3), 279.

[120] Laughlin, R. (1995). The Aqueous Phase Behavior of Surfactants. *Journal of the American Chemical Society*, *117*(42), 10603-10603.

[121] Gradzielski, M. A. (2003). Vesicles and vesicle gels-structure and dynamics of formation. *Journal of Physics: Condensed Matter*, *15*(19), R655.

[122] Panizza, P., Roux, D., Vuillaume, V., Lu, C. Y., Cates, M. E. (1996). Viscoelasticity of the onion phase. *Langmuir*, *12*(2), 248-252.

[123] Bangham, A. D., Horne, R. W. (1964). Negative staining of phospholipids and their structural modification by surface-active agents as observed in the electron microscope. *Journal of molecular biology*, *8*(5), 660-IN10.

[124] Bangham, A. D. (1961). A correlation between surface charge and coagulant action of phospholipids. *Nature*, *192*(4808), 1197.

[125] Pavelić, Ž., Škalko-Basnet, N., Schubert, R. (2001). Liposomal gels for vaginal drug delivery. *International journal of pharmaceutics*, *219*(1-2), 139-149.

[126] Regev, O., Guillemet, F. (1999). Various bilayer organizations in a single-tail non-ionic surfactant: unilamellar vesicles, multilamellar vesicles, and flat-stacked lamellae. *Langmuir*, *15*(13), 4357-4364.

[127] Papahadjopoulos, D., Poste, G., Schaeffer, B. E., Vail, W. J. (1974). Membrane fusion and molecular segregation in phospholipid vesicles. *Biochimica et Biophysica Acta (BBA)-Biomembranes*, *352*(1), 10-28..

[128]Hope, M. J., Bally, M. B., Mayer, L. D., Janoff, A. S., Cullis, P. R. (1986). Generation of multilamellar and unilamellar phospholipid vesicles. *Chemistry and physics of lipids*, *40*(2-4), 89-107.

[129]Barenholz, Y., Gibbes, D., Litman, B. J., Goll, J., Thompson, T. E., Carlson, F. D. (1977). A simple method for the preparation of homogeneous phospholipid vesicles. *Biochemistry*, *16*(12), 2806-2810.

[130]Bangham, A. D., Horne, R. W. (1964). Negative staining of phospholipids and their structural modification by surface-active agents as observed in the electron microscope. *Journal of molecular biology*, *8*(5), 660-IN10.

[131]Bangham, A. D. (1961). A correlation between surface charge and coagulant action of phospholipids. *Nature*, *192*(4808), 1197.

[132]Mayer, L. D., Hope, M. J., Cullis, P. R. (1986). Vesicles of variable sizes produced by a rapid extrusion procedure. *Biochimica et Biophysica Acta (BBA)-Biomembranes*, *858*(1), 161-168.

[133]Zasadzinski, J. A. (1986). Transmission electron microscopy observations of sonication-induced changes in liposome structure. *Biophysical journal*, *49*(6), 1119-1130.

[134]Richtering, W. (2001). Rheology and shear induced structures in surfactant solutions. *Current opinion in colloid & interface science*, *6*(5-6), 446-450.

[135]Talmon, Y., Evans, D. F., Ninham, B. W. (1983). Spontaneous vesicles formed from hydroxide surfactants: Evidence from electron microscopy. *Science*, *221*(4615), 1047-1048.

[136]Hoffmann, H., Gräbner, D., Hornfeck, U., Platz, G. (1999). Novel vesicles from single-chain surfactants. *The Journal of Physical Chemistry B*, *103*(4), 611-614.

[137]Caillet, C., Hebrant, M., Tondre, C. (2000). Sodium octyl sulfate/cetyltrimethylammonium bromide catanionic vesicles: aggregate composition and probe encapsulation. *Langmuir*, *16*(23), 9099-9102.

[138]Ghosh, S., Ambade, B., Ray, A. (2013). Stable catanionic vesicles as drug delivery vehicle. *Science of Advanced Materials*, *5*(12), 1837-1846.

[139]Vautrin, C., Zemb, T., Schneider, M., Tanaka, M. (2004). Balance of pH and ionic strength influences on chain melting transition in catanionic vesicles. *The Journal of Physical Chemistry B*, *108*(23), 7986-7991.

[140]Francisco, V., Basilio, N., Garcia-Rio, L., Leis, J. R., Maques, E. F., Vázquez-Vázquez, C. (2010). Novel catanionic vesicles from calixarene and single-chain surfactant. *Chemical Communications*, *46*(35), 6551-6553.

[141]Marques, E. F. (2000). Size and stability of catanionic vesicles: effects of formation path, sonication, and aging. *Langmuir*, *16*(11), 4798-4807.

[142] Schmölzer, St., Gräbner, D., Gradzielski, M., Narayanan, T. (2002). Millisecond-range time-resolved small-angle x-ray scattering studies of micellar transformations. *Physical review letters*, *88*(25), 258301.

[143]Raghavan, S. R., Fritz, G., Kaler, E. W. (2002). Wormlike micelles formed by synergistic self-assembly in mixtures of anionic and cationic surfactants. *Langmuir*, *18*(10), 3797-3803.

[144]Basilio, N., García-Río, L. (2009). Sulfonated Calix [6] arene Host–Guest Complexes Induce Surfactant Self-Assembly. *Chemistry – A European Journal*, *15*(37), 9315-9319.

[145]Francisco, V., Basilio, N., Garcia-Rio, L., Leis, J. R., Maques, E. F., Vázquez-Vázquez, C. (2010). Novel catanionic vesicles from calixarene and single-chain surfactant. *Chemical Communications*, *46*(35), 6551-6553.

[146] Vlachy, N., Renoncourt, A., Drechsler, M., Verbavatz, J. M., Touraud, D., Kunz, W. (2008). Blastulae aggregates: New intermediate structures in

the micelle-to-vesicle transition of catanionic systems. *Journal of colloid and interface science*, *320*(1), 360-363.

[147]Murphy, R. M. (1997). Static and dynamic light scattering of biological macromolecules: what can we learn?. *Current opinion in biotechnology*, *8*(1), 25-30.

[148]Sun, Y. (2011). Investigating Static and Dynamic Light Scattering. *arXiv preprint arXiv:1110.1703*.

[149]Burchard, W. (1983). Static and dynamic light scattering from branched polymers and biopolymers. In *Light scattering from polymers* (pp. 1-124). Springer, Berlin, Heidelberg.

[150]Øgendal, L. (2013). Light Scattering Demystified: Theory and Practice. *University of Copenhagen*, *125*.

[151]Sartor, M. (2003). Dynamic light scattering. *University of California, San Diego*, 2-21.

[152]Pecora, R. (2000). Dynamic light scattering measurement of nanometer particles in liquids. *Journal of nanoparticle research*, *2*(2), 123-131.

[153]Goldburg, W. I. (1999). Dynamic light scattering. *American Journal of Physics*, *67*(12), 1152-1160.

[154]Andersen, K. E., Hansen, M. B. (2000). Static light scattering. In *Methods and Applications of Inversion* (pp. 1-14). Springer, Berlin, Heidelberg.

[155]Yoo, S. H., Jane, J. L. (2002). Molecular weights and gyration radii of amylopectins determined by high-performance size-exclusion chromatography equipped with multi-angle laser-light scattering and refractive index detectors. *Carbohydrate polymers*, *49*(3), 307-314.

[156]Frisken, B. J. (2001). Revisiting the method of cumulants for the analysis of dynamic light-scattering data. *Applied optics*, *40*(24), 4087-4091.

[157] Zhu, B. Y., Gu, T. (1991). Surfactant adsorption at solid-liquid interfaces. *Advances in colloid and interface science*, *37*(1-2), 1-32.

[158] Zhang, R., Somasundaran, P. (2006). Advances in adsorption of surfactants and their mixtures at solid/solution interfaces. *Advances in colloid and interface science, 123*, 213-229.

[159] Atkin, R., Craig, V. S., Biggs, S. (2000). Adsorption kinetics and structural arrangements of cationic surfactants on silica surfaces. *Langmuir, 16*(24), 9374-9380.

[160] Atkin, R., Craig, V. S., Biggs, S. (2001). Adsorption kinetics and structural arrangements of cetylpyridinium bromide at the silica− aqueous interface. *Langmuir, 17*(20), 6155-6163.

[161] Atkin, R., Craig, V. S., Wanless, E. J., Biggs, S. (2003). Mechanism of cationic surfactant adsorption at the solid–aqueous interface. *Advances in colloid and interface science, 103*(3), 219-304.

[162] Tiberg, F., Joensson, B., Tang, J. A., Lindman, B. (1994). Ellipsometry studies of the self-assembly of non-ionic surfactants at the silica-water interface: equilibrium aspects. *Langmuir, 10*(7), 2294-2300.

[163] Eskilsson, K., Yaminsky, V. V. (1998). Deposition of Monolayers by Retraction from Solution: Ellipsometric Study of Cetyltrimethylammonium Bromide Adsorption at Silica− Air and Silica− Water Interfaces. *Langmuir, 14*(9), 2444-2450.

[164] Shi, L., Ghezzi, M., Caminati, G., Lo Nostro, P., Grady, B. P., Striolo, A. (2009). Adsorption isotherms of aqueous C12E6 and cetyltrimethylammonium bromide surfactants on solid surfaces in the presence of low molecular weight coadsorbents. *Langmuir*, *25*(10), 5536-5544.

[165] Wu, S., Shi, L., Garfield, L. B., Tabor, R. F., Striolo, A., Grady, B. P. (2011). Influence of surface roughness on cetyltrimethylammonium bromide adsorption from aqueous solution. *Langmuir*, *27*(10), 6091-6098.

[166] Gutig, C., Grady, B. P., Striolo, A. (2008). Experimental Studies on the Adsorption of Two Surfactants on Solid− Aqueous Interfaces: Adsorption Isotherms and Kinetics. *Langmuir, 24*(9), 4806-4816.

[167] Naderi, A., Claesson, P. M. (2006). Adsorption properties of polyelectrolyte− surfactant complexes on hydrophobic surfaces studied by QCM-D. *Langmuir*, *22*(18), 7639-7645.

[168] Voinova, M. V., Jonson, M., Kasemo, B. (2002). 'Missing mass' effect in biosensor's QCM applications. *Biosensors and Bioelectronics*, *17*(10), 835-841.

[169] Schumacher, R. (1990). The Quartz Microbalance: A Novel Approach to the In-Situ Investigation of Interfacial Phenomena at the Solid/Liquid Junction [New Analytical Methods (40)]. *Angewandte Chemie International Edition in English*, *29*(4), 329-343.

[170] Rodahl, M., Höök, F., Krozer, A., Brzezinski, P., Kasemo, B. (1995). Quartz crystal microbalance setup for frequency and Q-factor measurements in gaseous and liquid environments. *Review of Scientific Instruments*, *66*(7), 3924-3930.

[171] Fusetani, N. (2004). Biofouling and antifouling. *Natural product reports*, *21*(1), 94-104.

[172] Höök, F., Kasemo, B., Grunze, M., Zauscher, S. (2008). Quantitative biological surface science: challenges and recent advances.

[173] Fendler, J. H. (1996). Self-assembled nanostructured materials. *Chemistry of Materials*, *8*(8), 1616-1624.

[174] Ward, M. D., Buttry, D. A. (1990). In situ interfacial mass detection with piezoelectric transducers. *Science*, *249*(4972), 1000-1007.

[175] Cady, W. G. (2018). *Piezoelectricity: Volume Two: An Introduction to the Theory and Applications of Electromechanical Phenomena in Crystals*. Courier Dover Publications.

[176] Beck, R., Pittermann, U., Weil, K. G. (1988). Impedance analysis of quartz oscillators, contacted on one side with a liquid. *Berichte der Bunsengesellschaft für physikalische Chemie*, *92*(11), 1363-1368.

[177] Reviakine, I., Johannsmann, D., Richter, R. P. (2011). Hearing what you cannot see and visualizing what you hear: interpreting quartz crystal microbalance data from solvated interfaces.